University of California

Los Angeles

Applications of Network Science to Criminal Networks, University Education, and Ecology

A dissertation submitted in partial satisfaction

of the requirements for the degree

Doctor of Philosophy in Mathematics

by

Charles Zachary Marshak

2017

Abstract of the Dissertation

Applications of Network Science to Criminal Networks, University Education, and Ecology

by

Charles Zachary Marshak
Doctor of Philosophy in Mathematics
University of California, Los Angeles, 2017
Professor Andrea Bertozzi, Co-Chair
Professor Mason Alexander Porter, Co-Chair

Networks are a powerful tool to investigate complex systems. In this work, we apply network–theoretic tools to study criminal, educational, and ecological systems.

First, we propose two generative network models for recruitment and disruption in a hierarchal organized crime network. Our network models alternate between recruitment and disruption phases. In our first model, we simulate recruitment as Galton–Watson branching. We simulate disruption with an agent that moves towards the root and arrests nodes in accordance with a stochastic process. We prove a lower bound on the probability that the agent reaches the kingpin and verify this numerically. In our second model, we propose a network attachment mechanism to simulate recruitment. We define an attachment probability based on an existing node's distance to the leaf set (terminal nodes), where this distance is a proxy for how close a criminal is to visible illicit activity. Using numerical simulation, we study the network structures such as the degree distribution and total attachment weight associated with large networks that evolve according to this recruitment process. We then introduce a disruptive agent that moves through the network according to a self-avoiding random walk and can remove nodes (and an associated subtree) according to different disruption strategies. We quantify basic law enforcement incentives with these different disruption strategies and study costs and eradication probability within this model.

In our next chapter, we adapt rank aggregation methods to study how Mathematics students navigate their coursework. We first translate 15 years of grade data from the UCLA Department of Mathematics into a network whose nodes are the various Mathematics courses and whose edges encode the flow of students between these courses. Applying rank aggregation on such networks, we extract a linear sequence of courses that reflects the order students select courses. Using this methodology, we identify possible trends and hidden course dependencies without investigating the entire space of possible schedules. Specifically, we identify Mathematics courses that high–performing students take significantly earlier than low–performing students in various Mathematics majors. We also compare the extracted sequence of several rank aggregation methods on this data set and demonstrate that many methods produce similar sequences.

In our last chapter, we review core–periphery structure and analyze this structure in mutualistic (bipartite) fruigivore–seed networks. We first relate classical graph cut problems to previous work on core–periphery structure to provide a general mathematical framework. We also review how core–periphery structure is traditionally identified in mutualistic networks. Next, using a method from Rombach et al., we analyze the core–periphery structure of 10 mutualistic fruigivore–seed networks that encode the interaction patterns between birds and fruit–bearing plants. Our collaborators use our network analysis with other ecological data to identify important species in the observed habitats. In particular, they identify certain types of birds (*mashers*) that play crucial roles at a variety of sites, which are though to be less important due to their feeding behaviors.

The dissertation of Charles Zachary Marshak is approved.

University of California, Los Angeles

2017

To Nade

Table of Contents

1 Introduction 1

2 Growth and Disruption of a Hierarchical Criminal Network 5

2.1 Related Models for Criminal Organization and Behavior 6

2.2 Criminal Recruitment and Disruption Model I 10

2.2.1 Recruitment Mechanism 10

2.2.2 Pursuit Mechanism 15

2.2.3 Conclusions from Model 21

2.3 Criminal Recruitment and Disruption Model II 22

2.3.1 Model Overview and Related Network Processes 23

2.3.2 Recruitment Mechanism 30

2.3.3 Pursuit Mechanism 39

2.3.4 Conclusions from Model 53

2.4 Conclusions and Future Work 55

3 Rank Aggregation for Course Sequence Discovery 58

3.1 Introduction 59

3.2 Related Work 61

3.3 Student Data 64

3.4 Models and Methods for Rank Aggregation 69

3.5 Matrix Methods for Rank Aggregation 74

3.5.1 Preliminary Networks 75

3.5.2 PageRank 77

3.5.3 Rank Centrality 79

3.5.4 SerialRank 80

3.5.5 SyncRank 82

3.5.6 Least Squares 84

3.5.7 Ranking via Singular Value Decomposition 84

3.5.8 Evaluating a Course Sequence 85

3.6 Course-Sequence Discovery 87

3.6.1 Evaluating the Matrix Methods 87

3.6.2 Identifying Hidden Course Dependencies 95

3.7 Conclusions and Future Work 97

4 Core–Periphery Structure in Frugivore–Seed Networks 103

4.1 Notations and Related Graph Calculus 104

4.2 Core–Periphery Structure 110

4.2.1 Combinatorial Quantities Related to Core–Periphery Structure 113

4.2.2 Models for Core–Periphery Structure 118

4.3 Core–Periphery Structure in Frugivore–Seed Networks 135

4.4 Conclusions and Future Work 140

A Rank Aggregation for Course–Sequence Discovery 143

A.1 Course Numbers 143

B Core-Periphery Structure in Fruigivore–Seed Networks 145

B.1 Simulated Annealing 145

References 148

List of Figures

2.1 The recruitment process at $t = 3$ with $\xi \sim \text{Pois}(1.3)$. The darkest node at the top is the kingpin. The yellow nodes at the bottom are those recruited at $t = 3$. These yellow nodes are the only nodes eligible to recruit during $t = 4$. The variable ξ_i^t indicates the number of criminals recruited at time t by the ith criminal previously added during $t - 1$. We have enumerated criminals recruited at time t from left to right. The variable C_t indicates the total number of criminals added at time t. 12

2.2 We estimate the expected height $E(H)$ in two different ways for varying λ for $\mathbf{R}(\xi)$ and ξ Poisson-distributed with mean λ. First, we estimate $E(H)$ using the experimental mean $\widehat{H}$ over 10,000 simulations. We set the height threshold $m = 250$ and stop the recruitment process when this height is reached. Alternatively, we inspect $m(1 - r)$, numerically solving for r using Eq. (2.2) with $\varphi(s) = e^{\lambda(s-1)}$. 16

2.3 An example of a $\mathbf{P}(\xi, \mathrm{N}^0, z)$ during the first time step. Let N^0 be the network found in Figure 2.1. Let $z \in [0, 1]$ and $\xi \sim \text{Pois}(1.3)$. The agent uniformly at random selects a node eligible to recruit; these are the yellow nodes in Figure 2.1. The agent begins their investigation at v_1, moves to v_2, and then ends at v_3. At v_3, the agent is unable to move upwards once more and removes the subtree below their current position. The arrested criminals are in blue with thick boundary. The yellow node at the bottom right, labeled with an l, is still able to recruit, and the network has not been terminated. 18

2.4 The experimental mean $\widehat{H}$ and the upper bound from Eq. (2.5) for various z. We use 10,000 simulations to compute $\widehat{H}$ and initialize a network to be a perfect binary tree of height 2. We set the height threshold m to be 250. . . 20

2.5 A simulated recruitment process for $t = 0, 1, 2, 3$. The network starts with a single criminal (the kingpin) and then evolves according to the proposed attachment mechanism. Here the number of new criminals introduced into the network is given by the recruitment index $k = 5$. The leaf nodes (light yellow) represent criminals without underlings. In our model, these leaf nodes are called street criminals. Of these, the nodes with the darker boundary are those freshly recruited at a given time step. For example, the number of street criminals when $t = 3$ is 8, of which 5 are new recruits. 29

2.6 The criminal network at $t = 3$ with the values of $w(j; t)$ shown. Here, the recruitment index $k = 5$ and the initial configuration consists of a single kingpin. All criminals j in $\mathcal{S}(t)$ have attachment weight $w(j; t) = 1$. 31

2.7 The out-degree distribution $P_\infty(d)$ of nodes on a criminal network determined from numerical simulations for $t \to \infty$. The three curves correspond to recruitment indices $k = 1, 10, 20$. We terminate a simulation when the total number of criminals reaches or exceeds 5×10^3. Each curve for $P_\infty(d)$ represents 100 simulations. The tail of the degree distribution is noisier as high degree nodes are rarer than low degree nodes. As discussed in the text, we fit the distribution to a decaying exponential distribution. The numerics indicate that $P_\infty(d = 0) \approx 0.39$ for all the values of k we considered. 32

2.8 We show the distribution of distances from the kingpin. These distributions are the average over 100 runs, stopping each simulation at $t = 100$, 200, or 300. We set the recruitment index $k = 10$ and the initial configuration to be the kingpin alone. We then fit the measured distributions using a shifted gamma density $\rho_{\alpha,\beta,s}(y)$ (Eq. (2.12)). We label this fit γ-distribution as $\gamma(\alpha, \beta, s)$. . 35

2.9 (Top) The number $s(t)$ of street criminals as a function of time t for recruitment rates $k = 10, 50, 100$. In each simulation, we terminate the recruitment process when the total number of criminals exceeded 5×10^3. Each data point is the average of 250 simulations. We fit the data to $s(t) = r_s t + 1$ and expect $r_s \approx P_\infty(d = 0)k$, where $P_\infty(d = 0) \approx 0.39$. This scaling is confirmed with the fit values of r_s in the legend. (Bottom) The slope values r_s as a function of k with the r_s values from the top display shown in dark symbols with corresponding shapes. We then fit the data with a line as indicated in the bottom legend, providing evidence of our conjecture $r_s \approx P_\infty(d = 0)k$. 36

2.10 Schematic of the addition of new nodes from time t to time $t + 1$. Here, the recruitment index k is 3. We depict the leaf nodes in yellow and those nodes added from t to $t + 1$ with thick boundary. We indicate the attachment of a new leaf node to an internal node with a solid gray halo seen on the lower left hand side of the image. We also indicate the attachment of new leaf nodes to previously leaf nodes with a the dashed ring. In this recruitment phase, the total number of street criminals at time $t + 1$ increase by 1 from time t. In other words, this recruitment phase dictates $s(t + 1) = s(t) + 1$. 37

2.11 Total attachment weight $\sum_{j \in \mathcal{C}(t)} w(j; t)$ of the network as a function of time averaged over 100 runs for $k = 10, 20, 30, 40$. We initialized the network as the kingpin alone. We terminate each simulation when the number of criminals reaches 5×10^3. We fit the data to a linear form $\mathcal{W}t + w_0$ and find that the extrapolated values of $\mathcal{W}$ in the figure legend are in excellent agreement with the ones predicted from Eq. (2.18), given by $\mathcal{W} = 6.39, 12.79, 19.18, 25.57$ for $k = 10, 20, 30, 40$, respectively. 40

2.12 The pursuit phase as we describe in Section 2.3.3. We initialize the network as a perfect ternary tree of height three. The network consists of the light and dark colored nodes. The light nodes are those nodes invisible to our agent during the pursuit phase. The dark nodes are those nodes that have been investigated or arrested. (Left) At time $t = 1$ the agent begins their pursuit from the yellow criminal and without having perfect knowledge of the network. He investigates three other nodes, highlighted in red marked by a solid dark line. The last node, surrounded by a dark ring, is the criminal that is currently under investigation. (Right) The criminal that is under investigation is arrested. Once a criminal is arrested, they are removed from the network along with all of their direct underlings, their direct underlings, and so on. The arrested nodes are depicted in blue and have a darker boundary. Note that not all criminals arrested are investigated and vice versa. 43

2.13 Network eradication probability as a function of the recruitment index k, obtained by averaging over 10,000 simulations for different strategies. We consider a total population of $n^* = 500, 1000, 2000$ individuals and halt our simulations when the criminal network reaches this size. For each strategy, the Beat(Q) denotes the maximum recruitment index k for which the network is eradicated with probability 1, over all simulations. 45

2.14 Varying initial conditions prior to law enforcement intervention. (Left) Eradication probabilities on a complete initial tree with b branches and forty criminals for $k = 30$ and law enforcement strategy $Q_D(q = 3)$. When a graph consists of a single path ($b = 1$), the eradication probability is 1, because dead ends cannot be reached. Increasing b allows more dead ends to be encountered, so that the eradication probability decreases until $b = 3$ and plateaus until $b = 6$. After $b = 6$, the height of the network becomes small enough to allow for easier access to the kingpin. (Center and Right) Eradication probabilities using perfect initial trees with branching factor b and height h as initial conditions and using strategy $Q_D(q = 3)$. The initial number of criminals is $(b^{h+1} - 1)/(b - 1)$. 46

2.15 (Top) Costs incurred by law enforcement conditioned on kingpin capture as a function of the recruitment index k. Shades in the data points represent the probabilities of network eradication. We consider 10000 simulations and allow the network to grow to $n^* = 1000$. There is the emergence of maxima for certain curves because we condition on the eradication of the network. As k increases initially for such curves, the network grows more rapidly and so too does the number of investigations necessary for eradication. Upon reaching a threshold in k (maxima), the number of possible pursuit phases greatly decreases. In particular, for large k, a network must be eradicated within fewer pursuit phases and thereby reducing cost. (Bottom) The mean eradication time as a function of k for various strategies. Similarly as in the above panel, there is an emergence of maxima only now for all curves. Note that cost and time curves for $Q_A(p = 1)$ and $Q_D(q = 1)$ are identical and that $Q_I = Q_A(p \to \infty) = Q_D(q \to \infty)$. 57

3.1 A subgraph corresponding to the proportion matrix $\mathbf{P}$ defined Eq. (3.9) for Applied Mathematics majors. Each node represents a course; for this subgraph, we selected Linear Algebra I (Math 115A), Real Analysis I (Math 131A), and Discrete Structures (Math 61). The edge weight P_{ij} from course i to j indicates the proportion of students that took i in an earlier quarter than j out of all those students that took the pair of courses in different quarters. 79

3.2 The proportion matrix $\mathbf{P}$ for Pure Mathematics students with A-range GPA. We order courses with PageRank. 94

4.1 Two examples weight matrices for networks with characteristic mesoscale structures: community structure (a) and core–periphery structure (b). We illustrate strong, intermediate, and weak edge weight. In Figure 4.1a, C_1 and C_2 are two disjoint communities with strong edge weight within a community and weak edge weight between communities. In Figure 4.1b, C_1 is the core and C_2 the periphery such that the core is strongly connected to itself, the core is connected to the periphery with intermediate weight, and the periphery is connected weakly to itself. 110

4.2 The barbell graph in which there are two complete graphs on 10 vertices connected by a single edge. The shaded regions indicate the disconnected subgraphs when a single edge connecting these two subgraphs is removed. . . 113

4.3 The k-cores for $k = 1, 2, 3$ enclosed in increasingly dark concentric ellipses, respectively. Note that the largest degree node is not considered part of the core for $k > 1$ as it is connected to several degree one nodes. Using the k-core requires a core structure to be well connected with itself, though not necessarily with the periphery. 115

4.4 (a) A realization of a network from the stochastic block model from Eq. (4.23)–(4.24) with parameters $n_c = n_p = 50$, $p_{cc} = .8$, and $p_{cp} = p_{pp} = .5$ specified. (b) A histogram of degrees in the same network. 120

4.5 (a) A rank-2 adjacency matrix of a core–periphery structure. (b) An adjacency matrix that we generate from a stochastic block model with parameters $p_{cc} = p_{cp} = .8$ and $p_{pp} = .5$. (c) A rank-2 approximation of the adjacency matrix with entrywise thresholding such that each entry $\widetilde{w}_{ij}$ in rank-2 matrix is set to 0 if $\widetilde{w}_{ij} < .5$ else we set $\widetilde{w}_{ij}$ to 1. 122

4.6 $S(\alpha, \beta, n)$ where $\alpha = .7$, $\beta = .5$, and $n = 30$. We consider $\mathbf{f}_{\alpha,\beta}$ with range $S(\alpha, \beta, n)$. 131

4.7 Core matrices for an instance of a stochastic block model using three different centralities. The network was generated using tje stochastic block model specified with Eq. (4.23)–(4.24) and parameters $n_c = n_p = 50$, $p_{cc} = .8$, $p_{cp} = p_{pp} = .5$. We set t in Eq. (4.55) to be the median of nonzero entries. . 134

4.8 The weight matrix associated to Pozo Verde, one of the 10 sites. Each frugivore is labeled with an '(F)'. The weight between frugivores and plants is determined from the number of recorded interactions. A related network visualization is in Figure 4.9. 136

4.9 The network from Pozo Verde with weight matrix shown in Figure 4.8. The nodes's sizes are proportional to their aggregate core score (Eq. (4.51)). The edges are proportional to the weight. The two darker nodes are core-nodes. These nodes define a cut that maximizes CP-Cut from (Eq. (4.52)). 137

4.10 The matrix of $R_{\alpha,\beta}$ from Eq. (4.50). 141

4.11 The profile of CP-Cut(C_k, P_{n-k}) as a function of k, where we scaled each entry of $\mathbf{W}$ dividing by the maximum entry. 142

4.12 A scatter plot for degree versus core scores for two sites. We compute the correlation coefficient ρ. 142

List of Tables

2.1 A table comparing the terminology used for our recruitment and disruption model and that of standard network theory. 10

2.2 A table comparing the terminology used in this paper and that of standard network theory. 28

2.3 The parameters of the recruitment mechanism. 33

3.1 Sample of data provided by department of mathematics. 65

3.2 Course Sequences for Applied Mathematics Majors obtained by three of the six methods discussed in this chapter. 88

3.3 Course Sequences for Applied Mathematics Majors obtained by the three of the six methods discussed in this chapter. 89

3.4 K($\mathbf{q}$) coefficients for Applied Mathematics, Applied Science, and Pure Mathematics. Each major has n_s total students. We subdivide each majors into GPA categories: All ([0, 4.3]), A-range ([3.7, 4.3]), B-range ([2.7, 3.7)), and C-range ([1.7, 2.7)). 93

3.5 First 11 courses for A students in five different majors using SerialRank. . . 98

3.6 Comparing the A and C students in three majors using SyncRank. 99

A.1 Course names and numbers. 144

Acknowledgments

This thesis is the culmination of several years of study, research, and collaboration. It is an honor and a privilege to move through the doctoral process at UCLA. I am appreciative of the exceptional academic guidance of my supervisors: Professor Andrea Bertozzi and Professor Mason Porter. It was a joy to work under Professor Bertozzi. She gave me interesting applied problems to study, freely shared her mathematical insights, provided fascinating datasets for me and colleagues to explore, and connected me with the talented students, postdocs, and professors in her group. Professor Porter generously shared his time, energy, expertise, and humor in my final quarter and pushed me to be a better applied mathematician and analytic thinker. His passion and integrity has been inspiring even before he became an official supervisor. I also want to acknowledge the mentorship of Professor Puck Rombach, who was my guide through the wonderful world of networks since she first introduced me to Galton-Watson branching in the Fall of 2013. I am appreciative of my fruitful collaborations with Professor Mihai Cucuringu, Professor Maria D'Orsogna, and Dillon Montag. Professor Cucuringu, in particular, helped me to ask great questions of large data sets. I am also grateful to my committee: Professor Brantingham, Professor Teran, and Professor Yin. Each were available for discussions and guidance during this research.

I feel fortunate to have been apart of an amazing community at UCLA. I am grateful to Ryan Compton for sparking my interest in applied mathematics. He pointed me toward important computational tools, inspired me with his knack for data-centric problems, provided endless encouragement and shared a love for international cuisine. I am very grateful to the numerous classes that I took at UCLA in mathematics, each building confidence and skills that made this research tenable. Specifically, I am particularly grateful for Professor Teran's great courses on computational linear algebra; Professor Yin's insights into the field of numerical optimization, in which he plays a pivotal role; and Professor Petersen's perspective of differential geometry. It's hard to quantify all the mathematics I learned in informal conversations with colleagues, but these have been truly the most integral to my development as a mathematician. Gergley Klar shared his multilingual computational expertise; Andre Pradhana elucidated several numerical methods; and Joseph Woodworth intuitively explained many machine learning models. I am also grateful to Juan Carlos Apitz, Zach Boyd, Charles Chen, Brent Edmunds, Miguel Hidalgo, Ritvik Kharkar, Eric Larson, Stephen Lu, Xiyang Luo, Zhaoyi Meng, Cassidy Mentus, Travis Meyer, Shoo Seto, and Jessica Tran.

I also feel it is important to thank excellent instructors and teachers that challenged and nurtured my early mathematical interests. In that regard, I want to thank Cheryl Katz, Ira Moscow, Leigh Morris, Professor Arthur Ogus, Professor Ming Gu, Professor Joshua Sussan, Professor Fraydoun Rezakhanlou, and Professor John Kreuger. I also want especially thank Patrick Barrow for being the first to formally introduce me to a mathematical proof and for his friendship.

The UCLA staff Maida Bassili, Maggie Albert, Martha Contreras, Leticia Domingues, Jacquie Bauwens, and Babbette Dalton each helped me navigate the day-to-day logistics of the doctoral program and provided me the resources I needed to succeed as a graduate student.

I am also indebted to the support I received from my large extended family. Most importantly, I am forever grateful to my fiancée, Nadine Levyfield, who is a constant source of inspiration. She has constantly pushed me to always be my best self. I am grateful to my mom, Susan Zachary, for providing me with numerous educational opportunities and experiences (e.g. *QED*). I am extraordinary thankful to those who patiently supported me through life challenges: Thomas Kielty, Clare Sassoon, and Mona Field. This process was a little bit easier thanks to the regular hot food and good conversation of Ali Lake, Claude Zachary, Gregg Montefierre, Martin Goldstein, Ken Levy, Karen Hilfman, Ben Goldstein, Tania Verafield, Max Goldstein, Lois Levy, Jose Vera, Maggie Hasse, and Johanna Zetterburg.

All the research (models, methods, code, and analysis) is the shared work of several people, which I now discuss. Chapter 2 is a collaboration between myself, Andrea Bertozzi, Maria D'Orsogna, and Puck Rombach. We introduce a model that we proposed and published in [127]. Puck Rombach supervised the design of the generative network mechanism. James von Brecht was also involved in the preliminary stages of this project. I had helpful discussions on programming related to this project with Ryan Compton, Gergely Klar, and the Stackoverflow Community. The work was supported by ARO MURI grant W911NF-11-1-0332, AFOSR MURI grant FA9550-10-1-0569, NSF grant DMS-0968309, ONR grant N000141210838. We simulated the criminal networks and collected statistics using NetworkX, NumPy, and SciPy. The library d3.js was used for the network diagrams. All the code can be found at the site `https://github.com/cmarshak/GameOfPablos`.

In Chapter 3, we present an ongoing collaboration between Mihai Cucuringu, Puck Rombach and Dillon Montag. There is a preprint posted on the arXiv [139]. We thank Dimitri Shlyakhtenko and Andrea Bertozzi for acquiring the data from the UCLA Department of Mathematics and help with related administrative issues related to doing research on this data set. Mihai Cucuringu originally proposed the project, who initially explored a variety of approaches based on his recent work [53]. Dillon Montag provided crucial numerical investigation and analysis during the 2015 Research Experience for Undergraduates (REU) at UCLA. Afterwards, we supplemented his initial investigation with additional rank aggregation methodologies. We would like to acknowledge the invaluable conversations with Juan Carlos Apitz, Jessica Tran, Ritvik Kharkar, and Milicia Hadzi-Tanovic, with whom we worked extensively on processing and understanding this academic data set. This work will be the basis for a journal submission after this thesis is formally reviewed. This work was supported by NSF grant DMS-1045536, UC Lab Fees Research Grant 12-LR-236660, ARO MURI grant W911NF-11-1-0332, AFOSR MURI grant FA9550-10-1-0569, NSF grant DMS-1417674, and ONR grant N-0001-4121-0838.

In Chapter 4, we present two projects. The first is an ongoing work on core-periphery structure and a collaboration between Puck Rombach and Andrea Bertozzi. We present an exposition on core–periphery structure with an eye toward adapting an MBO-scheme [138]. The second is a brief description of our contribution to core–periphery network analysis appearing in [179]. This is joint work with Román A. Ruggera, Pedro G. Blendinger, and

M. Daniela Gomez, I am grateful for Puck Rombach's introduction to the team of ecologists and her permission to use her `Matlab` code, which was used for the network analysis.

Vita

2006 – 2010	B.A. Mathematics, University of California, Berkeley
2010	Dorothy Klumpke Award for Scholarship in Mathematics, University of California, Berkeley.
2010	Phi Beta Kappa
2010 – 2015	Teaching Assistant, University of California, Los Angeles
Summer 2014	M.S. Applied Mathematics, University of California, Los Angeles
Summer 2014	Graduate Student Asst. Mentor for Applied Mathematics REU at University of California, Los Angeles (Project: Criminal Networks)
Fall 2014	Research Assistant (Project: Criminal Networks)
Summer 2015	Graduate Student Mentor for the Applied Mathematics REU at University of California, Los Angeles (Project: Educational Data Mining)
Fall 2015	Research Assistant (Project: Core Periphery Structures)
2016	Graduate Student Instructor, University of California, Los Angeles
Summer 2016	Graduate Student Intern at Jet Propulsion Laboratory (Project: Two-layer Separation Problem)

Publications

Ritvik Y. Kharkar, Jessica Tran, and Charles Z. Marshak. Core Course Analysis for Undergraduate Students in Mathematics. (Submitted)

Charles Z. Marshak, Mihai Cucuringu, Dillon V. P. Montag, and Puck Rombach. Rank Aggregation for Course Sequence Discovery. (In Preparation)

Charles Z. Marshak, Puck Rombach, Andrea L. Bertozzi, and Maria R. D'Orsogna. Pursuit on an Organized Crime Network. *Physical Review E* 93.2 (2016): 022308.

Román A. Ruggera, Pedro G. Blendinger, M. Daniela Gomez, and Charles Z. Marshak. Linking Structure and Functionality in Mutualistic Networks: Do Core Frugivores Disperse More Seeds than Peripheral Species? *Oikos* 2015.

CHAPTER 1

Introduction

Networks are a powerful mathematical object to help understand data in our digital age. Networks represent a group of entities (humans, animals, servers, subway stops, politicians, college courses, films, websites, etc.) and the connections between them. They can model airplane flyways [38,111], political collaboration [149,176], pixels in an image [22,138], neuronal pathways [17], online social communities [132, 198], plant-animal interaction [136, 137, 167], and the authority of webpages [89, 166] to name but a few. Network science has matured in recent decades because of its varied contributions from mathematics [27], physics [154], social statistics [203], and computer science [72]. Generally, networks are a set of *nodes* and *edges*. Each node represents an entity and each edge a pairwise connections (e.g. a friendship in a social network or a hyperlink on the WWW). Many networks are described using the terminology of *graph theory* [27]. In addition to nodes and edges, networks often encode heterogeneous edge traits to study varied, nuanced relationships between nodes in empirical data sets. For example, not all connections are symmetric and one employs *directed edges* to encode such connections, as in a citation network [58]. In addition, an *edge weight* can quantify the strength of a particular connection, such as the distance between two airports [38, 111] or the frequency two politicians vote on the same bill [154, 176]. More recently, *multilayer networks* model relationships across networks [111], where nodes or edges between different networks can also be connected (though with a different edge type). Multilayer networks can model the evolution of political bodies over time [149] or the different types of interactions (trophic, mutualistic, or parasitic) in ecological systems [169]. This dissertation discusses the application of network science to model recruitment and disruption in organized crime networks (Chapter 2), to study course selection at the university level

(Chapter 3), and to investigate core–periphery structure in ecological networks (Chapter 4). We have organized this dissertation so that each of the chapters can be read independently. Each chapter develops its own mathematical machinery and discusses the pertinent related work.

In Chapter 2, we model the evolution and disruption of a hierarchal organized crime network. We propose two models to analyze recruitment and disruption in a hierarchal organized crime network. For both models, we represent an evolving hierarchal structure using a rooted tree, in which the root node represents the kingpin. We alternate between a recruitment phase, in which new criminals are added, and a disruption phase, in which a single disruptor moves through the network stochastically towards the kingpin. In our first model, we study a recruitment phase simulated using a dynamical process from population biology (Galton–Watson braching [85]). We then introduce a disruptive agent that climbs the network and arrests nodes according to a stochastic process. We prove a lower bound on the probability that the network is eradicated depending on the initial conditions of the model. In our second model, we propose a general attachment mechanism to simulate recruitment. Our attachment model adds new nodes at a constant rate. Each new node has a single edge and attaches to an existing node in the network according to an evolving probability distribution. For this recruitment process, we assume that nodes without any criminal underlings (terminal nodes) are those most involved in visible illicit activity. We then define the attachment probability in terms of a criminal's distance to these nodes without underlings. Specifically, those that are closer to visible illicit activity are more likely to recruit. We then study statistics associated to large networks generated from this recruitment mechanism. We then introduce a single disruptor that moves through the network according to a self-avoiding random walk. This agent may select nodes to arrest according to certain disruption strategies. We numerically analyze the eradication probability and costs related to these disruption strategies. Although these models are far from explaining empirical criminal behavior, they introduce a template to quantify basic criminal and law enforcement incentives for future study.

In Chapter 3, we study how Mathematics students at University California–Los Angeles

(UCLA) navigate their coursework. We build several weighted, directed networks to model the varied way that hundreds of students select their Mathematics courses. We weight each directed edge according to the frequency one course was taken in an earlier term. We use these networks to aggregate course selection habits, rather than focusing on numerous possible schedules and orderings. We apply rank aggregation methods [53, 71] to uncover course sequences and investigate possible trends in course selection and hidden dependencies between courses. Rank aggregation has been used to rank athletes [37], sports teams [53], movies [71], or webpages [166]. This application applies the same techniques to extract a sequence of courses. Using this methodology, we explore how different Mathematics majors (there are seven different Mathematics majors in total at UCLA) navigate their courses and compare differences in the course selection of high– and low–performing students. Our preliminary research suggest that certain classes taken early in a student's schedule are indicative of strong performance, and in future work, we plan to investigate causal relationships between our extracted sequence and performance.

In Chapter 4, we review core–periphery structure in networks and discuss an application to ecological networks. Core–periphery structure represents a fundamental mesoscale structure. Core nodes are those well-connected to an entire network and periphery nodes are those connected to a network's core, but not with each other. However, this is not a mathematically precise definition and there has been a great deal of work to identify this structure in networks [54, 120, 167, 176, 216]. We originally became interested in quantifying core–periphery structure with total variation minimization, which enjoys great computational efficiency [34, 99, 138]. In the first part of this chapter, we relate core–periphery structure to several classical combinatorial optimization problems as a first step towards this end. Then, we analyze core–periphery in an empirical ecological network. Typically, ecologists study core structure using nestedness [16, 167]. Due to the recent advances in core–periphery detection [176], there is great interest understanding the relationship between nestedness and other core–periphery methods [119]. We briefly discuss the relationship between these two notions and related open questions. Then, we analyze the structure in an ecological data set collected from 10 sites in northeastern Argentina that encodes birds (fruigivores) and seed interactions using a particular method from [176]. Using our network analysis, our collaborators identify several species that are core within the context of the interactions of each site. They discover that certain types of birds (*mashers*) typically ignored in ecological analysis play crucial roles in these ecological networks.

CHAPTER 2

Growth and Disruption of a Hierarchical Criminal Network

This chapter explores two new models for the growth and disruption of hierarchal organized crime networks. In this work, a hierarchal crime network is modeled with a rooted tree. Each criminal is represented by a node, their criminal connections by edges, and the network's kingpin by the root. Both models follow the same general organization. We first introduce a recruitment mechanism to add nodes to the criminal network. We then measure certain network structures such as the height or degree distribution when a network grows under this recruitment. After studying this growth, we introduce a disruptive agent and a pursuit mechanism specifying how this agent can remove nodes. We then allow networks to evolve alternating between recruitment and pursuit phases. We perform a sensitivity analysis on parameters associated to this network process.

The rest of the chapter is organized as follows. In Section 2.1, we discuss related work on criminal organization and behavior. In Section 2.2, we propose a model for recruitment and disruption in a criminal network based on a classical generative processes. We provide a bound on the probability of the network's eradication for a certain class of examples. In Section 2.3, we introduce another model for recruitment and disruption and study the process numerically. For the recruitment, we propose a new attachment mechanism using graph distance. This discussion elaborates on our work in [127].

2.1 Related Models for Criminal Organization and Behavior

In recent years, researchers have applied statistical mechanics, network science, partial differential equations, and game theory to model criminal organization and behavior [39,42,65]. This interdisciplinary effort has shed light onto crime hotspots [43,185,186], community policing [19,64], gang rivalries [192] and recidivism [20]. In this work, we propose two models for the recruitment and disruption on hierarchal criminal networks.

Large organized crime networks are successful illicit business operations. To avoid government detection, these networks are extremely secretive about their operations and membership. Crime researchers refer to such secretive criminal networks as *dark networks* [209]. Dark networks are those with nodes and the edges hidden, or at least partially so, from possible disruptors [209]. Criminals balance the threat of arrest with the profits of greater criminal collaboration. In addition to organized crime networks, dark networks encompass a wide range of criminal networks including terrorist networks [209], drug trafficking networks [67], and gang networks [145]. Each class of dark network has a different power and organizational structure. For this work, we concentrate on hierarchal organized crime networks such that nodes represent criminals and edges represent their professional connections within the criminal organization.

Broadly speaking, network disruption may represent the destabilization of communication, operations, or decision processes in a network [67]. In our models and those we review below, disruption is the *permanent* removal of nodes and edges. There are other mechanisms to simulate network disruption that we do not consider. For example, network disruption may be modeled as the *temporary* removal of nodes and edges [147,148]. In other models, disruption is the *weakening* of edges of a network to minize the flow of illicit goods such as drugs [94,207].

There are three important parts of the disruption models we consider. First, a model must specify the information available to this disruptive agent. For clarity of our discussion, we assume that a single disruptive agent orchestrates all disruption. This information must specify which nodes and edges the agent is allowed to remove. We refer to this as the *disruption mechanism.* Second, the model specifies one or more *disruption strategies* that a disruptive agent follows in removing nodes and edges. Third, a model must specify a *disruption measure* to evaluate the impact of a given disruptive act. In some models, the agent uses this numerical quantity to inform their disruption strategy. Each of the models we review and the new models that we propose in Section 2.2 and Section 2.3 specify these three parts.

In [29], the authors proposed a disruption model in which the disruptor has complete information of a network's structure. The agent selects a node to remove according to the measure of network *fragmentation.* Suppose a network has n nodes and k connected components each of size s_i for $i = 1, \ldots, k$. The fragmentation f of a network is

$$f = 1 - \frac{\sum_{i=1}^{k} s_i(s_i - 1)}{n(n-1)}.$$

The fragmentation varies on a scale from 0 to 1, in which a network without any edges has $f = 1$ and a connected network has $f = 0$. Using this measure, the agent selects a node along with its incident edges to remove to maximize f for the resulting network. To effectively compute f in these different scenarios, the disruptor must have full information about a network's structure. To address this shortcoming, the models of McBride *et al.* studied disruption when only a portion of a network's structure is known to the disruptive agent [133, 134]. In their work, a disruptive agent can see all the nodes but only a portion of the edges. This agent then removes a node and its incident edges using this limited information. The agent's goal is to minimize a measure of criminal activity that is determined using the entire criminal network. The *criminal activity* of a network is given by

$$A = \sum_{j=1}^{n} c_j d_j,$$

where d_j is the *degree* of each node j and c_j are fixed positive scalars associated to each node j. The degree of a node is the number of edges connected to this node. If the full network structure is known and $c_j = 1$ for all j, then removing the node with the largest degree maximizes the decrease in A. However, the disruptor has only partial information about a network's edges–this information is determined as follows. The disruptor chooses some subset of nodes uniformly at random to monitor. The edges that are visible to the disruptor are those incident to at least one monitored criminal. In [134], the authors showed for this model that, when $c_j = 1$ for all j, a disruptor removing a node with highest monitored degree maximizes the expected decrease in A for Erdős-Rényi random graphs [75]. Erdős-Rényi graphs are a class of artificial networks that consider n nodes such that an edge between any pair of nodes occurs with probability $p \in (0, 1)$.

The above two models do not directly employ any criminal data. In [67], however, the authors reconstructed a drug trafficking network using several years of Dutch police data and designed a disruption model on top of this network. Their disruption model considers an additional categorical variable called the *role* of a criminal–a role determines a criminal's contribution to drug production and distribution. These roles include the sale of drugs at local coffee shops or the disposal of wastes during the care of illicit crops. Using these roles, Duijn *et al.* defined a new network in which each node represents a different role. This network is called the *value-chain network.* Edges between distinct roles in the value-chain network are weighted by the number of times an edge connects two criminals with the same roles in the original drug trafficking network. Duijn *et al.* studied several disruption mechanisms including the random removal of nodes or removal of all nodes whose role had the highest degree in the value-chain network. Their model also considered several different recovery mechanisms, in which, once nodes and edges are removed due to disruption, new edges are created according to these mechanisms. Duijn *et al.* evaluated the disruption mechanisms according to measures of *efficiency* and *density.* These measures were defined using the structures associated to the drug trafficking network and the value-chain network. For the several disruption strategies and recovery mechanisms they investigated, they concluded that disruption become less effective over time as each recovery resulted in greater decentralization (low density) and efficiency. In [209], Xu and Chen investigated a disruption model both on artificial networks and several well-known terrorist networks. The agent's disruption strategy is to first order the nodes from highest to lowest according to a particular node centrality and then remove some proportion of nodes with highest centrality. Xu and Chen investigated two centralities: degree and *betweenness.* Roughly speaking, the betweenness measures the proportion of shortest paths that a particular node i lies on between all nodes. We define the betweenness g_i as

$$\widetilde{g}_i = \sum_{\substack{j \neq k \\ j \neq i; k \neq i}} \frac{\sigma_{jk}(i)}{\sigma_{jk}}$$

where $\sigma_{jk}(i)$ are the total number of shortest paths between j and k that pass through i, while σ_{jk} are the total number of shortest paths from j to k. The model assumes that a disruptive agent knows the full network structure and can thus compute these node centralities to select those nodes to remove. They compared the efficacy of these two disruptions according to the size decrease of the largest connected component. Measuring this size decrease, the authors found that removing nodes with high betweenness was more effective than removing nodes with high degree on the several terrorist networks they investigated. However, the two strategies were comparable for a class of artificial networks similar to the Barabási–Albert model [14]. The model we propose will simultaneously introduce new nodes (*recruitment*) while a disruptive agent removes nodes and edges in search of a kingpin (*pursuit*). To our knowledge, this alternation between two competing processes is a new way to organize and understand criminal network disruption.

In the remainder of the chapter, we describe two growth disruption models. We focus on hierarchal crime networks, commonly present in vertically-organized criminal networks such as the Central and South American drug cartels [12, 13, 121, 131]. Both models are organized so that they alternate between a recruitment phase and disruption phase. In the recruitment phase, a recruitment mechanism specifies how new nodes enter a network. In the disruption phase, a disruption mechanism specifies how a disruptive agent moves through a network, remove nodes and can capture the kingpin. We henceforth label the disruption mechanism as the *pursuit mechanism* as the disruptors primary objective is to capture the kingpin. The two mechanisms lead to interesting dynamics and implications for criminal network eradication.

This model	Network theory
Criminal network	Rooted directed tree
Kingpin	Root
Criminal j	Node j
Direct underlings of criminal j	Children of node j
Underlings of criminal j	Subtree under node j
Criminal superior of node j	Parent of node j

Table 2.1: A table comparing the terminology used for our recruitment and disruption model and that of standard network theory.

2.2 Criminal Recruitment and Disruption Model I

In this section, we propose our first model for criminal recruitment and disruption. This section is organized as follows. In Section 2.2.1, we discuss the recruitment mechanism, which is the Galton–Watson process. We provide numerical experiments to approximate the height of such networks when the process terminates. In Section 2.2.2, we introduce the pursuit mechanism. We specify how the agent investigates criminals and pursues the kingpin. We provide a lower bound on the probability the kingpin is removed by the disruptive agent.

2.2.1 Recruitment Mechanism

Since its 1874 publication [85], the Galton–Watson process has become a powerful apparatus in population biology [62, 100] and random graph theory [7, 26, 125]. There are many important variations of this process that model social phenomena [36, 106]. In this work, we use the Galton–Watson process to model criminal recruitment.

We now discuss the classical Galton–Watson setup, though we use the terminology of criminal recruitment. All the material here is well-known and a rigorous treatment can be found in [68]. Our discussion is heuristic.

The recruitment process is a generative network model. A network evolves according to this process. Networks we consider are rooted trees, in which the root represents a network's kingpin. Nodes represent criminals and edges are the professional ties between them. We view such a network as representing a criminal hierarchy in which the orientation of edges away from the kingpin determines relative seniority. We also refer to the node's children as the criminal's direct underlings. We say the node's underlings are the subtree consisting of the node itself, the node's children, their children, and so on. We also call a node's parent their superior. We summarize this terminology and relate it to standard network theory in Table 2.1. In our model, only those recruited in the previous time step are eligible to recruit. For clarity, we often assume that leaf nodes are initially the only nodes eligible to recruit unless we state otherwise. Let the number of new criminals recruited by each eligible criminal be independent and identically distributed as a nonnegative random variable ξ. Let N^0 be the initial network. We denote the recruitment process as $\mathbf{R}(\xi, \mathrm{N}^0)$. We write $\mathbf{R}(\xi)$ when the initial network is the kingpin alone. In Figure 2.1, a network evolves according to $\mathbf{R}(\xi)$ with $\xi \sim \mathrm{Pois}(1.3)$. Each level indicates the order the nodes were added with the kingpin at the top. The yellow nodes at the bottom of the figure are those who can recruit during the next time step. Let the random variable C_t be the number of new criminals recruited at time step t. For $\mathbf{R}(\xi)$, there is only one new criminal, the kingpin, and $C_0 = 1$. Additionally, for $t > 0$, we have

$$C_t = \begin{cases} \xi_1^t + \xi_2^t + \ldots + \xi_{C_{t-1}}^t & \text{if } C_{t-1} > 0 \\ 0 & \text{if } C_{t-1} = 0, \end{cases} \tag{2.1}$$

where ξ_i^t for $1 \leq i \leq C_{t-1}$ denotes the number of criminals recruited by the ith criminal at the bottom of the network hierarchy during the time step t. All ξ_i^t are independent and identically distributed with $\xi_i^t \sim \xi$. Figure 2.1 shows the values of these random variables for the particular example. At $t = 1$, the kingpin recruits two new criminals, so $\xi_1^1 = 2$ and $C_1 = 2$. At $t = 2$, the left criminal recruits 1 new criminal into the network and the right criminal recruits 2. Therefore, $\xi_1^2 = 1$, $\xi_2^2 = 2$, and $C_2 = 3$. We say that criminal network process *terminates* if $C_t = 0$ for some $t > 0$. Let $p_k := P(\xi = k)$ and $\varphi(s) := E(s^\xi) = \sum_{k=0}^{\infty} p_k s^k$ be the probability generating function.

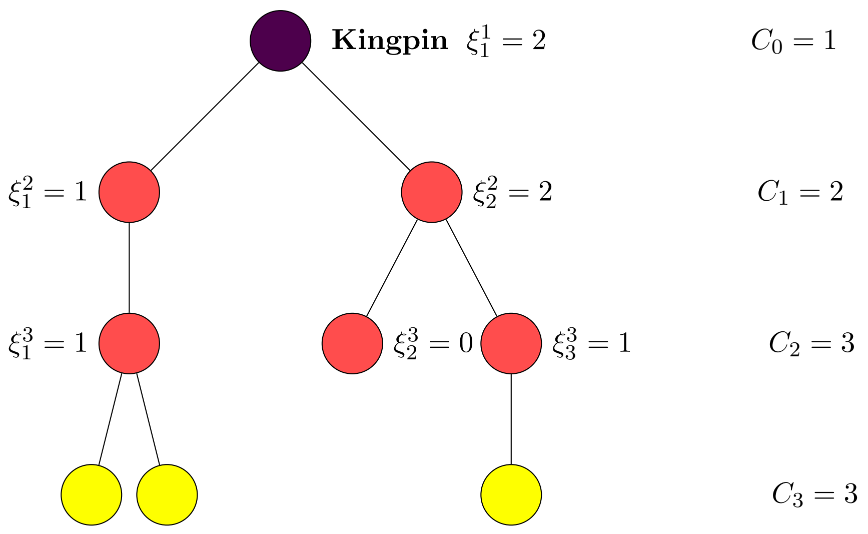

Figure 2.1: The recruitment process at $t = 3$ with $\xi \sim \text{Pois}(1.3)$. The darkest node at the top is the kingpin. The yellow nodes at the bottom are those recruited at $t = 3$. These yellow nodes are the only nodes eligible to recruit during $t = 4$. The variable ξ_i^t indicates the number of criminals recruited at time t by the ith criminal previously added during $t - 1$. We have enumerated criminals recruited at time t from left to right. The variable C_t indicates the total number of criminals added at time t.

Proposition 2.2.1. *[107]. Consider a recruitment process* $\mathbf{R}(\xi)$*. Let* r *be the probability the process terminates. The termination probability* r *is the smallest nonnegative solution to the fixed-point equation*

$$s = \varphi(s). \tag{2.2}$$

We verify that r solves the fixed-point equation (Eq. (2.2)). If the kingpin recruits k criminals, then the probability that a network terminates is r^k. From this and the law of total probability, we see that

$$r = \sum_{k=0}^{\infty} P(\xi = k) r^k = \sum_{k=0}^{\infty} p_k r^k = \varphi(r). \tag{2.3}$$

The next proposition shows that such networks grow rapidly or terminate quickly.

Proposition 2.2.2. *[68] Consider the recruitment process* $\mathbf{R}(\xi)$ *and let* C_t *be be the number of new criminals recruited at time* t*. If* $\lambda = E(\xi)$*, then* $E(C_t) = \lambda^t$*.*

A proof is found in [68]. In summary, when $\lambda > 1$, the expected growth of a network is exponential in time t. Moreover, the rate is $E(\xi)$, the expected number of criminals recruited per eligible criminal. When $\lambda < 1$, the expected number of criminals decreases exponentially, implying that termination occurs quickly.

We now use these propositions to approximate expected height of a network. The height of our network, a rooted tree, is the maximum distance from the root to another node in the network. Let h_t denote the height of a network at time t. For $\mathbf{R}(\xi)$, h_t is equal to t as long as a network has not terminated.

For the remainder of this section, consider $\mathbf{R}(\xi)$ with Poisson distributed ξ and $E(\xi) = \lambda$. The probability generating function of the Poisson distribution is $\varphi(s) = e^{\lambda(s-1)}$ [68]. From Proposotion 2.2.1, the smallest nonnegative solution to the equation $s = e^{\lambda(s-1)}$ determines termination probability r. We know that $s = 1$ is a solution to the fixed-point equation Eq. (2.2) for all possible λ. When $\lambda \leq 1$, this is the only solution by the intermediate value theorem. When $\lambda > 1$ there is a unique solution in $(0, 1)$.

For the remainder of Section 2.2.1, we consider processes of the form $\mathbf{R}(\xi)$ with $\xi \sim \text{Pois}(\lambda)$. We make the following assumptions to relate the expected height at which the recruitment process terminates and the termination probability r.

Assumption 1. *If a network reaches a large enough height m, then the recruitment process does not terminate.*

We give a heuristic justification of this assumption. By Proposition 2.2.2, the expected number C_t of recruits at time t is λ^t. Because $h_t = t$ for $\mathbf{R}(\xi)$, it follows that $E(C_t) = \lambda^{h_t}$. Moreover, the probability of termination becomes negligible as the number of criminals eligible to recruit increases because the probability that the process terminates at $t+1$ is

$$P(\xi_1^{t+1} = 0) \cdots P(\xi_{C_t}^{t+1} = 0) = P(\xi = 0)^{C_t}.$$

We see that $P(\xi = 0)^{C_t} \to 0$ as $C_t \to \infty$. We assume a stronger version of the contrapositive of Assumption 1. Specifically, termination is completely characterized by the recruitment of the kingpin.

Assumption 2. *If a network terminates, the height is 0.*

In the case when $\lambda \gg 1$, the above assumption can be justified similarly to Assumption 1. Specifically, $P(\xi = 0) \to 0$ as $\lambda \to \infty$. However, when $\lambda \approx 1$, the assumption becomes poorer as termination becomes more likely, so termination may occur at nontrivial heights. Indeed our numerics confirm this. When $\lambda \to 1^-$ (λ approaches 1 from the left), the height at termination is as large as 42, though averages never exceeded 8 when $m = 100$ for 10,000 simulations. For λ between 4 and 6, any terminating tree never grew past height 3.

We can now use these assumptions to investigate the mean height of these networks. Let m be the height for which Assumption 1 holds. Let H be the random variable denoting the height of $\mathbf{R}(\xi)$ after it terminates or reaches height m. Let the termination probability r be as in Proposition 2.2.1. If Assumptions 1 and 2 hold, then the following approximation holds

$$E(H) \approx m(1-r). \tag{2.4}$$

We can also average the heights of several networks that follow $\mathbf{R}(\xi)$ to approximate $E(H)$. We call this average the *experimental mean* $\widehat{H}$. In Figure 2.2, we show the expected height $E(H)$ approximated as $\widehat{H}$ and $m(1-r)$. Again, we note that the height for the process $\mathbf{R}(\xi)$ with $\lambda \leq 1$ may terminate with height larger than 0, contrary to Assumption 2. For $\lambda \leq 1$, the approximation $m(1-r)$ is strictly smaller than $E(H)$. In our numerics of Figure 2.2, the difference was no more than 8 in the regime $\lambda \leq 1$. The approximation gets better as λ increases past 1 as apparent from Figure 2.2. In particular, the experimental mean is within one decimal place of the approximation $m(1-r)$ for 10,000 simulations for $\lambda \in [5, 6]$ (not shown). We note that the approximation in Eq. (2.4) (when viewed as a function of λ) has a discontinuous derivative with respect to λ at $\lambda = 1$ (confirmed in Figure 2.2), which contrasts with the experimental mean $\widehat{H}$ over 10,000 simulations. We expect that $E(H)$ is smooth with respect to λ as this is approximately a mean over several simulations and a small change in λ should not impact the terminating height. However, the approximation $m(1-r)$ is proportional to the probability of the process not terminating. This must have a derivative change change at $\lambda = 1$ between those process with $r = 1$ for $\lambda < 1$ and those with $r < 1$ for $\lambda > 1$. This change in qualitative behavior at $\lambda = 1$ is referred to as a *phase-transition* or *critical-branching process* [68]. In Section 2.2.2, we introduce the pursuit mechanism. We then study the termination probability of this new process using the same assumptions we discussed in this section.

2.2.2 Pursuit Mechanism

In this section, we introduce the pursuit mechanism of this model. The agent has an opportunity between each recruitment to investigate and arrest criminals in a network. The agent's primary objective is to reach the kingpin during one of these pursuit phases. The recruitment here is identical to the mechanism associated to $\mathbf{R}(\xi, \mathrm{N}^0)$ discussed in Section 2.2.1. We assume that ξ is Poisson-distributed or constant. The initial rooted tree N^0 must have nonzero height otherwise the disruptor always captures the kingpin. The agent selects, uniformly at random, one of the nodes eligible to recruit and then investigates this node. The agent then moves up a network by one edge to the node's superior with some probabil-

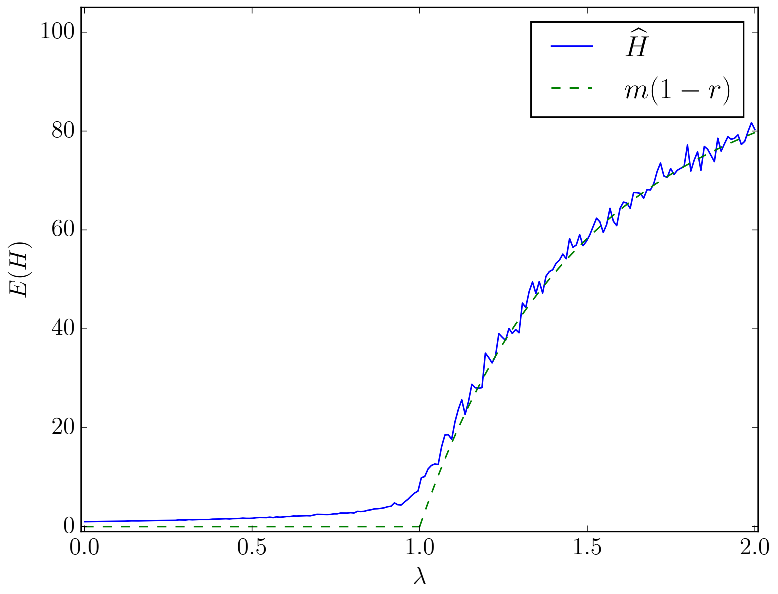

Figure 2.2: We estimate the expected height $E(H)$ in two different ways for varying λ for $\mathbf{R}(\xi)$ and ξ Poisson-distributed with mean λ. First, we estimate $E(H)$ using the experimental mean $\widehat{H}$ over 10,000 simulations. We set the height threshold $m = 250$ and stop the recruitment process when this height is reached. Alternatively, we inspect $m(1-r)$, numerically solving for r using Eq. (2.2) with $\varphi(s) = e^{\lambda(s-1)}$.

ity z. Each upward movement indicates a successful *investigation* by the agent. This might reflect successful surveillance or a criminal informing on their superior. A successful investigation permits the agent to continue their pursuit of the kingpin. When the agent reaches the kingpin, the agent captures the kingpin, and eradicates the criminal network. Once the agent fails to move upward in a network, the agent arrests the criminal under investigation and all of their underlings. The probability of a failed investigation is $1 - z$. Removal of the subtree of a network slows the growth of a network because it removes several nodes eligible to recruit. After making an arrest, the agent has to wait until the next time step, after another recruitment occurs. To reach and capture the kingpin, the agent must make consecutive investigation successfully. In certain instances, the agent effectively eradicates a network even when this agent does not reach the kingpin. This occurs when the subtree that the agent removes includes all nodes eligible to recruit. In this situation, the recruitment process does not move forward. The agent is then able to eradicate a network in some finite time. The longer the kingpin is not captured and a network grows, the harder for the agent to reach the kingpin. A network *terminates* when either the agent reaches the kingpin or removes all nodes that are eligible to recruit. We use the notation $\mathbf{P}(\xi, \mathrm{N}^0, z)$ to refer to the alternating recruitment process with the parameters ξ, N^0, and z. In Figure 2.3, we illustrate the first pursuit process of $\mathbf{P}(\xi, \mathrm{N}^0, z)$ with $\xi \sim \mathrm{Pois}(1.3)$, $z \in [0, 1]$ and N^0 as in Figure 2.1. The agent begins their pursuit at v_1, moves to v_2 and ends at v_3. Two successful investigations up the network occur with probability z^2. Their failure to move up once more results in an arrest of the node v_3 and all of their underlings. The arrested criminals are indicated in blue with a thick boundary. The network is not eradicated because there is still a yellow node eligible to recruit at the bottom right labeled l.

For the process $\mathbf{P}(\xi, \mathrm{N}^0, z)$ with $\xi = c$ and $c > 0$, we can bound the probability of termination r from below. For clarity, we will consider initial networks that are *perfect trees.* A perfect b-ary tree of height h is a tree such that all internal nodes have exactly b children and leaf nodes have distance h from the root. We call b the *branching factor* of such a network.

Proposition 2.2.3. *Let* $\mathbf{P}(\xi, \mathrm{N}^0, z)$ *be an alternating recruitment and pursuit process with*

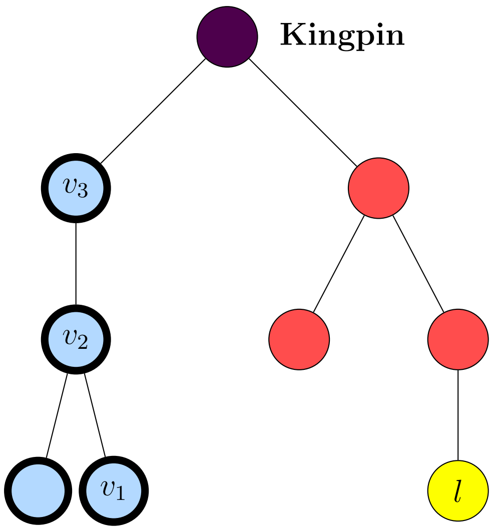

Figure 2.3: An example of a $\mathbf{P}(\xi, \mathrm{N}^0, z)$ during the first time step. Let N^0 be the network found in Figure 2.1. Let $z \in [0, 1]$ and $\xi \sim \mathrm{Pois}(1.3)$. The agent uniformly at random selects a node eligible to recruit; these are the yellow nodes in Figure 2.1. The agent begins their investigation at v_1, moves to v_2, and then ends at v_3. At v_3, the agent is unable to move upwards once more and removes the subtree below their current position. The arrested criminals are in blue with thick boundary. The yellow node at the bottom right, labeled with an l, is still able to recruit, and the network has not been terminated.

$\xi = c > 0$ and $c \in \mathbb{Z}$. Let the probability of a successful investigation be z. Let N^0 be a perfect tree of height 2 in which only leaves are eligible to recruit . If r_k denotes the probability the agent reaches the kingpin while there are still nodes eligible to recruit, then:

$$r_k = \frac{z^2}{1 + (z^2 - 1)z}.$$

In particular, the termination probability r is bounded below by r_k, that is $r \geq r_k$.

For the proof, see Section 2.2.2.1. We note that the argument in the proof can be adapted for an initial perfect tree of any height and any branching factor as long as only leaf nodes are eligible to recruit. The proof assumes the agent does not remove all criminals who are eligible to recruit, a valid method for terminating the process $\mathbf{P}(\xi, \mathrm{N}^0, z)$. When $\xi = 1$, a single arrest guarantees all criminals eligible to recruit have been removed and termination probability r is 1. However, for $\xi = c > 1$, a more rigorous treatment of this stochastic network process would be required and is beyond the scope of this work.

Proposition 2.2.2 also provides an upper bound for the expected height of a network. We use Assumptions 1 and 2 again for the process $\mathbf{P}(\xi, \mathrm{N}^0)$. Assumption 2 now holds because the termination of a network occurs precisely when the agent reaches the kingpin and then arrests all criminals. In other words, the height is 0. However, Assumption 1 may not lead to appropriate approximations of $E(H)$. As z increases, the agent has a higher probability of reaching the kingpin even for networks with large height. In particular, as the height reaches m, there is a nontrivial chance of termination. In our numerics, we observed that the maximum height over terminating networks did not reach a height of $m = 100$ for $z \in [.9, 1]$. In other words, as z gets very close to 1, networks terminate quickly, so Assumption 1 is acceptable in this regime. For $z \leq .9$, we observed in our numerics (not shown) an increase in m from 100 to 200 also increased the probability of termination, though the probabilities of termination only changed in their second decimal. We conjecture that the probabilities of termination converge for large enough m and that indeed Assumption 1 is acceptable. Precisely, if r_m is the approximation of the termination probability r when we stop a network once it reaches height m (Assumption 1), then we conjecture that $r_m \to r$ as

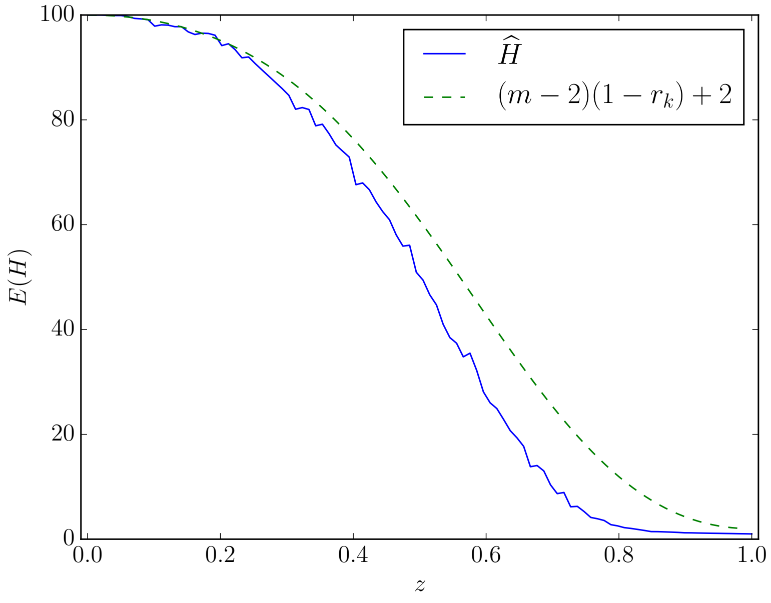

Figure 2.4: The experimental mean $\widehat{H}$ and the upper bound from Eq. (2.5) for various z. We use 10,000 simulations to compute $\widehat{H}$ and initialize a network to be a perfect binary tree of height 2. We set the height threshold m to be 250.

$m \to \infty$. We approximate the mean height and determine an upper bound:

$$E(H) \approx (1-r)(m-2) + 2 \leq (1-r_k)(m-2) \tag{2.5}$$

where we have assumed the height of N^0 is 2. In Figure 2.4, we compare the bound of Eq. (2.5) to $\widehat{H}$. Observe that the discrepancy between our bound and $\widehat{H}$ grows as z increases away from 0 and then decreases for z close to 1. We expect that as z increases there are more instances in which a network is eradicated due to the removal of all nodes eligible to recruit. However, as z approaches 1, we expect the agent to reach the kingpin while the network is still growing and $r_k \approx r$.

2.2.2.1 Proof of Proposition 2.2.2

In this section, we prove Proposition 2.2.2.

Proof of Proposition 2.2.2. Let r_k be the probability the agent reaches the kingpin while a network has criminals eligible to recruit. There are two cases to consider. The first case is when the agent reaches the kingpin at $t = 0$. This requires two successful investigations and has probability z^2. The second case is when $t > 1$. Because we assume a network still has criminals eligible to recruit, the height of this network increases by 1. Reaching the kingpin now requires an extra successful investigation and the probability is zr_k. By the law of total probability, $r_k = z^2 + (1 - z^2)zr_k$. Solving this equation for r_k determines the bound. As noted in the hypothesis regarding the existence of criminals eligible to recruit, r_k does not consider termination when the agent's arrests removes all criminals eligible to recruit. $\square$

2.2.3 Conclusions from Model

In this section, we introduced a model for the recruitment and disruption of a hierarchal organized crime network. The recruitment mechanism adapts a well-known tree model from population biology known as the Galton–Watson process [85]. The disruption mechanism introduces an agent that removes nodes from a network after each recruitment. The agent moves up through a network beginning at those nodes eligible to recruit. Each movement upwards is a successful investigation. When the investigations fail and the agent does not move upwards, the agent arrests the criminal under investigation and all of their underlings. If the agent reaches the kingpin, the entire process terminates. The model alternates between these recruitment and pursuit phases.

We briefly explored the disruption process numerically and theoretically. We measured the likelihood an agent terminates the network process (i.e. reaches the kingpin) and the expected height of such networks. We also related these quantities to model's parameters and initial conditions. To do so, we recalled a fixed-point equation (Eq. (2.2)) to determine the termination probability for the Galton–Watson process. Using this formula, we approximate the expected height of networks that grow according to $\xi \sim \text{Pois}(\lambda)$ and do not grow past some fixed height m. In Figure 2.2, we showed numerically that our approximation is reasonable comparing this approximation to the experimental mean $\widehat{H}$. We observed some discrepancies in our approximation, particularly for λ near 1. In this regime, the expected height $E(H)$ has smooth derivative, whereas our approximation does not. However, the method for obtaining the approximation exploits the recursive nature of the recruitment process and can be adapted for the full disruption model. Using the same setup, we investigate the termination probability and expected height of networks for the full disruption model. We provide a lower bound on the probability of termination for a special class of networks in Proposition 2.2.2. We again numerically approximate the expected height of networks using this proposition and investigate the bound for various $z \in [0, 1]$. We did not give precise analytic formulas for the termination probabilities nor the heights of terminating networks, even in the special case $\xi = c > 0$. These questions we hope to answer in future work, though we will require a more rigorous framework.

Unfortunately, this model in its current form is far from explaining the complex formation and disruption of real-world criminal networks. Ultimately, we hope this work provides researchers with new tools for modeling the recruitment and disruption on a criminal network.

2.3 Criminal Recruitment and Disruption Model II

In this section, we describe a different model for recruitment and disruption on an organized crime network [127]. Our recruitment mechanism introduces a model for attachment. We then propose a disruptive mechanism and examine various disruption strategies for a disruptive agent. The rest of the section is outlined as follows. We first provide a general overview in Section 2.3.1 of the recruitment and pursuit model. We then elaborate on the specific construction of the recruitment mechanism and its numerics in Section 2.3.2. In Section 2.3.3, we propose a disruptive mechanism and various disruption strategies for the agent to follow. We propose measures to study the effectiveness of these disruption and briefly explore them numerically. Finally, in Section 2.3.4, we evaluate the disruption strategies and discuss future work.

2.3.1 Model Overview and Related Network Processes

In this section, we overview the recruitment and pursuit mechanisms of this model. Our model alternates between two phases: the recruitment of criminals into the network and the subsequent disruption by law enforcement. We define the processes precisely in Section 2.3.2 after providing this high level overview of our model and review of related processes on networks.

To recruit new criminals into a network, we propose a new attachment mechanism, a schematic of which we show in Figure 2.5. An attachment model refers to a diverse class of generative network models in which nodes are added to a network and attach to existing nodes according to an evolving probability distribution [154]. An attachment model begins as an initial network at $t = 0$ and then new nodes are added during each subsequent discrete time step t ($t = 1, 2, \ldots$). Each incoming node has a positive number of edges and each edge attaches to an existing node according to a probability distribution that evolves with t. The number of incoming nodes and the number of edges per incoming node can change from time step to time step [58, 154]. Such attachment models considers either directed networks [58] or undirected networks [14]. The evolving probability distribution is determined according to a non-negative quantity called the *attachment weight* $w(j;t)$ that depends on the existing node j and the time step t. These attachment weights are often a function of node centrality (e.g. degree). If an incoming node i has m edges and each edge attaches to the network independently, then each edge attaches to an existing node j at time t with probability:

$$p(i, j; t) = \frac{w(j;t)}{\sum_{i' \in \mathcal{V}(t)} w(i';t)},$$

where $\mathcal{V}(t)$ are the nodes in the network at time t. Certain models specify that edges from an incoming node are not permitted to the same node in the network [154]. For such models, each edge's probability of attachment is no longer independent and the probability $p(i, j; t)$ that an incoming node i attaches to node j for a particular edge changes as each of i's edges attach to the network. Some attachment models also introduce mechanisms for the stochastic removal and addition of nodes and edges [47, 50, 142]. In [47, 50], nodes follow a normal attachment mechanism with probability α_1, delete nodes uniformly at random with probability α_2, delete edges uniformly at random with probability α_3, and add edges between existing nodes are added with probability α_4. In addition to the constraint that $\alpha_1+\alpha_2+\alpha_3+\alpha_4 = 1$, the parameters α_1, α_2, α_3, and α_4 are chosen to ensure that the expected number of nodes and edges in a network at time t are both monotonically increasing (i.e. the expected size of the network grows over time, which is normally the case for attachment models).

We presented a definition of attachment weight is non-standard, and we now relate our notion of attachment weight to standard attachment model constructions. The most studied attachment models are those in which the degree determines the attachment weight $w(j;t)$. That is,

$$w(j;t) = \eta_j f(d_j^t),$$

where $f : \mathbb{R}_{\geq 0} \to \mathbb{R}_{\geq 0}$, η_j is a non-negative parameter depending on the node j, and d_j^t is the degree of node j at time t. When $\eta_j = 1$, f is known as the *attachment kernel* [101,113]. When $f(d_j^t) = d_j^t$ and η_j is some positive parameter depending on each j, then η_j is known as the *fitness* of a node [24]. When f is monotonically increasing, such models are known as *preferential attachment models* [14, 21, 58]. Preferential attachment models capture the heuristic that the "rich get richer" [14] or "cumulative advantage" [187] with respect to degree, meaning that nodes with the greatest degree are the most likely to increase their degree in future time steps. Udny Yule used a stochastic mechanism, which has since been shown to be equivalent to a particular preferential attachment model [21], to describe the distribution of species in genera over time [215]. Herbert Simon generalized this model to discuss the distribution of words in prose and the distribution of wealth [187]. More generally, the stochastic process known as the Polya urn model is equivalent to a large class of preferential attachment models [21, 46]. Although the preferential attachment models of Yule, Simon, and Pólya do not explicitly consider networks, the analysis has proven crucial for the mathematical investigation of preferential attachment [21,68]. Derek de Solla Price used a preferential attachment model to describe the directed network of academic citations [58]. Barabási and Albert proposed an undirected preferential attachment model to study the growth of the World Wide Web (WWW) [14, 102]. Although the Barabási–Albert model renewed interest in the preferential attachment models, there is significant doubt as to their claim that preferential attachment describes the creation of webpages and links on the WWW [2, 205].

An important feature of networks that grow according to preferential attachment is their *degree distributions*. Let $P(d;t)$ be the probability a node chosen uniformly at random on a network has degree d. We refer to $P(d;t)$ as the *degree distribution at time* t. Because we are interested in the degree distribution for large t, we consider the formal distribution as $t \to \infty$. Assuming this distribution is well defined [68], we denote this limiting distribution as $P(d;t \to \infty)$ or $P_\infty(d)$. To investigate this limiting distribution, one usually measures the degree distribution for sufficiently large t. For a wide class of attachment models, Chayes *et al.* showed that as $t \to \infty$, the degree distribution $P_\infty(d) \approx Cd^{-\alpha}$ for suitable positive constants C and α. The degree distributions of the form $Cd^{-\alpha}$ obey a *power law*. More generally, the degree distributions of attachment models are *heavy-tailed* if

$$\lim_{d\to\infty} \frac{e^{-d}}{P_\infty(d)} = 0.$$

In [14], a large subset of the WWW was measured to have degree distribution approximately Cd^{-3}. Measuring a heavy tail distribution on a network does not imply that a preferential attachment mechanism accurately describes the method of attachment [2, 205]. For example, for certain large subsets of the WWW, there was no correlation between the number of links on a webpage and the time it was created as the Barabási–Albert preferential attachment model suggests [2]. Additionally, measuring the link structure of webpages is quite complicated, and can erroneously detect high degree nodes [205]. There are several more statistical challenges to validating a power-law distribution on real-world degree distributions [88, 122, 194] In light of these challenges, it has been reported that scientific citation networks is governed by some preferential attachment mechanism [153]. Generally speaking, validating any attachment mechanism (preferential or otherwise) requires careful statistical analysis beyond the simple measurement of a network's degree distribution.

There are some attachment models that consider quantities other than degree. For example, in [25, 40], each node has an associated feature vector $\mathbf{x}_i$ of dimension N encoding some node metadata. In [25], the attachment weight depends only on these feature vectors and is independent of the time step t. The attachment weight was defined as

$$w(i,j) = \sum_{k=1}^{N} \frac{\omega_k}{1 + \nu_k \cdot d_k(\mathbf{x}_i^k, \mathbf{x}_j^k)^{\zeta_k}}, \tag{2.6}$$

where ω_k, ν_k and ζ_k are positive constants; $\mathbf{x}_i^k$ aren $\mathbf{x}_j^k$ are the kth feature of $\mathbf{x}_i$ and $\mathbf{x}_j$ respectively; $d_k(\cdot,\cdot)$ is a distance function in which two nodes with relatively high similarity with respect to their features $\mathbf{x}_i^k$ and $\mathbf{x}_j^k$ have relatively small distance with respect to d_k. The authors claimed that their generative model shared similar statistics with the Pretty Good Privacy (PGP) network such as the distribution of the *local clustering coefficient.* The local clustering coefficient of a node j is the proportion of pairs of nodes adjacent to j that are themselves connected. If a node j has n_j neighbors, then the local clustering coefficient c_j of a node j is

$$c_j = \frac{|\{e_{st} \mid s \text{ and } t \text{ are adjacent to } j\}|}{\binom{n_j}{2}},$$

where e_{st} denotes the edge between nodes s and t. The authors then studied the mean of the local clustering coefficient of nodes with degree k both in their attachment model as well as the PGP network. Because the similarity considered in [25] is transitive (two nodes that are similar to a third node are similar to each other), the attachment model produces networks with high local clustering coefficient relative to those generative models in which edges are assigned uniformly at random such as the Erdős-Rényi model [75, 154]. In particular, the local clustering coefficient can be used to differentiate this generative process from the Erdős-Rényi model [154]. However, the several parameters and inputs such as $\mathbf{x}_i$, d_k, ω_k, ζ_k, and ν_k makes validating this generative mechanism in real-world networks extraordinarily challenging.

We now propose a new attachment mechanism for our recruitment phase. In our model, incoming nodes have attachment weight negatively correlated with the distance from the leaf set. This distance between a criminal and the leaf set represents the criminals distance to visible illicit activity. We refer to this visible illicit activity as *street activity.* Therefore, our model specifies that leaf nodes are the closest to street activity with distance 0. We refer to leaf nodes as *street criminals*. The closer a criminal is to visible street activity the more vulnerable they are to detection and arrest [1]. Indeed, in organized crime networks, senior criminals maintain a buffer between themselves and any direct illicit activity [51, 109, 143]. Our model introduces new nodes at constant rate and they attach to one existing node of the network preserving the hierarchal structure. The attachment weights reflect that street criminals have the greatest visibility to new recruits due to their visible street activity [61]. The constant rate mechanism assumes that a criminal network can continue to recruit from a large pool of criminals. For large Central and South American drug cartels, this is often the case as their substantial revenue streams provide incentive to poor populations to join their ranks [66, 121]. In fact, such cartels can even lure middle-class, highly-trained soldiers and military personal away from their government jobs due to the promise of higher pay and a more lavish lifestyle [66]. We provide a precise mathematical formulation of this recruitment in Section 2.3.2.

Now we turn to the pursuit phase of the model. Our pursuit mechanism simulates an agent's whose primary target is the kingpin of a criminal network. When a criminal enterprise is large, arresting low-level criminals may not be effective as such criminals are usually the most easily replaced [1, 12]. Law enforcement thus pursue the so-called "kingpin strategy" targeting the highest ranking criminals for arrest [108]. For instance, the Colombian government in collaboration with the Drug Enforcement Administration (DEA) successfully employed this strategy against the Medellín cartel targeting Pablo Escobar and his inner circle [108]. The Mexican government is pursuing the same strategy in its current war on drugs [165], although with mixed results.

In a pursuit phase, the agent begins their pursuit from visible street criminals, progressively moving to more nested criminals. Each node encountered by law enforcement represents an investigation, and their path is determined using a self-avoiding random walk. Because the agent's information about the criminal network is incomplete or inaccurate, their movements may appear random to a neutral observer with perfect information. At any point during the pursuit, the criminal under investigation can be arrested with all of the

This model	Network theory
$\mathcal{C}(t)$: Criminals (including kingpin) at time t	Nodes (including root) at time t
$\mathcal{S}(t)$: Set of criminals without underlings (street criminals) at time t	Set of leaves at time t, (nodes of out-degree 0)
$\mathcal{C}(t)\backslash\mathcal{S}(t)$: Set of criminals with at least one underling at time t	Internal nodes (nodes with out-degree at least 1) at time t

Table 2.2: A table comparing the terminology used in this paper and that of standard network theory.

node's associated underlings. Although we refer to node removal as "arrest", the removal can also represent exile, extradition, or assassination [31, 196]. Because the overall structure of a network is unknown to the agent, the random walk may also lead to another street criminal with no further investigation possible. In this case, the pursuit is terminated and deemed unsuccessful. If instead the kingpin is reached, the kingpin is captured and the criminal network is eradicated. We remark this fundamental assumption that kingpin capture is equivalent to the network's eradication underlying this disruption mechanism is invalid for decentralized networks such as terrorist networks and gang networks [114, 144].

We employ the same criminal terminology for network structures as in Section 2.2. A summary of this terminology is found in Table 2.1. In Table 2.2, we list additional terminology we require along with the corresponding network theory terms. As mentioned before, our criminal network is a tree with criminals as nodes and the kingpin as the root. The edges are directed away from the kingpin, from superior to underling in the power structure. The street criminals are leaf nodes while the nodes above the leaves are internal nodes. Internal nodes are those nodes that are not leaf nodes, or equivalently, those nodes that have out-degree at least 1. We use the criminal terminology interchangeably with those from network science.

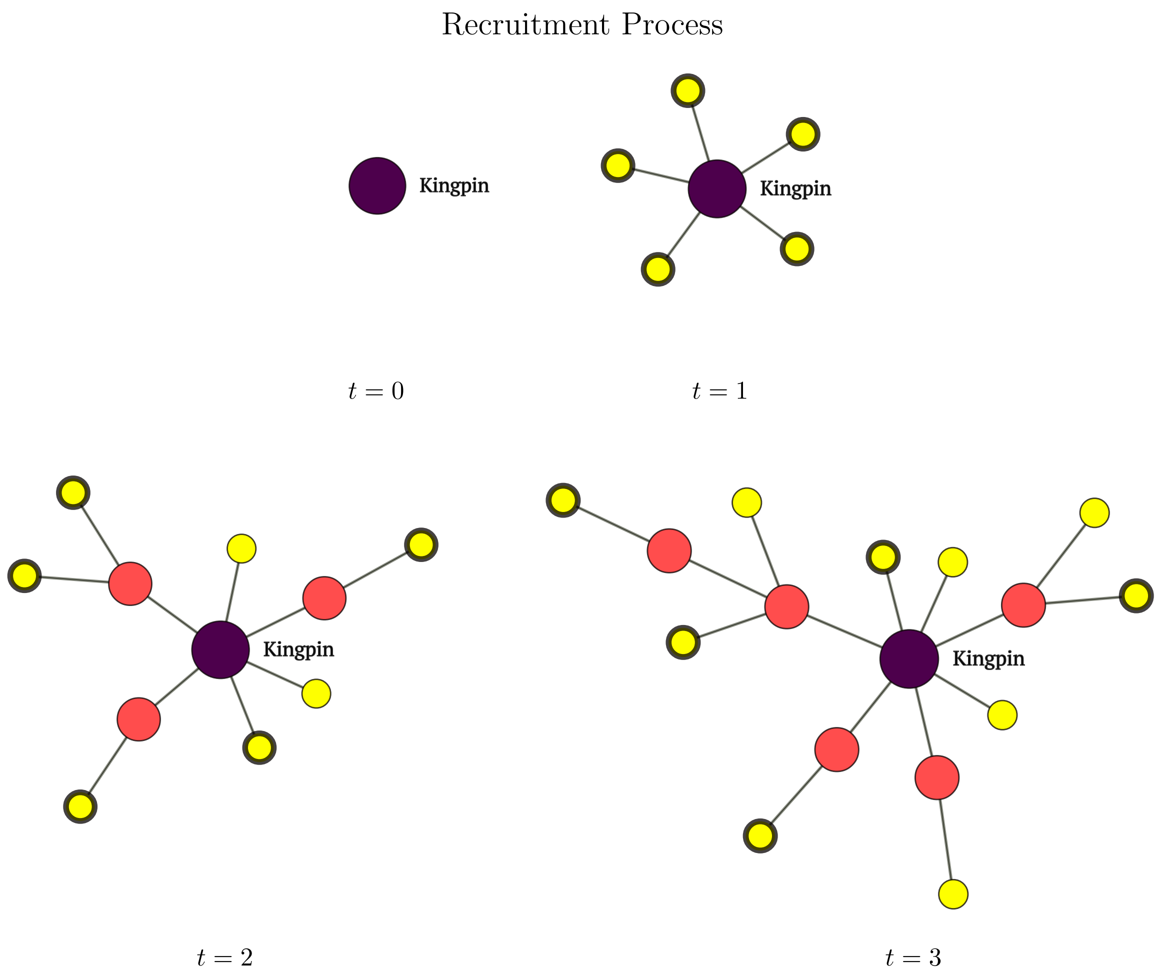

Figure 2.5: A simulated recruitment process for $t = 0, 1, 2, 3$. The network starts with a single criminal (the kingpin) and then evolves according to the proposed attachment mechanism. Here the number of new criminals introduced into the network is given by the recruitment index $k = 5$. The leaf nodes (light yellow) represent criminals without underlings. In our model, these leaf nodes are called street criminals. Of these, the nodes with the darker boundary are those freshly recruited at a given time step. For example, the number of street criminals when $t = 3$ is 8, of which 5 are new recruits.

2.3.2 Recruitment Mechanism

We now precisely define the recruitment process. We start with an initial tree. We often assume the network begins as a the kingpin alone for clarity. The network recursively evolves so that with each new time step, new criminals and edges are added to the existing network. Let $\mathcal{C}(t)$ denote the set of criminals at time t. Let $\mathcal{S}(t)$ be the set of leaf nodes, also referred to as the set of street criminals. Let $\text{dist}(j;t)$ denote the graph distance separating node j from $\mathcal{S}(t)$ at time t. Recall the distance between a node j and a leaf node is the shortest path between them. The distance from a node j to the set $\mathcal{S}(t)$ is the minimum of all such distances. From t to $t+1$, we add k new recruits to the network according to an attachment mechanism. Every node j is assigned a *attachment weights* $w(j;t)$. We define $w(j;t)$ to be

$$w(j;t) = \frac{1}{\text{dist}(j;t) + a}, \tag{2.7}$$

where a is a positive parameter. Roughly speaking, $w(j;t)$ determines the proximity of criminal j to visible street activity on a scale from 0 to 1. If node j is a street criminal and $a = 1$, then $\text{dist}(j;t) = 0$ and $w(j;t) = 1/a = 1$, the maximum possible value. However, as the network keeps growing, internal nodes j that have been in the network for large t can become progressively more detached from street activity with $d(j;t)$ becoming large for such nodes j. Before adding criminals, we first evaluate $w(j;t)$ for all existing nodes in the network. We then introduce k new criminals and link them to a single existing criminals with probability proportional to $w(j;t)$. Specifically, this probability $p(i,j;t)$ that an incoming node i attaches to node j is

$$p(i,j;t) = \frac{w(j;t)}{\sum_{i' \in \mathcal{C}(t)} w(i';t)}. \tag{2.8}$$

Note that each existing node can recruit multiple nodes within a single time step, though each new recruit is connected to a single node. We call k the *recruitment index*. In Figure 2.6 we show a particular network configuration, including the explicit weights $w(j;t)$ assigned to each criminal j. Note that as the weight parameter a approaches ∞, the attachment weight $w(j;t)$ becomes identical for all nodes j. In this instance, the recruitment process reduces to the recursive tree model [126, 189]. If the parameter approaches 0, then recruitment is

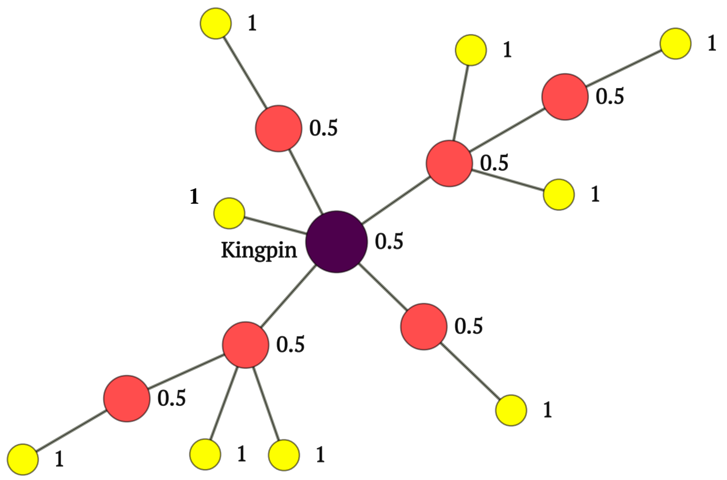

Figure 2.6: The criminal network at $t = 3$ with the values of $w(j;t)$ shown. Here, the recruitment index $k = 5$ and the initial configuration consists of a single kingpin. All criminals j in $\mathcal{S}(t)$ have attachment weight $w(j;t) = 1$.

limited to street criminals and the model reduces to the model from Section 2.2 with $\xi = k$. We set $a = 1$ so that the model balances the two different attachment weights that govern these other models.

2.3.2.1 Out-degree Distribution

We numerically examine the statistics associated network properties associated with the recruitment process. We first study the degree distribution (specifically, the out-degree). The out-degree represents number of direct underlings of a criminal. For example, in Figure 2.6 the out-degree of the kingpin is 5. Of these five, the upper left two have out-degree 1 and the other three have out-degree 2. Let $P(d;t)$ equal the probability a node selected uniformly at random has out-degree d at time t. At the beginning of network growth, when the only criminal present is the kingpin, $P(0;0) = 1$. As the number n of nodes increases, we conjecture that for $d \geq 1$, $P(d;t \to \infty)$ can be approximated as

$$P_\infty(d) \equiv P(d;t \to \infty) = c_1 e^{-c_2 d}, \tag{2.9}$$

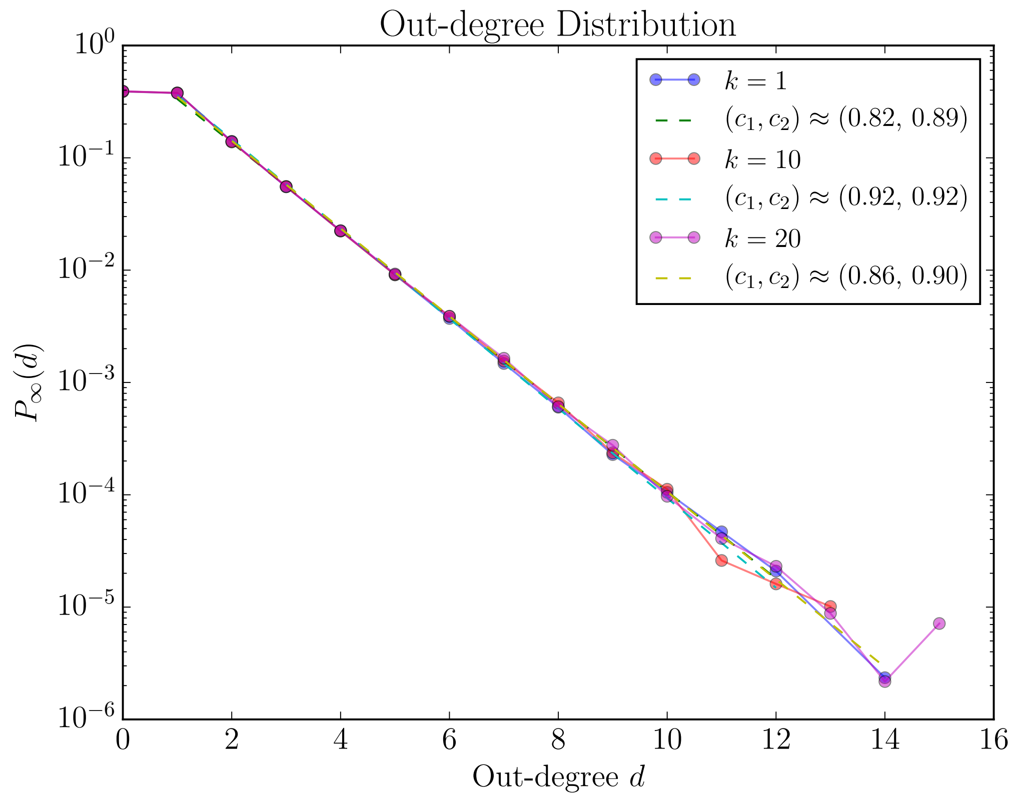

Figure 2.7: The out-degree distribution $P_\infty(d)$ of nodes on a criminal network determined from numerical simulations for $t \to \infty$. The three curves correspond to recruitment indices $k = 1, 10, 20$. We terminate a simulation when the total number of criminals reaches or exceeds 5×10^3. Each curve for $P_\infty(d)$ represents 100 simulations. The tail of the degree distribution is noisier as high degree nodes are rarer than low degree nodes. As discussed in the text, we fit the distribution to a decaying exponential distribution. The numerics indicate that $P_\infty(d = 0) \approx 0.39$ for all the values of k we considered.

Parameter	Description
t	Time
k	Recruitment index: number of new criminals added to the network at each time step
a	attachment weight parameter in $w(j;t)$; often set to 1
n	Number of criminals on network at time t; when network begins as kingpin alone obeys $n = kt + 1$

Table 2.3: The parameters of the recruitment mechanism.

for constants c_1, c_2. In Figure 2.7, we plot the conjectured distribution of Eq. (2.9) versus the degree distribution averaged over 100 different network realizations. In these computations, we grow a network until there are 5×10^3 total criminals. We expect that as $t \to \infty$ most of the new criminals connect to existing street criminals, resulting in $P_\infty(d = 0) \approx P_\infty(d = 1)$. Using this approximation and Eq. (2.9) for $d \geq 1$, we expect $c_1, c_2, P_\infty(d = 0)$ to be related by

$$c_1 \approx [1 - P_\infty(d = 0)](e^{c_2} - 1). \tag{2.10}$$

We observe that when c_1 and c_2 are numerically fit with Eq. (2.9), then the relationship between c_1 and c_2 specified with Eq. (2.10) is valid to 1 decimal place. In Figure 2.7, we vary the recruitment index k between 1 and 20 and do not notice substantial variations in c_1 and c_2. We also examine networks with 500 criminals (not shown) and find that their degree distributions are well approximated with the exponential form of Eq. (2.9). These results suggest that, as $t \to \infty$, the degree distributions converge $P(d;t) \to P_\infty(d)$ and this distribution $P_\infty(d)$ is independent of k. In Section 2.3.2.3, we give further evidence that $P_\infty(d = 0)$ is independent of k. Using this degree distribution, we see that the expected out-degree d is given by

$$\langle d \rangle \approx c_1 \sum_{d=1}^{\infty} d e^{-c_2 d} = \frac{1 - P_\infty(d = 0)}{1 - e^{-c_2}} \approx 1. \tag{2.11}$$

For any large rooted tree, the mean out-degree approaches 1 because

$$\langle d \rangle = \frac{|E|}{|V|} = \frac{n-1}{n} \to 1$$

as $n \to \infty$, where n is the number of nodes and we recall that a tree has precisely $n-1$ edges. As in other attachment models in which all incoming nodes have the same number of edges [68], we expect as $t \to \infty$ that the mean out-degree $\langle d \rangle$ to approach the number of new edges per incoming node, which in our model is 1.

2.3.2.2 Criminal Density and Position

We now focus on the distribution of distances from the kingpin–the distances from the root node. In Figure 2.8, we stop the process at a fixed time t, and then we measure the distribution $\rho(y)$, which is the fraction of criminals at a distance y from the kingpin. We fit $\rho(y)$ to a shifted gamma probability density [21]

$$\rho_{\alpha,\beta,s}(y) = \frac{\beta^{\alpha}}{\Gamma(\alpha)}(y-s)^{\alpha-1}e^{-\beta(y-s)} \tag{2.12}$$

for $y > s$ and $\alpha > 1$. Our choice is motivated by the fact that this distribution is supported on the positive y-axis. Using the fitted values of $\rho_{\alpha,\beta,s}(y)$ the probability that a criminal is a distance y from the kingpin can be estimated by

$$\int_{s}^{y} \rho_{\alpha,\beta,s}(y')\, dy'. \tag{2.13}$$

Figure 2.8 shows that as t increases, the expected distance from the kingpin increases. Additionally, examining different initial conditions, we see that the shifted gamma probability density appears to be a good approximation for $\rho(y)$. We expect the parameters associated to the distribution to depend on k, the initial configuration of the network, and the time t which $\rho(y)$ is measured.

2.3.2.3 Street Criminals

We now study the population of street criminals over time. Recall the street criminals are the leaf nodes of a network. By our construction of the recruitment process, street criminals

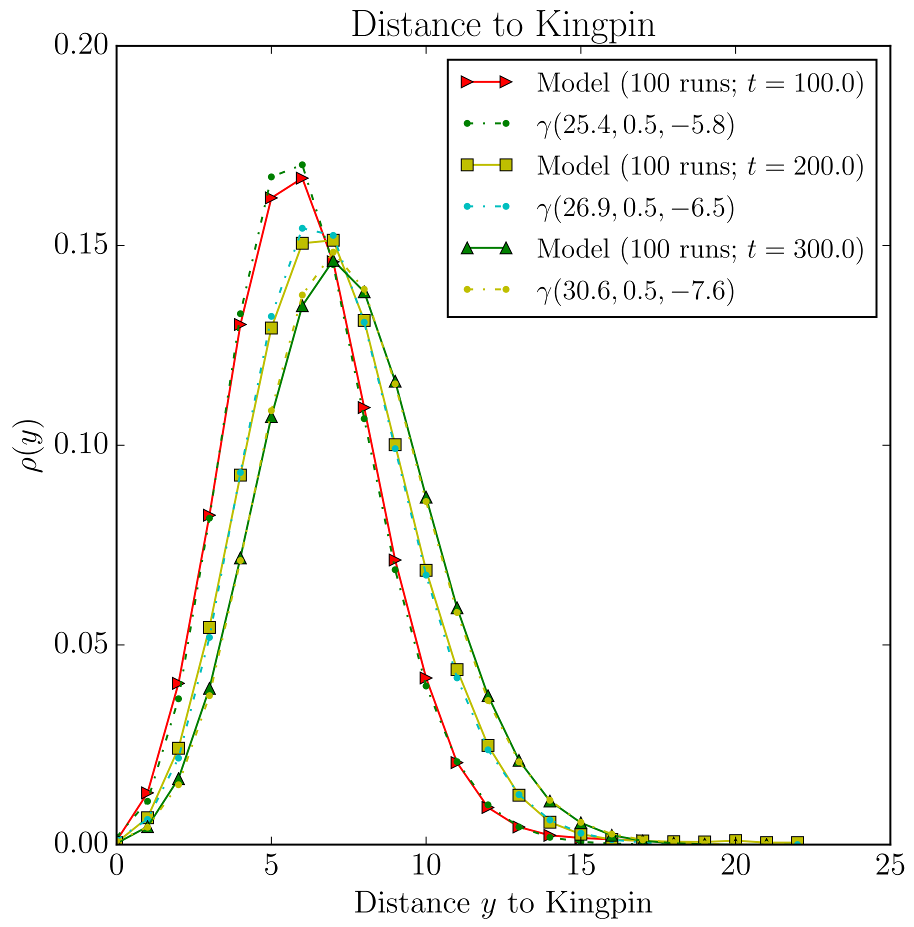

Figure 2.8: We show the distribution of distances from the kingpin. These distributions are the average over 100 runs, stopping each simulation at $t = 100$, 200, or 300. We set the recruitment index $k = 10$ and the initial configuration to be the kingpin alone. We then fit the measured distributions using a shifted gamma density $\rho_{\alpha,\beta,s}(y)$ (Eq. (2.12)). We label this fit γ-distribution as $\gamma(\alpha, \beta, s)$.

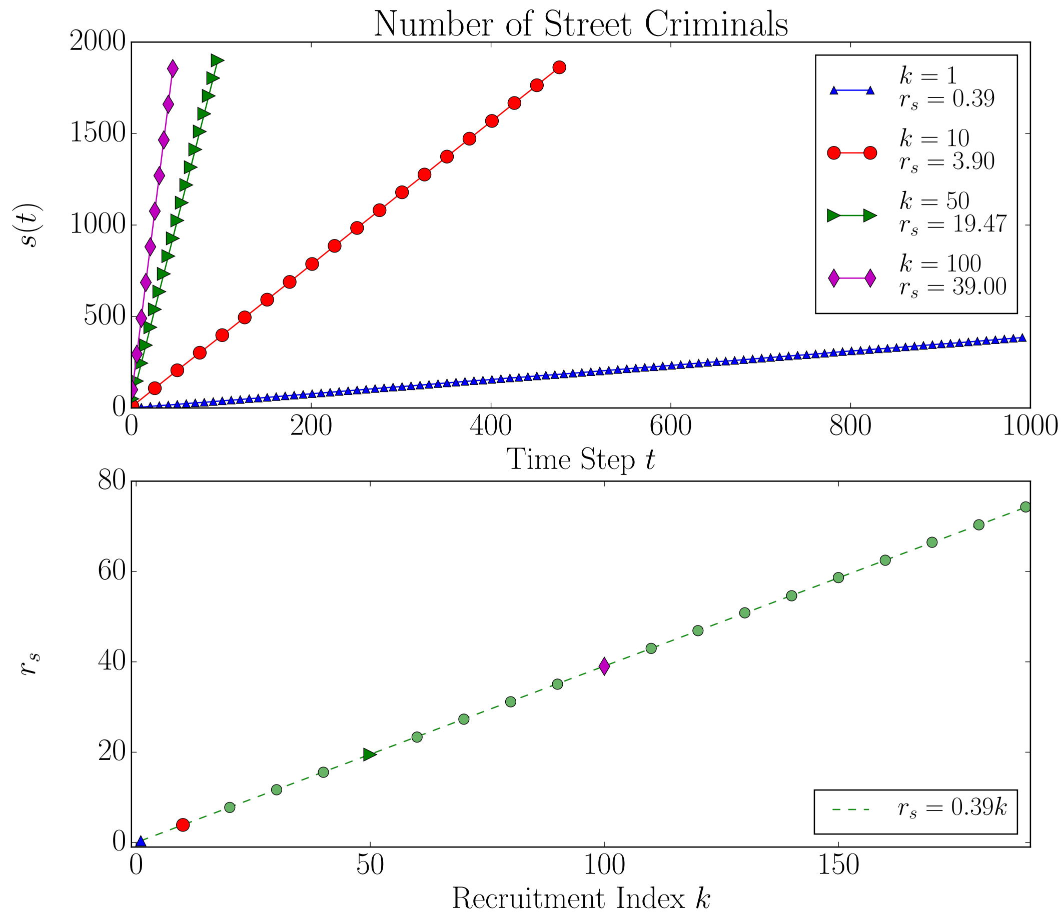

Figure 2.9: (Top) The number $s(t)$ of street criminals as a function of time t for recruitment rates $k = 10, 50, 100$. In each simulation, we terminate the recruitment process when the total number of criminals exceeded 5×10^3. Each data point is the average of 250 simulations. We fit the data to $s(t) = r_s t + 1$ and expect $r_s \approx P_\infty(d = 0)k$, where $P_\infty(d = 0) \approx 0.39$. This scaling is confirmed with the fit values of r_s in the legend. (Bottom) The slope values r_s as a function of k with the r_s values from the top display shown in dark symbols with corresponding shapes. We then fit the data with a line as indicated in the bottom legend, providing evidence of our conjecture $r_s \approx P_\infty(d = 0)k$.

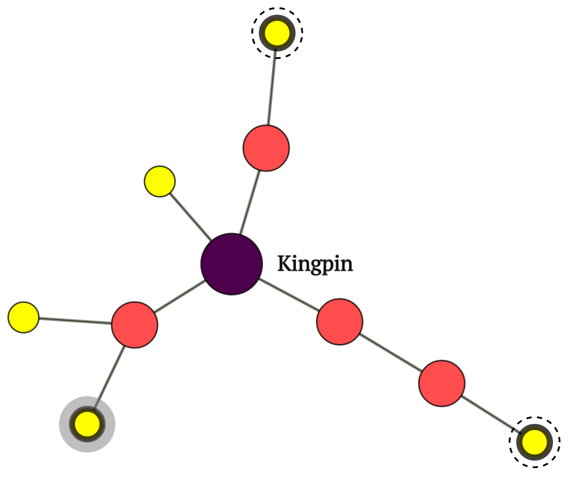

Figure 2.10: Schematic of the addition of new nodes from time t to time $t+1$. Here, the recruitment index k is 3. We depict the leaf nodes in yellow and those nodes added from t to $t+1$ with thick boundary. We indicate the attachment of a new leaf node to an internal node with a solid gray halo seen on the lower left hand side of the image. We also indicate the attachment of new leaf nodes to previously leaf nodes with a the dashed ring. In this recruitment phase, the total number of street criminals at time $t+1$ increase by 1 from time t. In other words, this recruitment phase dictates $s(t+1) = s(t)+1$.

are those most likely to recruit new members into an organization. Let $s(t)$ be the number of street criminals in a network at time t. Because a network grows linearly in time t, we might expect $s(t)$ to increase linearly as well. Recall from our numerics in Section 2.3.2.1, we found that $P_\infty(d=0) \approx 0.39$ for large t. This also implies that leaves grow linearly in t because for fixed k we have

$$s(t) \approx P_\infty(d=0)n = P_\infty(d=0)(kt+1),$$

when the initial configuration of the network is the kingpin alone. In Figure 2.9, we plot $s(t)$ and fit the data to a linear form $s(t) = r_s t + 1$. Note we enforce $s(0) = 1$ as all of our simulations start as a single node (i.e. the kingpin). Indeed, the fit slope r_s satisfies $r_s \approx P_\infty(d=0)k$ as verified in the lower panel of Figure 2.9.

Recall the attachment weight that we define in Eq. (2.7). We now relate the total attachment weight for all nodes in a network at time t to $s(t)$. We first write an iterative equation for $s(t)$ [68, 154]. At time t, the likelihood of increasing the total number of street criminals to the network is approximately the probability that an internal node recruits. We observe that the number of leaf nodes does not change if a leaf node recruits a single new node. However, if a leaf node recruits multiple new nodes into the network, then the total number of leaf nodes increases. We assume for large networks that each street criminal recruits *at most one* new criminal. We justify this assumption as follows. If we assume that each of the k incoming nodes attach to one of the n existing nodes uniformly at random and $k \ll n$, then the probability that no two nodes attach to the same existing node approaches 1 because

$$\lim_{n\to\infty} \frac{n!}{(n-k)!} \cdot \frac{1}{n^k} = 1.$$

If we condition that the k new nodes each connect to leaf nodes, the same argument implies that, as long as $k \ll s(t)$, the probability that no two new nodes attach the same leaf node approaches 1 as well. Indeed, we have found the leaf nodes grows linearly in time, and therefore, for large enough t, we must have $k \ll s(t)$ and the assumption should be reasonable. With this assumption, we conclude the only observed increase to $s(t)$ occurs when internal nodes recruit. We illustrate how $s(t)$ increases for $k = 3$ in Figure 2.10. First, we compute the total attachment weight of internal nodes as the difference between the total attachment weight and the attachment weight of leaf nodes; explicitly, this is

$$\sum_{j\in C(t)\setminus\mathcal{S}(t)} w(j;t) = \sum_{j\in\mathcal{C}(t)} w(j;t) - s(t). \tag{2.14}$$

In Eq. (2.14) above, we use that the attachment weight of leaf nodes are 1 implying that the total attachment weight of all leaf nodes is $s(t)$. The probability of adding a criminal to an internal node can be found with Eq. (2.14) after it is normalized with respect to the total attachment weight $\sum_{j\in\mathcal{C}(t)} w(j;t)$. We now write our iterative equation for $s(t)$ as

$$s(t+1) \approx s(t) + \frac{\sum_{j\in\mathcal{C}(t)} w(j;t) - s(t)}{\sum_{j\in\mathcal{C}(t)} w(j;t)} k. \tag{2.15}$$

We use the approximation in Eq. (2.15) to determine the attachment weight of the entire tree $\sum_{j\in\mathcal{C}(t)} w(j;t)$ in terms of the constant $P_\infty(d = 0)$. To do so, we assume that the total attachment weight scales linearly when t is large which is confirmed by the numerics displayed in Figure 2.11. Let $\mathcal{W}$ be the constant such that $\sum_{j\in\mathcal{C}(t)} w(j;t) \approx \mathcal{W}t$ for large t. We now substitute that $s(t) \approx r_s t$ into Eq. (2.15) and obtain

$$r_s \approx \frac{\mathcal{W} - r_s}{\mathcal{W}} k. \tag{2.16}$$

Now, Eq. (2.16) yeilds

$$\mathcal{W} \approx \frac{k r_s}{k - r_s} \tag{2.17}$$

$$\approx \frac{k P_\infty(d=0)}{1 - P_\infty(d=0)}, \tag{2.18}$$

where the the approximation in Eq. (2.18) follows from $r_s \approx kP_\infty(d=0)$. In Figure 2.11 we plot the total attachment weight of the network as a function of time for $k = 10, 20, 30, 40$ and find that it scales linearly, as we had assumed. We also find that the corresponding numerical estimation of $\mathcal{W}$ agrees with the estimates from Eq. (2.18) within two decimal places.

2.3.3 Pursuit Mechanism

In this section, we introduce the mechanism for pursuit and subsequent disruption by law enforcement. For this model, the primary objective of law enforcement is to find and arrest the kingpin. We represent law enforcement as a single disruptive agent. We equate the dismantling of the network with this agent's capture of the kingpin. With this pursuit mechanism, we then define a network evolving in time t, in which a single time step consists of a recruitment phase and a pursuit phase. The recruitment phase is described in Section 2.3.2. We now define the pursuit mechanism for the pursuit phase.

During the pursuit phase, the agent moves through the network according to a self-avoiding random walk. A self-avoiding walk ensures that each new investigation leads to a criminal that has not previously been investigated. This self-avoiding mechanism may reflect a negative cost associated to the agent's reinvestigation of a criminal within a pursuit phase. However, we select this mechanism primarily for its simplicity and computational considerations. Indeed, a random walk with repetitions or a biased random walk are viable alternatives to a self-avoiding walk. In the case of a random walk with repetitions, the pursuit

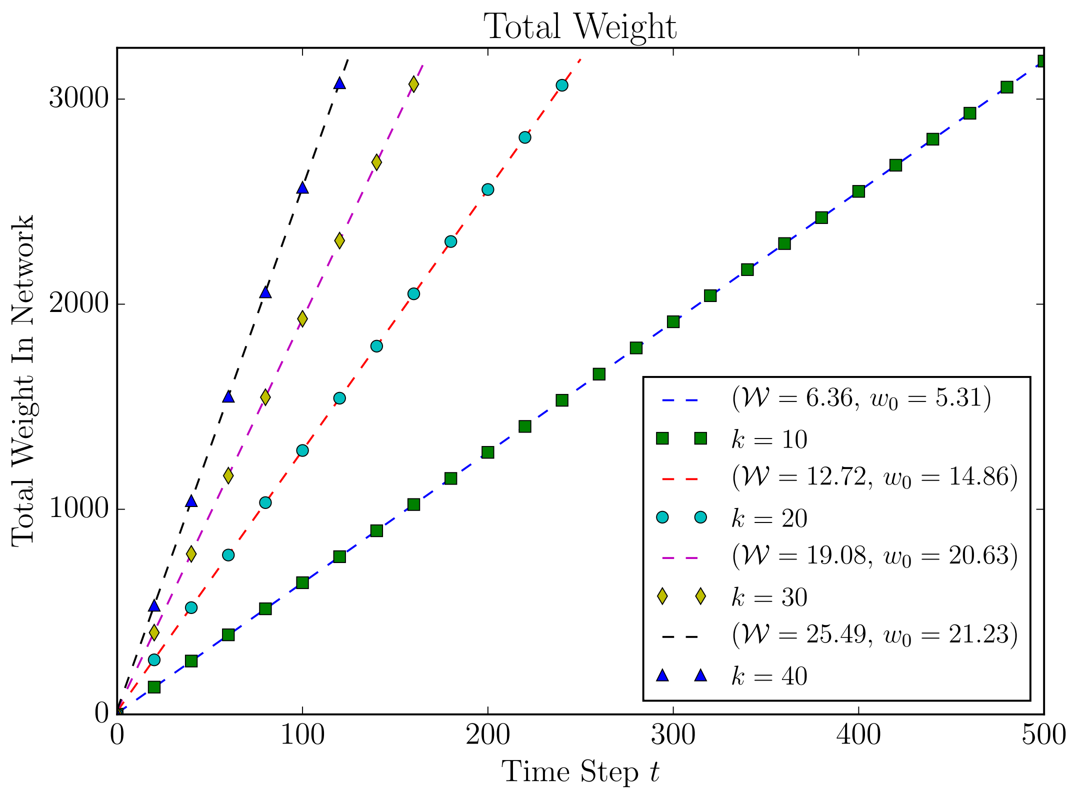

Figure 2.11: Total attachment weight $\sum_{j \in \mathcal{C}(t)} w(j;t)$ of the network as a function of time averaged over 100 runs for $k = 10,\ 20,\ 30,\ 40$. We initialized the network as the kingpin alone. We terminate each simulation when the number of criminals reaches 5×10^3. We fit the data to a linear form $\mathcal{W}t + w_0$ and find that the extrapolated values of $\mathcal{W}$ in the figure legend are in excellent agreement with the ones predicted from Eq. (2.18), given by $\mathcal{W} = 6.39, 12.79, 19.18, 25.57$ for $k = 10, 20, 30, 40$, respectively.

phases may become arbitrarily long and make our simulations significantly slower. This is an important consideration because our numerical experiments require a large number of simulations and each test an array of parameters and initial conditions. We note that since the average degree in a criminal network is 1 (Section 2.3.2.1), the self-avoiding random walk exhibits qualitatively different behavior than a random walk with repetitions. As a result, this selection impacts our numerical experiments. We did not select the biased random walk in order to avoid the introduction of a new parameter. The self-avoiding mechanism implies that if the agent does not reach the kingpin, then the agent eventually ends the pursuit phase at a different leaf node. We refer to the latter situation as the agent reaching a *dead end*. The agent's current position in a network indicates the criminal under investigation. We allow the agent to investigate only one criminal at a time. This agent begins their investigations with a street criminal (leaf node) as these criminals are assumed to be the most visible in the network. Before moving to an adjacent node, the agent is given the opportunity to make an arrest. When the agent arrests a criminal under investigation, the agent also arrests all of this criminal's underlings. Because a node at which the arrest takes place can be a few edges removed from the original leaf node, an arrest does not necessarily imply that the first criminal investigated is removed. The removal of criminals may decrease the the distance between the kingpin and street criminals, therefore increasing the likelihood the agent reaches the kingpin in subsequent pursuit phases. In Section 2.3.3.1, we propose some arrest criteria for the agent and study their efficacies. The arrest criteria represent high-level strategies of law enforcement. The pursuit phase stops when the agent reaches the kingpin, makes an arrest, or reaches a dead end. If the agent reaches the kingpin during a pursuit phase, then the entire network process ends because the agent effectively dismantles the network. In this case, we say the network is *eradicated*. In the second scenario, the agent arrests the criminal and their underlings, and resumes their investigations during the next time step. Once the pursuit phase at time t is completed and assuming the kingpin has not been reached, we proceed to the next time step. During the next time step, the criminal network grows according to the recruitment process discussed in Section 2.3.2 followed by another pursuit phase. This proceeds until the network reaches or exceeds a given size n^*, with the network evolving dynamically in time. We note this pursuit mechanism implicitly assumes the agent does not retain information from previous pursuit phases. This assumption is for simplicity. Precisely defining how information is transmitted from pursuit phase to pursuit phase and specifying how the agent processes this information is beyond the scope of this work. To ensure that the kingpin is not inevitably captured, we assume there is some nontrivial number of edges between the kingpin and the street criminals. Many of our simulations initialize our network as in Figure 2.12 with a perfect ternary tree of height three with forty criminals. In some instances, we initialize networks as *complete* b-ary trees of height h. These are trees such that all leaf nodes have distance h or $h-1$ from the root and all nodes have b children except for nodes a distance h and possibly those $h-1$ from the root. Again, we call b the branching factor of the network just as we did for perfect trees. All perfect trees are complete trees, but not conversely. In the next section, we describe three arrest criteria for the pursuit process we have defined.

2.3.3.1 Disruption Strategies

We now consider some disruption strategies for arrest that the agent may employ within a pursuit phase. As discussed at the beginning of Section 2.3.3, we assume the agent only has knowledge of the criminals that they investigate during the current time step. From the agent's viewpoint, the decision to continue investigating could lead to a dead end or the kingpin.

The first arrest criterion we consider is the *fixed-investigation-number strategy.* For this strategy, the disruptor investigates p successive nodes before making an arrest, assuming they have not reached a dead end in that time. As usual, reaching a dead end halts the process for a given time step. We denote this strategy by $Q_A(p)$. In Figure 2.12, we show a disruptor pursuing strategy $Q_A(q=3)$ on an initial perfect ternary tree of height three.

The second arrest criterion is the *degree strategy*, where the agent arrests a node if the out-degree is at least q. Again, if the agent does not reach a node of out-degree q before a dead end, the pursuit stops for a given time step. In this case, the agent uses degree as a proxy for a criminal's influence in the network and this strategy selects criminals to arrest that possess a certain amount of influence. The agent may make a different number investigations within each pursuit phase, but the agent arrests a criminal with at least q direct underlings and likely many more total underlings. We denote this strategy by $Q_D(q)$.

Finally, we consider the *persistent-investigative strategy*, where the pursuit is stopped only upon reaching the kingpin or a dead end. We denote this strategy by Q_I.

The above pursuit strategies are meant to reflect real-world objectives of law enforcement. Strategy $Q_A(p)$ represents those law enforcement agencies that must regularly make arrests to

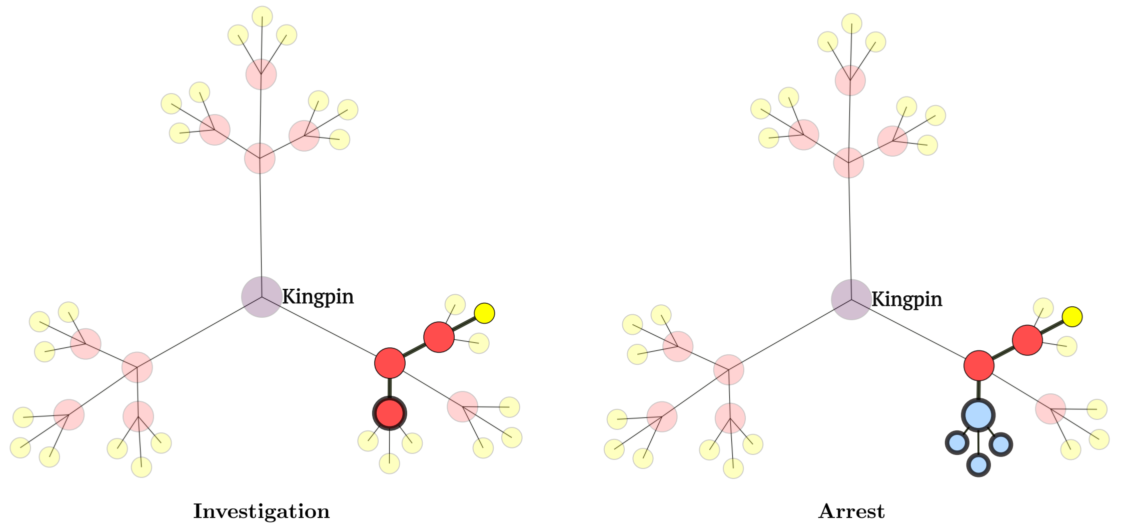

Figure 2.12: The pursuit phase as we describe in Section 2.3.3. We initialize the network as a perfect ternary tree of height three. The network consists of the light and dark colored nodes. The light nodes are those nodes invisible to our agent during the pursuit phase. The dark nodes are those nodes that have been investigated or arrested. (Left) At time $t = 1$ the agent begins their pursuit from the yellow criminal and without having perfect knowledge of the network. He investigates three other nodes, highlighted in red marked by a solid dark line. The last node, surrounded by a dark ring, is the criminal that is currently under investigation. (Right) The criminal that is under investigation is arrested. Once a criminal is arrested, they are removed from the network along with all of their direct underlings, their direct underlings, and so on. The arrested nodes are depicted in blue and have a darker boundary. Note that not all criminals arrested are investigated and vice versa.

demonstrate incremental success to the government or other regulating bodies [10]. One may also view this arrest criterion as the analogy of a so-called "broken windows policy" [78], in which regular arrests are a proxy for securing public confidence and deterring future offenses. Strategy $Q_D(q)$ reflects a disruption strategy that undermines the operations of a network's hierarchy removing nodes with many professional connections [1, 206]. Lastly, strategy Q_I represents law enforcement's choice to minimize violence and act covertly only arresting when the kingpin is reached [1]. In some cases, an arrest at any level may lead to deadly confrontation or violent reorganization. Keeping the pursuit covert until the kingpin is reached may generate less violence [13, 196]. We say two strategies are equal when the agent adhering to the two strategies is indistinguishable to an outside observer. The above strategies are related by the following equalities

$$\lim_{p\to\infty} Q_A(p) = \lim_{q\to\infty} Q_D(q) = Q_I, \tag{2.19}$$

$$Q_A(1) = Q_D(1). \tag{2.20}$$

Note that as the parameters p or q increase, the movements of agents adhering to $Q_A(p)$ or $Q_D(q)$ become indistinguishable from the agent adhering to Q_I. Additionally, note that under strategy $Q_A(1)$ law enforcement removes the node directly above the street criminal initially investigated. This is the same result that would arise from strategy $Q_D(1)$, because all nodes above street criminals have at least one direct underling.

We evaluate each strategy's performance versus the recruitment index k using numerical simulations. We continue simulations until either the kingpin is arrested or the network reaches or exceeds a population size n^*. In the former case, the network is eradicated. The latter case represents a failure of the agent to disrupt the network. We can thus compute the the eradication probability as the total number of successful runs divided by the total number of simulations run. In Figure 2.13 we plot the eradication probability for $Q_A(p)$, $Q_D(q)$ and Q_I as a function of the recruitment index k for various choices of p, q and n^*. For all strategies, as can be expected, the probability of eradication decreases with k. In other words, the faster criminals are added to a network, the less likely the agent reaches the kingpin. We also define Beat(Q), the *beat number* of strategy Q, as the maximum recruitment index k

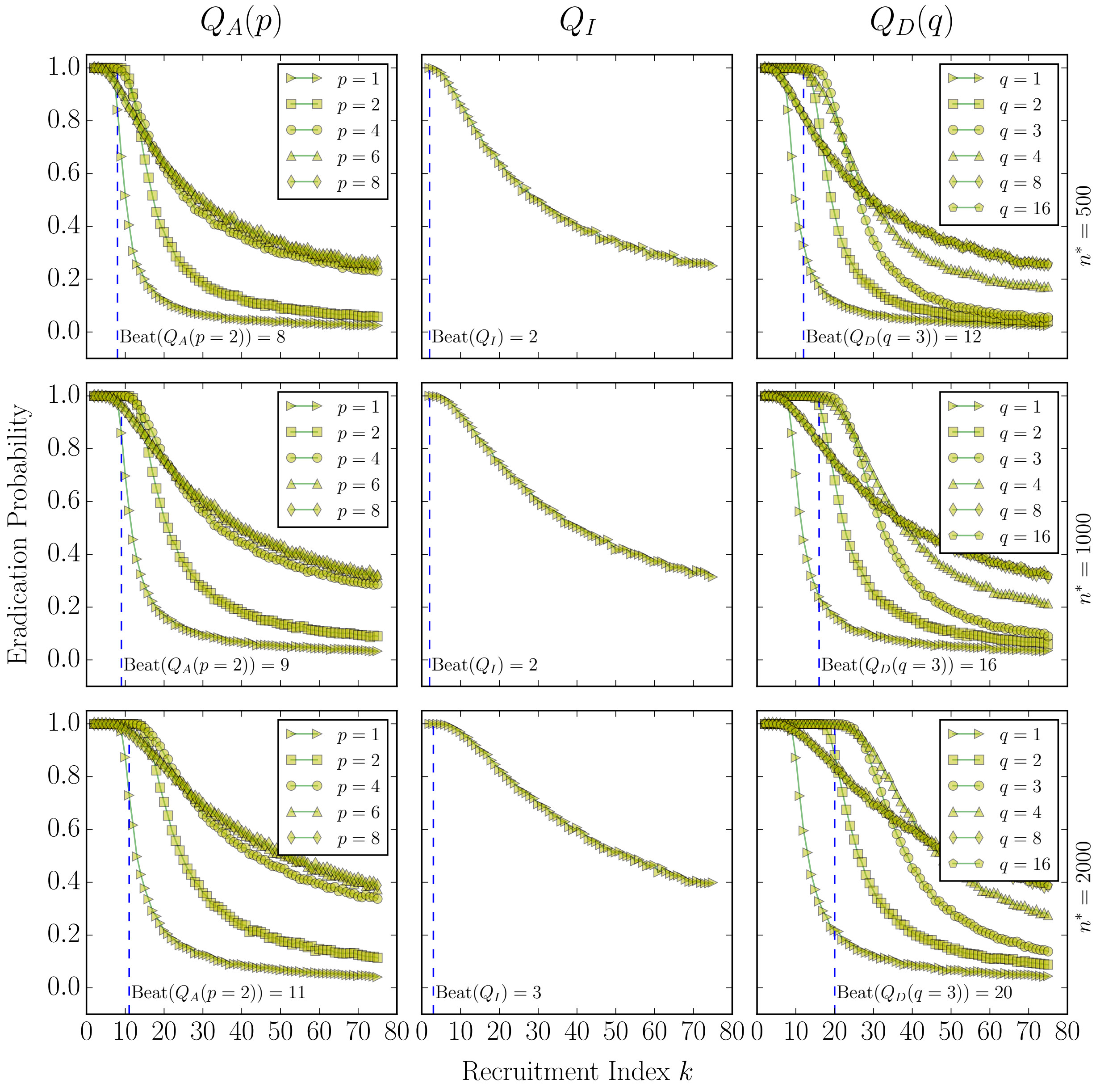

Figure 2.13: Network eradication probability as a function of the recruitment index k, obtained by averaging over 10,000 simulations for different strategies. We consider a total population of $n^* = 500, 1000, 2000$ individuals and halt our simulations when the criminal network reaches this size. For each strategy, the Beat(Q) denotes the maximum recruitment index k for which the network is eradicated with probability 1, over all simulations.

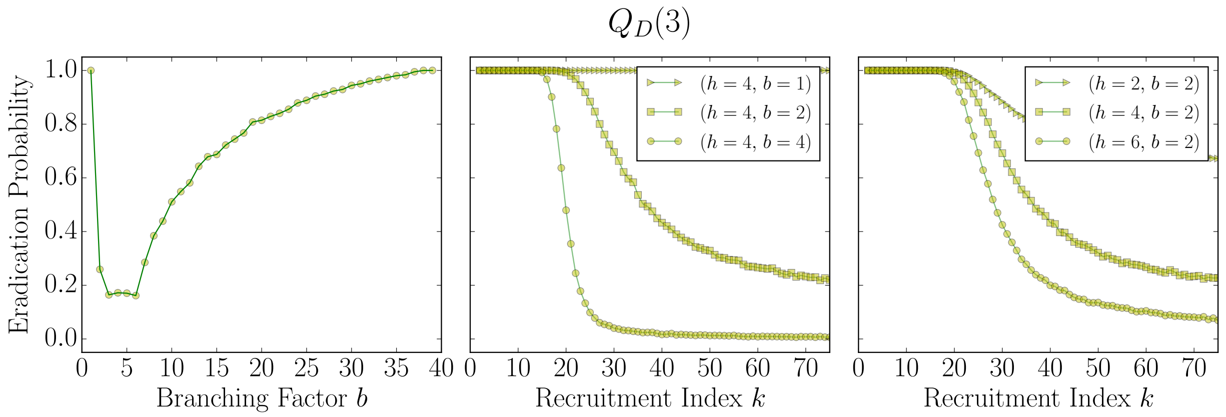

Figure 2.14: Varying initial conditions prior to law enforcement intervention. (Left) Eradication probabilities on a complete initial tree with b branches and forty criminals for $k = 30$ and law enforcement strategy $Q_D(q = 3)$. When a graph consists of a single path ($b = 1$), the eradication probability is 1, because dead ends cannot be reached. Increasing b allows more dead ends to be encountered, so that the eradication probability decreases until $b = 3$ and plateaus until $b = 6$. After $b = 6$, the height of the network becomes small enough to allow for easier access to the kingpin. (Center and Right) Eradication probabilities using perfect initial trees with branching factor b and height h as initial conditions and using strategy $Q_D(q = 3)$. The initial number of criminals is $(b^{h+1} - 1)/(b - 1)$.

of the network such that the agent reaches the kingpin with probability 1. The eradication probabilities and Beat(Q) depend on the total size n^* of the network. For instance, from the rightmost column of Figure 2.13, the beat number Beat($Q_D(q = 3)$) of strategy $Q_D(q)$ increases with $n^* = 500$, 1000, 2000 as 12, 16, 20, respectively. This comes as no surprise as larger values for n^* imply that there are more opportunities for the agent to capture the kingpin.

Fixing n^*, we can compare different strategies using the curves in Figure 2.13. The leftmost column of panels of Figure 2.13 illustrates results for strategy $Q_A(p)$. The simulations in Figure 2.13 are initialized as perfect ternary trees of height 3 (40 initial criminals). When $k \geq 30$ and $n^* = 2000$ are fixed, the eradication probability increases with the parameter p. In other words, for recruitment index k in this regime, increasing p provides more opportunity to reach the kingpin. For these recruitment indices, the growth is so rapid that arresting a smaller number of criminals than the number of new criminals added in the next time step is not advantageous for eradication. For fixed $k < 30$ and $n^* = 2000$, strategy $Q_A(p)$ requires different considerations. Specifically, the growth of a network is now slow enough that the arrest of a small number of criminals during a pursuit phase can compete with the addition of newly recruited criminals and improve the likelihood of eradication. Smaller p (for $p = 1, 2, 3, 4$) implies that the agent is more likely to arrest criminals during a pursuit phase, reduce the number of total nodes in a network, and eventually capture the kingpin. For example, $Q_A(p = 6)$ and $Q_A(p = 8)$ have smaller eradication probability than $Q_A(p = 1)$ and $Q_A(p = 2)$ in this regime of k. Similar analysis is true for lower values of total network size n^*. We also analyze $Q_D(q)$, whose eradication probabilities are shown in the rightmost column of Figure 2.13. For fixed $n^* = 2000$ and $k > 50$, a large degree threshold q increases the eradication probability. Therefore, for k in this regime, it is advantageous to allow the agent more investigations to reach the kingpin just as with $Q_A(p)$. However, for fixed $k \leq 50$ and $n^* = 2000$, a moderate degree threshold q ($q = 2, 3, 4$) has the highest eradication probability. Here, regular arrests of nodes with sufficiently high out-degree is more valuable for eradication than just searching for the kingpin. For $k \leq 50$, we see that $q = 4$ eradicates the network with highest probability of those considered. Again, similar analysis can be made for $n^* = 500$ or 1000. Lastly, the middle column of panels in Figure 2.13 shows results stemming from the persistent-investigative strategy Q_I. Comparing the the many panels of Figure 2.13 shows that the selection of an optimal disruption strategy depends on k. We see as p or q increase in the leftmost column or rightmost column of Figure 2.13 respectively, the eradication probabilities resemble those of Q_I due to Eqn. 2.19. Often, regular arrests must be balanced with supplying sufficient investigations to reach the kingpin. The local arrest criterion of $Q_D(q = 3, 4)$ is particularly effective for $k \leq 50$ as indicated in Figure 2.13.

Now we turn to the effect of the initial configurations on the eradication probability. Let an initial network be perfect or complete b-ary trees. If k and n^* are fixed, we expect that, as the number of initial nodes increases, so too does the eradication probability. The symmetry of perfect networks implies that the success of the agent's first pursuit does not depend on which leaf node the agent selects to investigate first. In other words, the agent is equally likely to reach the kingpin from any street criminal when the initial network is a perfect tree. With these initial configurations in mind, we examine the effect of the number b of branches and the height h on the eradication probability. Note that perfect trees have a total of $(b^{h+1} - 1)/(b - 1)$ criminals.

We first investigate the eradication probability as b and h vary for complete trees of fixed size. We note that as b increases, h decreases and vice versa. In particular, if we fix the number of criminals and maximize b, then $h = 1$ and the agent always reaches the kingpin. However, the choice of $b = 1$ turns the network into a line graph and the agent always reaches the kingpin given enough investigations. We now examine all possible b which the eradication probabilities are smallest. In the left hand panel of Figure 2.14, we show the eradication probability for $Q_D(q = 3)$ on an initial network of 40 criminals with varying b and a fixed value of $k = 30$. We see from this panel that the smallest eradication probabilities occur when b for an initial network is lies in the range 3 to 6. Similar trends related to the b of initial complete trees also arise for strategy $Q_A(p)$ and Q_I (not shown) although the sharp decrease for small b is less pronounced.

We next consider initial networks made of perfect trees with fixed b and variable h and vice versa without limits on a network's size (middle and right panels of Figure 2.14). We expect increases in b or h to lead to lower eradication probabilities, because the number of initial criminals is larger and there are more chances the investigation leads to a dead end. In the middle panel of Figure 2.14 we examined an initial network of height $h = 4$ for various b. In this panel, we see that when $b = 1$, the agent always reaches the kingpin for $Q_D(3)$. When b increases to 2 and then 4, the eradication probability decreases as we expect. In the right panel of Figure 2.14 we find similar results for an initial perfect binary tree with $b = 2$ and heights $h = 2, 4, 6$. Qualitatively similar results arise for other strategies $Q_D(q)$ and $Q_A(p)$ as those results as those in Figure 2.14.

2.3.3.2 Strategic Costs and Time to Eradication

In this section, we introduce two measures for costs associated to a pursuit, and we evaluate each strategy according to these measures. First, we associate a cost to investigations and arrests during a pursuit. We assume that the public and the government are the primary levers for replenishing law enforcement resources. For example, in the United States, each fiscal year Congressional representatives must negotiate and approve a detailed budget for all law enforcement agencies [158]. When the government assesses the cost of law enforcement actions, certain actions such as investigations are difficult to quantify while others such as arrest and seizures are more easily quantifiable and can help ensure future funding [140,174]. Moreover, arrests visibly reduce criminal activity, while investigations do not [174]. Additionally, the United States Justice Department program of asset forfeiture–the confiscation of criminal assets after an arrest–fund future criminal investigations [140]. We now define the cost associated to the pursuit mechanism of Section 2.3.3. We define the cost during a single pursuit phase as the number of investigations minus the number of criminals removed, if this difference is positive. In the event that the kingpin is reached, the cost is the number of investigations made minus the criminals in the network. In both cases, if this difference is negative, the cost is set to 0. The higher the numerical cost of a pursuit, the harder for law enforcement to replenish their resources. Our definition of cost implies that pursuit phases that reach a dead end occur at high cost. However, a pursuit phase that ends with an arrest may occur at low cost depending on the number of investigations and total number of investigations. We compute the cost of the pursuit phase shown in Figure 2.12. In the left diagram, four nodes are investigated: the street criminal (depicted in yellow) and three other criminals (depicted in green connected by a dark line). During the arrest phase, in the right panel of Figure 2.12, four criminals (depicted in red) are eliminated. Thus, the costs associated with this iteration is 0. We calculate the total cost as the cumulative cost over all time steps.

We study the costs associated to each strategy. There are two cases: when the network is eradicated and when it is not. We study the cost versus the recruitment index k for each case. We initialize the network as a perfect tree with $b = h = 3$. We first discuss the cost when the network is eradicated. The top row of Figure 2.15 shows the total cost of eradication with $n^* = 1000$. We average the total cost over 10000 simulations. We inspect strategies $Q_A(p)$ and $Q_D(q)$ starting on an initial perfect ternary tree. We also depict the probability of kingpin capture and criminal network eradication as shades in the data points. Costs are identically 0 for $Q_A(p = 1)$ and $Q_D(q = 1)$ because, in these cases, there are two investigations and at least two criminals removed at every time step. Similarly, costs stay relatively low for $p = 2, 3$ and $q = 2, 3$. For example, the total cost of eradication for $Q_D(q = 3)$ is nearly 0, indicating that the number of investigations is comparable to the number of arrests on average. For sufficiently large k, the cost of eradication decreases monotonically in k for $Q_A(p = 2, 3, 4, 5)$ and $Q_A(p = 3, 4, 5, 6)$ because we stop network growth at n^*. As k increases, the network reaches n^* more quickly and the agent must eradicate a network in less time with fewer investigations. In fact, strategies $Q_A(p = 3), Q_A(p = 4)$ and $Q_D(q = 4)$, the cost curves are monotonically decreasing for all k . As p and q increase further for strategies $Q_A(p)$ and $Q_D(q)$, the agent arrests less frequently and reaches more dead ends, increasing the costs particularly for fixed $k < 10$ (Figure 2.15). Moreover, the equivalence of strategies $Q_A(p \to \infty) = Q_D(p \to \infty) = Q_I$ is apparent in cost curves as the parameters p and q increase.

We now transition to the costs associated to networks that are not eradicated. For networks not eradicated, our numerics (not shown) indicate that cost monotonically decreases with k for all strategies. In this case, the cost of a strategy can only be studied for k that exceed this strategy's beat number $\text{Beat}(Q)$. Moreover, if we wish to compare two strategies, then we can only compare them for k that exceed both their beat numbers (otherwise, one strategy will not have a well-defined cost because all of the networks simulated were eradicated). As k increases past the beat number of a strategy, the number of pursuit phases decreases and so too does the cost. For networks that are not eradicated, arrests actually increase costs because arresting criminals increases the number of pursuit phases before the network reaches a size n^*. Our numerics (not shown) show that Q_I is the least expensive strategy. Strategy Q_I ensures that the network grows without arrests, and thus requires the least number of pursuit phases until n^* is reached.

We now examine the time until a network is eradicated or reaches total size n^*. We record the number T of time steps required for each case. For the former case, the lower panel of Figure 2.15 shows time versus recruitment index k. Unlike cost, the time of first eradication is always nonmonotonic: it increases in k before decreasing again. Here, as k increases initially, the network grows more rapidly requiring more time on average to reach the kingpin. However, for sufficiently large k, we see that T decreases in k. We can explain T's decrease as follows. Because the maximum network size n^* is fixed, if the network is eradicated, T must decrease in k. In particular, the larger k becomes, the fewer pursuit phases are possible. Additionally, peaks in the curves in Figure 2.15 are close to the beat numbers and correspond to drops in the eradication probability. For networks that are not eradicated, the time T is monotonically decreasing in k (not shown), identical to the cost scenario discussed in the previous paragraph. Moreover, the total time T is smallest for Q_I just as was the case with cost.

It is important to note that the exact cost curves depend significantly on the initial network configuration: different initial conditions yield different eradication probabilities, costs and eradication times. However, our comparison of strategies made in this section remain valid for many different initializations that are perfect tree. For networks that were initialized as perfect trees (all possible initializations with $b = 2, 3, 4$ and $h = 2, 3, 4$; numerics not shown), the cost comparisons we made remain valid. For instance, although the exact cost curve changes for an initial perfect tree with $b = 2$ and $h = 4$, strategy Q_I still has the lowest cost when compared to other strategies for networks not eradicated. We expect the cost comparisons to be valid for complete tree initializations, though future work will consider the precise dependence of eradication probability and costs associated to different initial conditions.

2.3.3.3 Evaluation of Disruption Strategies

In this section, we evaluate each disruption strategy with respect to the associated eradication probability (Section 2.3.3.1), pursuit cost (Section 2.3.3.2), and the total pursuit time (Section 2.3.3.2). For each measure of disruption, we studied the measure versus the recruitment index k. For this numerical analysis, we assume that an agent cannot influence the recruitment index k and we view this rate k as an intrinsic property of the network. This assumption is done for simplicity because we do not wish to introduce a new mechanism that influences k, though this is certainly an avenue for future research. We also assume the agent selects the parameter p or q associated to the appropriate strategy and never changes them during the process. Again, this assumption is made for simplicity and may be altered in future work. We use the numerical experiments performed in the previous sections. Figure 2.13 shows that for small values of k eradication probabilities were all 1 or close to it. As k increases and we move past the beat number of a strategy, we see some strategies ($Q_A(p = 2)$ and $Q_D(q = 2)$) have sharp decrease whereas others decrease more gradually ($Q_A(p = 6)$ and $Q_D(q = 8)$). For intermediate values of k ($10 \leq k \leq 30$), the degree strategy $Q_D(q)$ is associated with the highest eradication probabilities particularly when $q = 3$ compared to any $Q_D(q)$ or $Q_A(p)$. We also note that $\text{Beat}(Q_D(p = 3, 4)) > \text{Beat}(Q_A(q = 3, 4))$ for all values of n^*. However, as k increases past these intermediate values, Q_I becomes the most effective. Moreover, as the parameters p and q increase, $Q_A(p)$ and $Q_D(q)$ become indistinguishable to Q_I.

In our model, the agent's optimal strategy–in the sense of ensuring the highest likelihood of eradication–is to employ $Q_D(q)$ and select q based on an estimation of k. If the agent is interested in lowering costs–for instance, when the criminal organization is not engaged in activities that are deemed to be especially dangerous for the community–that agent should lower the parameter q to ensure regular arrests. From Figure 2.15, we see that $Q_D(q)$ costs are lower than those for $Q_A(p)$ costs for comparable eradication probabilities when the network is eradicated. Similarly, if the agent is concerned in reducing eradication time, the degree strategy also $Q_D(q)$ usually yields better results than $Q_A(p)$. Moreover, selecting q large enough makes the strategy indistinguishable from Q_I, which is best for large k.

2.3.4 Conclusions from Model

The recruitment and disruption model introduced in Section 2.3 provides a template for the formation and disruption of growing criminal networks. Although this model is far from providing an explanation of criminal network data, this generative network process may help future research into criminal organizations and their disruption. We focused on organized, hierarchical networks motivated by the vertical structure of the Medellín and Sinaloa drug cartels [1, 4, 12, 13, 79, 121, 131, 196]. There are other smaller hierarchal criminal organizations for which this work may be applicable such as the American and Sicilian Cosa Nostra mafia networks [57, 128, 129] and the Hells Angels biker gang [145].

In this model, we first proposed new attachment model for criminal recruitment. We first studied how a network evolved with respect to this mechanism. There is an important distinction between this model and preferential attachment, including the model of Barabási–Albert. The resulting degree distribution is not heavy tailed [15, 193]. Additionally, we examined the statistics of several network structures for large networks. We found the distribution of criminal position relative to the kingpin to be well approximated by a shifted gamma distribution. Our model also yields a linear relationship between the number of street criminals and the recruitment rate k. Moreover, we found the total attachment weight of the network scaled linearly in t for large t. We also conjecture the degree distribution to be independent of the recruitment index k. All these claims are supported by careful numerical simulations although rigorous analysis is still required.

We then introduced a pursuit mechanism into our model. The pursuit mechanism determines the movement and arrest patterns of a disruptive agent. During a time step of an evolving network process, a recruitment phase is followed by a pursuit phase. The network then evolves according this alternation between these recruitment and pursuit phases. We then analyzed the efficacy of three disruption strategies: $Q_D(p)$ with a preset number of investigations p before an arrest is made; $Q_A(q)$ in which the agent arrests only when a criminal with at least q underlings; and Q_I in which no arrests are made save for the kingpin. We used numerical simulation to examine the strategies in terms of their eradication probability, measured costs, and total time. We found $Q_D(q)$ to be effective from all these standpoints though selecting q depends on the recruitment index k. For example, from Figure 2.13 it appears that $Q_D(q = 8)$ is more effective than $Q_D(q = 4)$ only when $k \geq 40$ for all values of n^*. However, for $k \leq 50$, $Q_D(q = 4)$ has the highest probability of eradication for all strategies and all n^*. We remark that the removal of nodes with high degree has also been seen as effective in dark network models of [133,134,209] (see Section 2.1 for more discussion of this model). Our model also echoed the common sense strategy that the faster a network grows, the more quickly it needs to be eradicated if it is to be at all.

Finally, we briefly explored the effect initial configuration of the network played on disruption. We studied complete trees and varied their height and branching factor fixing the number of criminals available for each configuration. As we expect, networks with small or large branching factor b (large or small height respectively) are the easiest to eradicate. We found a range b for which the eradication probability is significantly lower particularly than other configurations.

In future work, we will further quantify the resilience of this network model. Specifically, we plan to quantify the flow of illicit goods or criminal information through a criminal networks in future work. For instance, we can simulate the flow of illicit goods stochastically and examine disruption as not only the removal of criminals but also the removal of goods. To do so, we may wish to adapt network interdiction for our generative network process [94,207].

In this work, we have only modeled a hierarchal network of criminals. However, we plan to generalize this model in future work to acyclic directed networks. We consider an initial acyclic directed network and consider the following attachment mechanism. There are k incoming nodes as usual, now each with m in-edges (in the current model each incoming node has 1 in-edge). We then set the attachment weight of an existing node j on the network to be:

$$w(j;t) = \frac{1}{1 + \text{dist}(j;t)},$$

where $\text{dist}(j;t)$ is the distance of node j to nodes of out-degree 0. The disruption strategies that we presented could be modified for this acyclic model. Another possible relaxation on the structure is to remove a single root node, and replace it with a larger set of criminal nodes that all equally oversee the organization. We also may want to consider different distances for the attachment weights to simulate other criminal considerations. For example, we may wish to instead to investigate the distance to a fixed set of nodes of high rank and set the attachment weight to be positively correlated with this distance. This model is in its current form is theoretical and quite simplistic. In future work, we plan to carefully motivate new generative network models (or adapt existing attachment models) to agree with the data found in such studies as [67,144]. We proposed a generative network model for the formation and disruption of criminal networks. This network process, although far from explaining real-world criminal networks, introduces new mechanisms that can be adapted for the dynamics of criminal recruitment and disruption.

2.4 Conclusions and Future Work

The network models we presented in Section 2.2 and Section 2.3 describe mechanisms for recruitment and disruption on a hierarchal criminal network. Both models will require significant modifications and improvement to resemble real-world dark networks. Nonetheless, this work proposes a new framework to model these complex criminal organizations and law-enforcement interactions. In Section 2.2, we presented our first model for recruitment and disruption. We adapted the Galton–Watson branching process to simulate recruitment into a hierarchal criminal network. We then introduced a disruptive agent who moves up the network and arrests according to a stochastic process. In Section 2.3, we presented our second model. We proposed a new attachment model to simulate recruitment based on certain criminal incentives. We then introduced a disruptive agent that followed a self-avoiding random walk through the network and arrested nodes according to certain disruption strategies. We designed each model so that they alternate between a recruitment phase and a disruption phase. Moreover, we equated the capture of the kingpin (the root) with the dismantling of the network. These simplifying assumptions, though unrealistic, allowed us to simulate the resulting network dynamics and discuss criminal disruption. In particular, for each model, we measured the probability a network was terminated (Section 2.2) or eradicated (Section 2.3). In Proposition 2.2.2, we proved a bound on this probability in Section 2.2. Using the model in Section 2.3, we compared several simplified disruption strategies for law enforcement. This attachment model (Section 2.3.2) may be adapted for more general network science applications. For example, our process resembles the online referral networks discussed in [8] because incoming nodes are most likely to attach to those most recently added to the network.

For this work, rather than using specific criminal network data, we designed our model considering high-level criminal incentives and law-enforcement goals. In future work, we plan to carefully integrate criminal network data into these models as in [67, 144, 209]. However, there are many challenges associated with the reconstruction of criminal network data [67, 144, 209]. For example, criminals must remain secretive about their connections to avoid government detection, and thus the reconstruction of a criminal network may be incomplete or inaccurate. Moreover, there are wide variety of incentive structures in various types of criminal networks such as terrorist networks [114, 209], gang networks [144], and drug trafficking networks [67, 144]. Additionally, to our knowledge, there is no real-world data relating the disruption and recovery of criminal networks [67]. As a result, we expect the validation of all aspects of a criminal disruption model to be largely untenable. However, using suitable criminal data, we plan to adapt the generative processes studied here to study real-world criminal organizations and support law enforcement objectives.

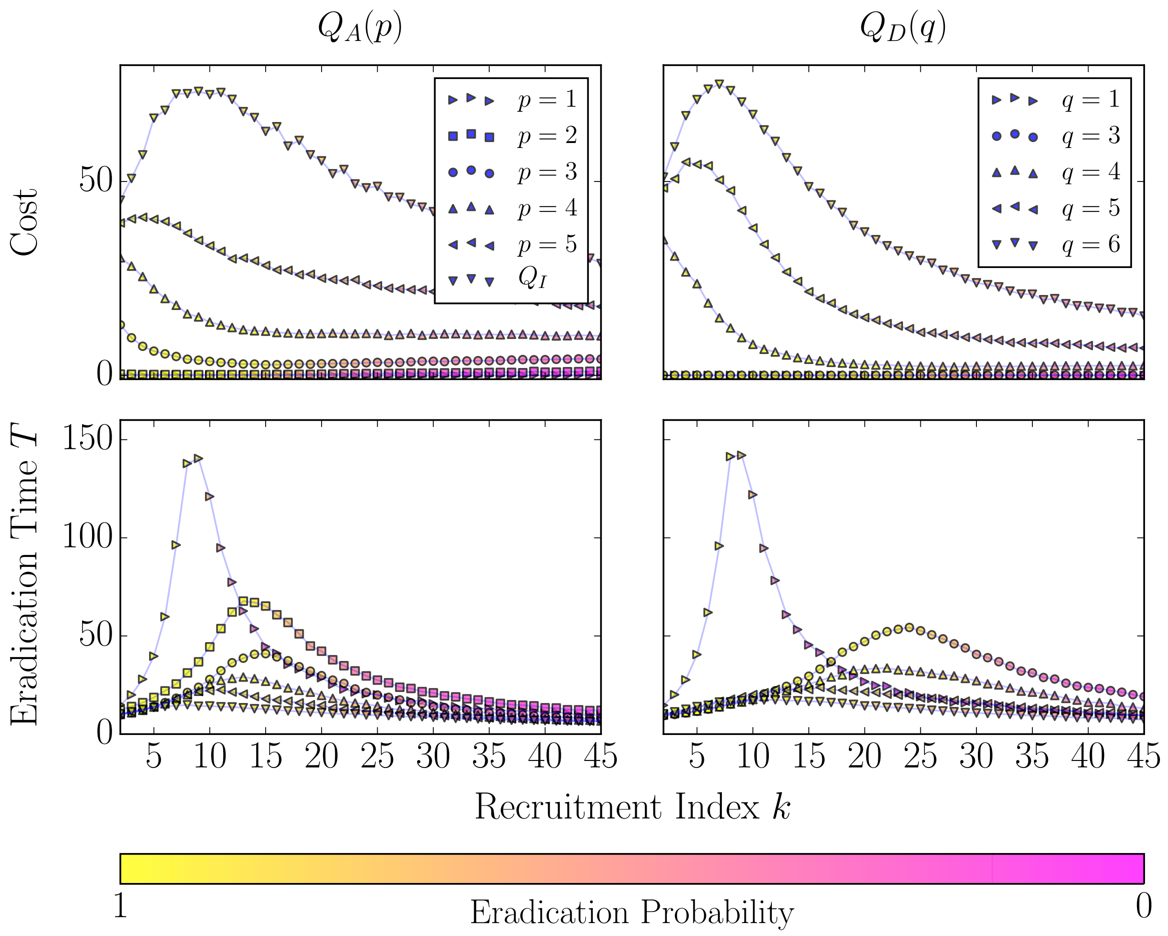

Figure 2.15: (Top) Costs incurred by law enforcement conditioned on kingpin capture as a function of the recruitment index k. Shades in the data points represent the probabilities of network eradication. We consider 10000 simulations and allow the network to grow to $n^* = 1000$. There is the emergence of maxima for certain curves because we condition on the eradication of the network. As k increases initially for such curves, the network grows more rapidly and so too does the number of investigations necessary for eradication. Upon reaching a threshold in k (maxima), the number of possible pursuit phases greatly decreases. In particular, for large k, a network must be eradicated within fewer pursuit phases and thereby reducing cost. (Bottom) The mean eradication time as a function of k for various strategies. Similarly as in the above panel, there is an emergence of maxima only now for all curves. Note that cost and time curves for $Q_A(p = 1)$ and $Q_D(q = 1)$ are identical and that $Q_I = Q_A(p \to \infty) = Q_D(q \to \infty)$.

CHAPTER 3

Rank Aggregation for Course Sequence Discovery

In this chapter, we adapt rank-aggregation for university-level course-sequence discovery of mathematics, we consider a large pool of undergraduate students and the sequence of mathematics courses they take. Our methodology aggregates the course sequences of these students and outputs a single linear ordering of courses. We refer to this methodology as *course-sequence discovery.* Although students rarely take courses in a strictly sequential fashion, our method's extraction of a course sequence can assist students in their selection of courses and determine hidden dependencies between courses.

For this chapter, we apply rank aggregation methods to 15 years of student data (2000–2015) from the UCLA department of mathematics. We obtained the data from the department and discuss it at length in Section 3.3. A student profile determines a partial pairwise ranking of courses, and a course is ranked higher than another if the course was taken in an earlier academic term than the other. These individual pairwise rankings are partial because a student only enrolls in a subset of all the courses offered in the mathematics department. Moreover, a mathematics student often takes several courses within the same academic term, in which no pairwise comparison can be made. Using these pairwise ranking of courses from each student profile, we construct network models, in which nodes represent courses and edges quantify the flow of students between courses from term to term. With these network models, we apply several rank aggregation methods and extract a single course sequence. Using this methodology, we explore the course sequences for different subsets of students. For instance, we compare the course sequences of high and low performing Pure Mathematics majors. We are able to identify a course (Discrete Mathematics/Math 61) that high-performing Pure Mathematics majors take earlier than low performing math majors.

Although we do not verify there is no causal relationship between a student's performance and the course sequence they take, identifying possible trends can assist students in their course selection and provide administrators information regarding how students are moving through the coursework of their major.

The rest of the chapter is organized as follows. In Section 3.1, we discuss how our work fits into larger university-level education and a literature review. In Section 3.2, we review machine learning and data mining techniques for course-sequence discovery and related tasks. In Section 3.3, we discuss the student data that we analyzed; specifically the data from the UCLA Department of Mathematics between 2000–2015. In Section 3.4, we review various methods and models for rank aggregation. In Section 3.5, we outline the methods we use for rank aggregation in this chapter. In Section 3.6, we apply these methods to analyze sequences of mathematics courses at UCLA. We use our findings to infer course sequences from these records and hidden dependencies between them. We also compare the performance of each rank aggregation method to demonstrate the many different approaches are fairly consistent for this data set. In our final Section 3.7, we review our findings and explore future directions.

3.1 Introduction

Many statistics suggest that a college education has become an increasingly important hurdle in securing one's financial future [56, 156]. In November 2016, the unemployment rate for college educated adults was 2.3%, which is less than half of the unemployment rate of adults with only a high school diploma (4.9%) and almost a quarter of the unemployment rate for adults who did not graduate high school (7.9%) [156]. Moreover, for 15–32 year olds in 2013, the median annual income for a college educated person was $45,500, whereas it was $30,000 for those with only a high school diploma-a more than 50% increase in median salary. Additionally, college enrollment has grown in recent decades. From 2003–2013, the proportion of 18–24 year olds in the United States enrolling in colleges has risen by 20% in addition to the population growth of this same segment (18–24 year old adults rose by 9% in the same period) [56]. To meet this increasing demand, universities must create systems to efficiently guide their undergraduate students towards the completion of their degrees. In this chapter, we focus on a specific aspect of the education process: how students navigate through their coursework required by their major. The expected sequence a student navigates through his/her educational coursework informs each course's sophistication, the instructor's expectations, a student's performance in the course, and the content covered [96, 182]. We apply rank aggregation to analyze temporal patterns of course sequences in the UCLA department of mathematics.

To earn a college degree, a student must pass a certain number of required classes. A department often encourages students to take required courses in a particular order, so that students are best prepared for each subsequent course. For example, departments of science, technology engineering, and mathematics (STEM) fields frequently have a list of required course work to provide foundational knowledge for advanced topics and research [96]. For example, in Department of Mathematics at UCLA, there are six introductory courses (Math 31AB, Math 32AB, Math 33AB) that every math major must complete in sequence at the beginning of his/her undergraduate study [161], although some students may fulfill this requirement in high school or community college. Moreover, the more advanced introductory courses that introduce linear algebra and differential equations (Math 33AB) do not formally require all the introductory calculus courses [161], but as we discuss in Section 3.3, a majority of students take Math 33AB after the calculus sequence is complete. Generally, the recommended ordering of courses is the product of practical considerations within a department and broader curriculum goals set by professors and educators to ensure students are building a core competency in their major [48, 96]. A university can ensure that courses are taken in a specific order by restricting enrollment to those who have fulfilled the specified prerequisites. For UCLA mathematics courses, course prerequisites are not enforced due to the changing availability of courses and the diverse needs of a large student population. Moreover, a popular professor or an early-morning lecture may also influence how a student selects his/her courses regardless of what a department recommends. Additionally, there large number of possible student schedules–too many to investigate separately. To do these considerations, it is important to have tools to identify trends in the order students select courses.

We apply rank aggregation to analyze the order students take courses within the UCLA Department of Mathematics. We obtain a single course sequence that aggregates the several different ways students navigate their coursework. From this sequence, we can infer and compare trends in course selection between different student populations. The ability to determine trends in student course selection is a challenge because of the number of possible schedules. We assume that an underlying sequence determines the distribution of how courses are arranged in a students schedule. With this assumption, we obtain the underlying ranking via rank aggregation and can more easily identify possible trends. For instance, comparing the course sequences of high- and low-performing Pure Mathematics students, we identify a course (Discrete Mathematics/Math 61) that high-performing students take significantly earlier than low-performing students.

To our knowledge, the application of rank aggregation methods to order temporal data and uncover patterns has not been thoroughly explored in the literature [95, 202]. We hope that this work can help provide a proof-of-concept and be adapted for other pattern-mining applications for the temporal ordering of events [73, 74, 112, 177]. In the next section, we discuss machine learning and data mining approaches for assisting students in their course scheduling, course-sequence discovery and related tasks.

3.2 Related Work

The mining and analysis of educational data allows universities to build effective systems to serve their diverse and intelligent undergraduate population. In recent years, researchers have applied machine learning techniques to model course selection, automate curriculum design, forecast educational consumption, and understand related student behaviors. For example, in [210], van der Schaar et al. propose a system to help UCLA engineering students select courses, term by term. Their model first considers two inputs: the prerequisites of each STEM course required to graduate and the availability of courses in past years (e.g. some engineering classes may be offered in a particular term). The system then selects candidate schedules for students that minimize a student's expected time to graduation, while ensuring a student only takes courses for which he/she has the official prerequisites. The system then groups students according to their past performance in university courses, Scholastic Aptitude Test (SAT) scores, and their high school ranking to select those schedules that maximize their expected grade point average (GPA) at UCLA based on students with similar profiles. As another example of the application of machine learning to educational systems, the authors in [213] applied natural language processing to extract a directed graph model called a *concept graph* that describes how physics and mathematics concepts depend on one another. The authors used materials from massive open online courses (MOOCs) and Wikipedia corpus to infer dependencies between concepts. This approach provides a system for automating curriculum design. However, it ignores that each university often customizes courses and particular curriculum to meet departmental goals. In [84], researchers constructed a *correlation network* to identify key STEM courses at Warsaw University of Technology. More specifically, for every pair of courses, they considered the students that took both and analyzed their grades in each. Suppose there n such students that take both course i and course j. Let $\mathbf{g}_i$ and $\mathbf{g}_j$ be $n \times 1$ vectors such that the kth student's grades in course i and course j are the kth component of $\mathbf{g}_i$ and $\mathbf{g}_j$, respectively. The covariance matrix $\mathbf{\Sigma}$ between any two courses has entries

$$\Sigma_{ij} = (\mathbf{g}_i - \mu_i \mathbf{1}_n)^T (\mathbf{g}_j - \mu_j \mathbf{1}_n)$$

where μ_i is the mean of the entries of vector $\mathbf{g}_i$ and $\mathbf{1}_n$ is the $n \times 1$ vector consisting entirely of 1's. They defined the correlation network be the weighted, undirected network in which nodes are the courses and edges between course i and j are weighted according to their *correlation coefficient*. The correlation coefficent ρ_{ij} between two courses is

$$\rho_{ij} = \frac{\Sigma_{ij}}{\sigma_i \sigma_j} \,. \tag{3.1}$$

In Eq. (3.1) above, σ_i and σ_j denote the standard deviation of grades in course i and j, respectively. Specifically, the standard deviation in course i is defined as

$$\sigma_i = \sqrt{(\mathbf{g}_i - \mu_i \mathbf{1}_n)^T (\mathbf{g}_i - \mu_i \mathbf{1}_n)} \,.$$

Using this framework, the authors of [84] performed elementary network analysis to identify key courses. Specifically, they calculated the degree of nodes in the correlation network to determine which courses had the highest aggregate correlation coefficient among those courses considered. They also explored *maximum spanning trees* to investigate how courses could potentially built on one another. Recall that a spanning tree is a sub-tree that contains all the nodes of a network. The maximum spanning tree has the additional property that the total edge weight is greater than or equal to any other spanning tree. Focusing only on student grades, their analysis suggested that courses such as "Introduction to Programming" and "Fundamentals of Physics" are key courses, which were both introductory STEM courses at Warsaw University of Technology.

Researchers have also used MOOC data to analyze how students move through coursework. On MOOC platforms, students watch lectures from a computer, submit problem sets electronically, and complete exams online. Even though many elite universities rarely grant undergraduate degrees strictly with online courses, many university professors have designed university-level courses for MOOC platforms [33, 105]. For example, many researchers adapted internet recommendation systems for MOOC platforms to analyze course navigation and material consumption [195, 204]. A recommendation system first clusters similar student profiles using personal data, previous course grades/scores, and usage patterns. The system then forecasts how students will perform in future courses analyzing the profiles of students with similar profiles. With the tools to forecast course grades/scores, educators can better recommend courses for students and identify features that correlate with course grades. For example, in [204], the authors deployed a recommendation system for six online business courses at the University of Taiwan. The system collected each students' gender, course grade and the order courses were taken (only one course was taken per term); the system also surveyed each student at the end of a course about the perceived level of difficulty. The students were then clustered according to the data allowing the administrators to help guide students through their coursework. After the system was deployed, 850 students were required to follow the recommended coursework and provide their feedback at the end of the online coursework. Over 80% of the students participating in the pilot program thought the recommendations were appropriate, although the work did not survey any online learners that were not confined to the recommendation system. Overall, MOOCs are very different than typical university classes: only 5–10% of students that sign up for a course complete it [33, 105]. Although MOOCs rarely provide the same level of accreditation that universities do (Georgia Institute of Technology is offering an online masters through a MOOC platform [135] with additional university support), they offer a glimpse into how students consume educational content and navigate through courses.

For this work, rather than using existing prerequisite structures or course content, we focus on the flow of students from course to course. We assume an underlying sequence determines the distribution of course selections and then use student data to infer this sequence. Our approach applies well-known rank aggregation techniques to infer this global sequence of courses. We also use this information to identify possible hidden dependencies between courses whose dependency is not listed in the course catalog.

Rank aggregation is widely applied and studied; it is a powerful tool in Web search [71, 166], sport rankings [37, 53], recommendation systms [44, 71], and other applications. In Section 3.5, we adapt it to extract course sequence from student schedules. In the next section (Section 3.3), we discuss the data set that we use for this application.

3.3 Student Data

We use student data from the UCLA Department of Mathematics between Fall 2000 and Spring 2015. We provide a snapshot of this data in Table 3.1. This table shows five courses taken by a student. Each row corresponds to a course taken by this student. Additionally, each row contains identification information and this student's grade.

This data set contains only a subset of courses taken by students. Specifically, it only reveals courses that a student was enrolled in the same term as a mathematics course. Although all science and engineering majors require completion of particular mathematics courses, we can only inspect those the terms that such students were enrolled in math courses. In this data set, there are 66,881 unique students, but many students have only a few terms

Table 3.1: Sample of data provided by department of mathematics.

Hashed ID	**Term**	**Major**	**Class Standing**	**Admit Class**	**Ethnicity**	**CA Resident**	**U.S. Resident**	**Subject**	**Course**	**Grade**
0x0009...	Fall 2010	Pure Math	Junior	Freshman	Chinese-American	No	No	Math	115A	2.7
0x0009...	Winter 2011	Pure Math	Junior	Freshman	Chinese-American	No	No	Math	131A	4.0
0x0009...	Winter 2011	Pure Math	Senior	Freshman	Chinese-American	No	No	Math	170A	4.0
0x0009...	Spring 2011	Pure Math	Senior	Freshman	Chinese-American	No	No	Math	172A	4.0
0x0009...	Fall 2011	Pure Math	Senior	Freshman	Chinese-American	Yes	Yes	Math	172B	3.0

visible for inspection. Each mathematics major (there are seven) has relatively few students. For example, this data set contains only 346 students declared as a Pure Mathematics Majors (Bachelor of Science Degree) during 2000–2015 that earned average passing grades in their mathematics courses.

We now discuss each field listed in Table 3.1. We also point out how certain information within a field that may be ambiguous or incomplete. The *ID* field is a student's unique identification number. To protect each student's privacy, the ID number has been encrypted using a Hash function from a Microsoft SQL database product. The *Term* field refers to the academic term from Fall 2000 to Spring 2015.

UCLA is on a quarter system and there are four academic terms each year: (in order) fall, winter, spring, and summer. Summer term is over 3 months long, while the other terms are approximately 10 weeks. Moreover, summer quarter is organized differently than the other quarters. There are three different summer sessions within a single summer quarter and Math courses are typically offered in two minimally overlapping sessions (the overlap is 1 week) [184]. Each of the two sessions that math is offered lasts 8 weeks. This means that an individual course is faster paced; however, instructors meet with students more frequently and generally students do not take as many courses during a single summer quarter (90% of students take no more than two Math courses). However, we only have records from the summer quarter from 2010–2014. We are also not able to differentiate between the different summer sessions; namely, if a student was able to take two math courses in different summer sessions then this appears the same in the data set as a student that completed two courses in a single summer session (the latter being much more demanding of a student's time). Additionally, summer courses may be taught by external faculty; and enrollment is open to international students, professionals, and students from other universities. If we consider all students that took at least five courses and at least one upper-division math course (a course beyond the six introductory courses required for all math majors), there are 5,327 students. Of these students, 1,384 students at least one summer course; 599 took multiple courses in a single summer quarter; and 119 students took courses in multiple summer quarters. These small percentages of students are not a reflection of the popularity in summer courses, but rather a reflection that we only have summer quarters beginning in 2010. Although summer quarter is a markedly different experience for students, we do not differentiate summer quarter from Fall, Winter, and Spring quarters.

The *Major* field indicates one of the several majors offered at UCLA [3]. The seven Mathematics majors are Pure Mathematics, Applied Mathematics, Mathematics & Economics, Financial and Actuarial Mathematics, Mathematics for Teaching, Mathematics for Applied Science, and Mathematics of Computation [157]. Since a student can change his/her major from quarter to quarter, we assume a student's major is the major he or she declared in their last quarter. Due to the current data pipeline in place, the department only records student's first major field in his/her student record. Although a student can major in multiple disciplines, this data set does not reveal those students who obtained multiple degrees. For this work, we do not ever consider students in the Mathematics for Teaching or the Financial and Actuarial Mathematics major because there so few students in each. In the entire data set, there are only 84 students who declare as a Mathematics for Teaching major and only 73 for Financial and Actuarial Mathematics. The Financial and Actuarial Mathematics is a new major and has only been able since Fall 2014. However, the Mathematics for Teaching has been available to students since Winter 2007.

The *Class Standing* deals with what academic rank a particular student has due to their completed units [159]. There are four possible choices "Freshman", "Sophmore", "Junior", or "Senior". Class standing does not refer to the number of years a student has completed.

The *Admit Class* field refers to the class standing given to an incoming student due to his/her prior college-approved course credits. There are two types of incoming undergraduate students: freshman admits and transfer admits. Each of these incoming students can have two different admit classes. A freshman admit can have either a "Freshman" or "Sophmore" admit class, but not higher because there are caps on the total number of outside credits that such students can use toward their degree. Transfer admits can have either "Junior" or "Senior" admit class. These two types of incoming student navigate their coursework differently: transfer students have 2 years at UCLA, while freshman students have a full 4 years.

The *Subject* field indicates the department of the course from a particular row. The *Course* field is the numerical value of a class found in the course catalog [161]. Although we often include the full course names in our discussion, there are some instances where we refer to a course in number only. For convenience, we have Appendix A.1 that includes a table with course name and number. Although there are honor track courses, we ignored honors labeling. For example there is both an honors Real Analysis I and a non-honors Real Analysis I, and for this work, we consider them the same. In the UCLA Mathematics Department, courses numbered from 0–99 are *lower-division* courses [157]. These courses are viewed as foundational and can frequently fulfill requirements for other STEM majors. Courses numbered from 100–199 are *upper-division* courses and cover more advanced material [157]. Typically, students enrolling in these courses are mostly Mathematics majors.

The *Grade* field is a numerical score from 0.0 to 4.3 corresponding to letter grades [160]. We note that A-range grades occur in the interval [3.7, 4.3], B-range grades occur in the interval [2.7, 3.7); and C-range grades occur in the interval [1.7, 2.7). We frequently refer to such students as A, B, and C students, respectively. We do not further subdivide GPA categories in this work because in certain instances further subdivision can lead to inference on very small populations. For example, for students that average an A- (GPAs that lie in $[3.7, 3.85)$) there are only 20 such Pure Mathematics students. The population of A-range Pure Mathematics students is still relatively small with only 87 students in our data set. We do not specifically consider D-range or F-range students because the GPA requirements to complete any of the seven math majors pose a significant obstacle. Specifically, for each major anywhere for 12-15 courses beyond the six introductory courses are submitted to fulfill major requirements. For each of these submitted courses, a student must at least C grade. If there are courses that a student receives a C- or worse, these cannot be counted towards his/her degree. For simplicity, we assume that students with at least a 1.7 major GPA are those that will be able to eventually earn his/her degree.

The *CA Resident* and *U.S. Resident* fields refer to residency status in California and the U.S., respectively. A student's tuition is determined using his/her residency status.

We also discuss an important aspect of the mathematics curriculum–namely the set of required calculus and related introductory courses [157]. There are six introductory math courses that all students must take: Calculus I (Math 31A), Calculus II (Math 31B), Multivariable Calculus I (Math 32A), Multivariable Calculus II (Math 32B), Linear Algebra for Applications (Math 33A), and Differential Equation (Math 33B). A majority of students take these courses in this order. However, because many STEM departments only require a strict subset of these six courses, the math department has made it easier for students take the sequence in different orders [161]. For example, chemistry students are required to take all these courses except for Math 33A [155]. As a result, Math 33B does not require Math 33A even though the course numbers may suggest that it does [161]. Twenty-six percent of students that have taken at least 5 math courses that includes an upper-division math course (6,250 students total) took the introductory courses in a way that violated the sequence in the listed order at the beginning of this paragraph. We do not view courses taken concurrently as inconsistent with this order. While this is a sizable population that did not follow the standard order of introductory math courses, our rank aggregation methods should order courses to reflect how the majority of students select their coursework.

In the following section (Section 3.4), we review matrix techniques for rank aggregation and discuss their applicability for extracting global course sequences that are most consistent with the given data. Rank aggregation has been a powerful tool in Web search [71], sport rankings [37, 53], and more recently, grading schemes [172]. To our knowledge, it has not been used to infer trends in ordering temporal data [202, 211, 212].

3.4 Models and Methods for Rank Aggregation

Rank aggregation is the process of obtaining a single ranking from incomplete and noisy comparisons [71, 80]. In this section, we review a few different methods and models to rank aggregation. When possible, we connect the methods to our particular application: ordering courses from student schedules.

Rank aggregation considers n items to rank using the information from a set of comparisons. There are numerous applications of rank aggregation methods spanning from information technology to social choice. Some of the earliest applications were to model the perceived degree of various criminal offenses from vagrancy to murder [197]. Rank aggregation has also been used to construct voting systems in which voters rank candidates [151, 214], and it can also be used to crowd-source comparisons of movies, video games skill levels, online seller ratings, etc. [44, 70, 163]. It is also used to rank professional teams and athletes [37, 53, 163]. Moreover, the internet company Google uses rank aggregation methods to help infer the authority of websites and search the WWW [35, 89, 166].

The manner items are compared and the number of items compared in a single comparison may vary in different data sets. We assume all comparisons are pairwise, but for many practical applications, comparisons can consider comparisons that are made on a larger subset of items [71, 80]. Aggregating rankings from pairwise comparisons is rather common in professional sports. For example, National Collegiate Athletic Association (NCAA) ranks each team according to how well it performs in its regular season games (a pairwise comparisons of two teams) [37, 163]. We remark that comparisons of multiple items arise frequently in recommendation systems [70, 71]. For instance, MovieLens aggregates user film ratings to determine a list of best films: each user rates a subset of films and thus ranks these films [70].

Two types of pairwise comparison data can arise. There are *ordinal* comparisons in which the data ranks two items relative to each other. For example, in a sports league, an ordinal comparison of two teams is the identification of the winner in a head-to-head match up as the better team. There are also *cardinal* comparisons in items are scored individually or relatively. Again, using the sports league, a cardinal comparison between two teams may be the point totals in a head-to-head matchup or the difference of such totals. A cardinal comparison not only ranks two items, but also provides data about how much better one item is relative to another.

For our data set, we break up a student's schedule into several pairwise ordinal comparisons. Specifically, we rank course i lower than course j if course i came before course j in a student's schedule. We do not make cardinal comparisons between courses, as we do not consider the number of terms between courses. Such comparisons invariably require more careful constructions and are beyond the scope of this work. Our simplifying construction allows us to ignore complications associated to the varying speeds a student moves through his/her coursework. We also avoid complications from our data associated to summer quarter such as several missing summer quarters and the different way summer courses are organized (see Section 3.3).

There are many challenges extracting a single ranking from pairwise comparisons. First, many pairs of items are never compared. Second, the comparisons between items may not be evenly distributed with respect to all possible pairs. For example, the distribution of head-to-head matchups in a sports league may not be evenly distributed because teams located in the same geographic region may play each other more frequently than teams that are not. For our application, because different math majors have different course requirements, certain pairs of courses may rarely be taken by a students, and thus we are not able to compare the order of these courses. However, certain courses may be taken frequently in sequence providing multiple comparisons reinforcing the order such courses. Third, some of the comparisons may be "noisy." For example, a hidden variable can influence how comparisons are being made. A sports team may win all of its head-to-head matchups except one because its star player was ill. For course-sequence discovery, a "noisy" comparison may be the result of course availabilities, early-morning lectures, or a popular professor that influenced a student to not take courses in the recommended order.

For many of our methods, we translate the pairwise comparison data to a directed network. Let $G = (V, E)$ be a network, in which V are the n items to be ranked and E encode the pairwise comparisons. There are various ways to model the edges to represent pairwise comparisons. For example, if the pairwise comparisons are ordinal comparisons, the direction indicates which item is ranked higher: if i is ranked higher than j, then the edge is directed from i to j. We often describe these networks using a weight matrix $\mathbf{W}$. We also define the *measurement graph* $G_M = (V_M, E_M)$ as the graph whose nodes are the n items and edges between items i and j whenever these items are compared at least once.

We now discuss some of the generative models associated with rank aggregation. These models describe how rankings (and associated parameters) generate a set of pairwise comparisons. These models also provide synthetic benchmarks to evaluate a rank aggregation methods. We first discuss the Bradley–Terry–Luce (BTL) model [32, 124]. The BTL model takes a vector $\mathbf{x} \in \mathbb{R}^n$ as input, where n denotes the number of items compared and x_i represents the skill parameter associated to the i^{th} item. We assume all the components x_i are nonnegative. The BTL model produces a set of pairwise ordinal comparisons of the n items. Let i and j be two items and consider the l^{th} comparison between them. Let Y_{ij}^l be a random variable that takes values in $\{0, 1\}$ such that $Y_{ij}^l = 1$ if i is ranked higher than j in the l^{th} comparison and 0 otherwise. Note that $Y_{ij}^l = 1 - Y_{ji}^l$. This construction assumes there are no ties when items are compared. The BTL model specifies that

$$P(Y_{ij}^l = 1) = \frac{x_i}{x_i + x_j} \, . \tag{3.2}$$

To obtain a more general form, we select v_i such that $x_i = e^{v_i}$ for all $i = 1, \dots, n$ and write

$$P(Y_{ij}^l = 1) = \frac{1}{1 + e^{-(v_i - v_j)}} \, . \tag{3.3}$$

We can rewrite Eq. (3.3) as

$$P(Y_{ij}^l = 1) = F(v_i - v_j) \, , \tag{3.4}$$

where $F(x) = 1/(1 + e^{-x})$. The form of Eq. (3.4) can be generalized to other ordinal comparison models as long as F is the cumulative distribution function of a random variable symmetric about the origin [41, 81]. When F is the cumulative distribution function for a normal distribution with mean 0 and fixed variance, Eq. (3.4) is an example of the Thurston model [41, 197]. These generative models can be used to provide synthetic data sets for rank aggregation [53, 81, 152] in addition to describing simple mechanisms to relate rankings and comparisons [197].

However, rankings alone often do not adequately describe cardinal comparisons. For example, models that forecast professional sport scores in head-to-head matchups consider weather, player profiles, coaching strategies, and other inputs [86, 91]. Because of this complexity, generative models that produce cardinal comparison data often make simplifying assumptions. In [53], Cucuringu proposed a generative model for cardinal ranking called the Erdős–Rényi–Outlier (ERO) model with parameters $\mathbf{v}$, p, and r. Here, $\mathbf{v}$ is a vector of skill parameters for each of the n items, similar to the BTL model. The vector $\mathbf{v}$ is a permutation on $\{1, \ldots, n\}$. In other words, the map $i \mapsto v_i$ is a bijective function. To reduce complexity, the model considers the *rank offsets* R_{ij} defined to be

$$R_{ij} = v_i - v_j \,. \tag{3.5}$$

The ERO Model then outputs a network $G = (V, E)$ with weight matrix $\mathbf{W}$ with entries

$$W_{ij} = \begin{cases} R_{ij} & \text{with probability } (1-r)p \\ U_{R_{ij}} & \text{with probability } rp \\ 0 & \text{with probability } 1-p \end{cases} \tag{3.6}$$

when $i < j$ where $U_{R_{ij}}$ is a uniform, integer-valued random variable on $[-R_{ij}, R_{ij}]$. When $i > j$, we define $W_{ij} = -W_{ji}$; when $i = j$, $W_{ii} = 0$. This model specified in Eq. (3.6) can be generalized replacing R_{ij} with $R_{ij} + \varepsilon_{ij}$, where ε_{ij} is a Gaussian random variable with 0 mean and represents noise in the measurements. Unfortunately, even with these generative models, estimating parameters of a model with maximum likelihood estimation is problematic because comparisons may be incomplete or unevenly distributed among pairs [55]. In [44], Chen et al. applied expectation maximization on a related graphical model to approximate the parameters of the BTL model in the presence of incomplete and noisy comparisons.

To circumvent the challenge associated to noisy and incomplete comparison data, rank aggregation can be posed as a combinatorial problem on a network whose edges encode pairwise comparison data [90, 104, 163, 164]. This approach requires two steps. First, the pairwise comparisons are translated into a network model. We assume the weight matrix $\mathbf{W}$ is skew-symmetric. The entry $W_{ij} > 0$ implies that i is ranked higher than j; $W_{ji} < 0$ implies that j is ranked higher than i; and $W_{ij} = 0$ means i and j were never compared. Next, one extracts the rankings from the structure of the network. There are numerous network constructions that are possible. Often, several different network constructions are used for rank aggregation and then compared [81, 90, 104, 163]. We describe a particular model explored in [90, 104, 163] to elucidate how such a combinatorial problem can be posed.

Let's assume that for each pair i and j, there are L_{ij} cardinal pairwise comparisons. We also associate a score R_i^l with i and a score R_j^l with j with the l^{th} comparison. We construct a weight matrix $\mathbf{W}$ with entries that are the mean of the rank offsets for these comparison. Specifically,

$$W_{ij} = \begin{cases} \frac{1}{L_{ij}} \sum_{l=1}^{L_{ij}} (R_i^l - R_j^l) & L_{ij} > 0 \\ 0 & L_{ij} = 0 \ . \end{cases} \tag{3.7}$$

In [104, 163], Jiang et al. and Osting et al. ranked items according to the vector $\widehat{\mathbf{x}}$ that solves

$$\widehat{\mathbf{x}} = \underset{\mathbf{x}\,:\,\mathbf{1}_n^T\mathbf{x}=1}{\arg\min} \sum_{(i,j)\in E_M} |x_i - x_j - W_{ij}|^p \tag{3.8}$$

where $p = 1$ or 2; the vector $\mathbf{1}_n$ of length n all of whose entries are 1; and E_M are the edges in the measurement graph defined earlier in this section. There is the constraint $\mathbf{1}_n^T\mathbf{x} = 0$ because the addition of any constant to $\mathbf{x}$ does not alter the objective Eq. (3.8). The minimization in Eq. (3.8) is a continuous, convex optimization problem and an optimal solution can be found using a linear program as in [104]. When $p = 2$, the above problem can be well-approximated using low-rank matrix approximations [53, 89]. We refer to the later approach as a matrix method because it is reduced to a well-known numerical matrix routine such as the computation of eigenvalues/eigenvectors [60]. In the following section (Section 3.5), we discuss the matrix methods for rank aggregation that we apply for course-sequence discovery.

3.5 Matrix Methods for Rank Aggregation

We now discuss the methods for rank aggregation that we use for course-sequence discovery. These methods reduce rank aggregation to a numerical matrix computation. For clarity, we first discuss some preliminary network constructions in Section 3.5.1 to more easily describe ordinal course comparisons data. We then describe the different matrix methods in Sections 3.5.2–3.5.6 for rank aggregation and course-sequence discovery.

3.5.1 Preliminary Networks

In this section, we introduce some preliminary networks and notation to help describe this pairwise ordinal comparison data. Each method either uses or modifies the networks described here. Each network has nodes that represent courses. We consider directed edges to encode the frequency a course i was taken before course j.

The first model we consider defines directed edge weights to be the ratio of students that took courses in a particular order out of all the total students that took the courses in different quarters. Let $l = 1, \ldots, n_s$ be an enumeration of students. Let i and j be an enumeration of courses with $i, j = 1, \ldots, n_c$. We first define the indicator variable I_{ij}^l if student l took course i before course j

$$I_{ij}^l = \begin{cases} 1 & \text{if student } l \text{ took course } i \text{ before } j \\ 0 & \text{otherwise}. \end{cases}$$

Let the *count matrix* $\mathbf{C}$ be an $n_c \times n_c$ matrix such that

$$C_{ij} = \sum_{l=1}^{n_s} I_{ij}^l \quad \text{when } i \neq j,$$

and $C_{ij} = 0$ when $i = j$. Let the *proportion matrix* $\mathbf{P}$ be

$$P_{ij} = \frac{C_{ij}}{C_{ij} + C_{ji}}, \tag{3.9}$$

whenever $C_{ij} + C_{ji} > 0$. If $C_{ij} = C_{ji} = 0$, then we define $P_{ij} = P_{ji} = 0$. By construction, $P_{ij} + P_{ji} = 1$ when course i and course j have been taken in different quarters at least once. The proportion matrix $\mathbf{P}$ defines a directed multigraph in which an edge weight P_{ij} approximates the flow of students moving from course i to course j. In Figure 3.1, we illustrate a portion of the network model using three courses: Discrete Structures (Math 61), Linear Algebra I (Math 115A), and Real Analysis I (Math 131A). We have only considered Applied Mathematics students to construct the edge weights of the network; there were 672 students total. Of these students, there were 437 Applied Mathematics Students that took Real Analysis I (Math 131A) and Linear Algebra I (Math 115A) in different quarters. Only 24 students of the 437 took real analysis first. The appropriate proportion is applied in the edge weight (0.056) from Real Analysis I to Linear Algebra I.

We now define the *flow matrix* $\mathbf{F}$. Let $\mathbf{F}$ be a skew-symmetric matrix of size $n_c \times n_c$ with $|F_{ij}| \in [0.5, 1]$. Using P_{ij} (Eq. (3.9)), define F_{ij} as

$$F_{ij} = \begin{cases} P_{ij} & \text{if } P_{ij} \geq 0.5 \\ P_{ij} - 1 & \text{if } P_{ij} < 0.5 \ . \end{cases} \tag{3.10}$$

For example, if 70% of the students (who took both courses i and j) attended course i before j, then we set $F_{ij} = 0.7$ and $F_{ji} = -0.7$. The matrix $\mathbf{F}$ defines a multigraph such that edge weights encodes the flow of the majority of students between two courses. Many of the rank aggregation methods require a skew-symmetric matrices as in Eq. 3.8. Several other choices for candidate skew-symmetric matrices are explored in [90] such as $\mathbf{F}_p = \mathbf{P} - \mathbf{P}^T$, where $\mathbf{P}$ is the proportion matrix defined in Eq. (3.9).

We also briefly review the terminology of a (discrete time) *Markov chain* in the context of a student moving through coursework. A complete treatment can be found in [69]. We assume a student is enrolled in precisely one of the n_c courses at time discrete time steps $t = 1, 2, \ldots$. The model assumes that, with each subsequent time step, the student can move to a new course repeating courses as needed. We define the probability that a student enrolls in course j is taken after course i as the the *transition probability* T_{ij} and T_{ij} does not depend on t (time homogeneity). We also assume that the probability that course j is taken after i is independent of the courses taken prior to i (Markov property). The *transition matrix* $\mathbf{T}$ associated with this Markov chain has entries given as T_{ij}. We can associate a directed network structure with $\mathbf{T}$ if we view $\mathbf{T}$ as a weight matrix.

For Markov chains, we investigate systems as $t \to \infty$. Let $\mathbf{q}_t$ be the $n_c \times 1$ vector whose i^{th} entry denotes the probability that a student is at course i in the t^{th} time step. For normalization, $\sum_{i=1}^{n_c} (q_t)_i = 1$. From our construction above, the following equation holds for all t

$$\mathbf{q}_t^T = \mathbf{q}_{t-1}^T \mathbf{T} \ . \tag{3.11}$$

We define the *stationary distribution* $\mathbf{q}_\infty$ associated to Markov chain as the vector that satisfies

$$\mathbf{q}_\infty^T = \mathbf{q}_\infty^T \mathbf{T} \ .$$

This defines a linear system of equations. In certain cases, we can compute the stationary distribution as

$$\mathbf{q}_\infty^T = \lim_{t\to\infty} \mathbf{q}_0^T \mathbf{T}^t \ , \tag{3.12}$$

independent of an initial condition $\mathbf{q}_0$ as is common for several rank aggregation methods [89]. In [69,123], there are conditions that guarantee the limit in Eq. (3.12) exists and equals the stationary distribution. As another example, if we assume that a Markov chain denotes the movement of a walker along an undirected graph, then Eq. (3.12) holds as long as the graph is not bipartite [123]. We use Eq. (3.12) to approximate a stationary distribution via power iteration (a spectral method discussed [60]).

3.5.2 PageRank

PageRank ("bringing order to the Web" [166]) ranks the authority of websites by computing the stationary distribution of a random web surfer who either moves to an adjacent website via a hyperlink or moves uniformly at random anywhere in the network [35,89,166]. In [37], the authors adapted a similar framework to model voters in the NCAA poll and extract football rankings based on regular season matchups.

We use PageRank to determine a course sequence. Recall our construction of the proportion matrix $\mathbf{P}$ from Eq. (3.9). We define a transition $\mathbf{S}_\alpha$ to describes the motion of a student. This transition matrix $\mathbf{S}_\alpha$ is

$$\mathbf{S}_\alpha^{\text{pr}} = (1-\alpha)\mathbf{D}^{-1}\mathbf{P} + \alpha\left(\frac{1}{n_c}\mathbf{1}_{n_c\times n_c}\right) \ , \tag{3.13}$$

where $\alpha \in (0,1)$, $\mathbf{1}_{n_c\times n_c}$ is the $n_c \times n_c$ matrix of all 1s, and $\mathbf{D}$ is the diagonal matrix of out degrees related to $\mathbf{P}$ (i.e. $d_{ii} = \sum_j P_{ij}$). The first term $(1-\alpha)\mathbf{D}^{-1}\mathbf{P}$ indicates that with probability $(1-\alpha)$ a student at course i travels to an adjacent node j in the network with probability $p_{ij}/\sum_{j'} p_{ij'}$. The second term $\alpha\left(\frac{1}{n_c}\mathbf{1}_{n_c\times n_c}\right)$ determines with probability α that the student moves to any other course uniformly at random. One observes that

$$\frac{1}{n_c}\mathbf{1}_{n_c\times n_c} = \mathbf{1}_{n_c} \cdot \left(\frac{1}{n_c}\mathbf{1}_{n_c}^T\right) \ ,$$

and the latter vector $\frac{1}{n_c}\mathbf{1}_{n_c}^T$ is the uniform distribution on the n_c courses. One can generalize Eq. (3.13) replacing $\frac{1}{n_c}\mathbf{1}_{n_c}^T$ with an arbitrary distribution $\mathbf{v} \in \mathbb{R}^{n_c}$ on the n_c courses with $\sum_i v_i = 1$ from normalization. Specifically,

$$\mathbf{S}_\alpha^{\text{pr}} = (1-\alpha)\mathbf{D}^{-1}\mathbf{P} + \alpha\left(\mathbf{1}_{n_c}\mathbf{v}^T\right) \ . \tag{3.14}$$

The movement determined in the second term of Eq. (3.14) is called *teleportation* and $\mathbf{v}$ as the vector of *teleportation probabilities.* One associates a Markov chain with states $\mathbf{q}_t$ at time t with $\mathbf{S}_\alpha^{\text{pr}}$ and the transition rule:

$$(\mathbf{q}_{t+1})^T = (\mathbf{q}_t)^T\mathbf{S}_\alpha^{\text{pr}} \ . \tag{3.15}$$

The *PageRank vector* $\mathbf{q}_\infty$ is defined to be the stationary distribution associated to the Markov chain in Eq. (3.15) and computed as a limit, $\lim_{t\to\infty}\mathbf{q}_t$. In our case, the ith component of $\mathbf{q}_\infty$ gives the ranking of course i. The smaller $(\mathbf{q}_\infty)_i$ for a course i, the more likely a student is to take course i early in his/her sequence. From this ordering, we extract a global ranking for ordering courses. We use power iteration to obtain $\mathbf{q}_\infty$ and find that 200 iterations are sufficient to ensure a relative error $||\mathbf{q}^{k+1} - \mathbf{q}^k||_1 < 10^{-10}$. We remark that PageRank is guaranteed to converge to the stationary distribution via power iteration as noted in Theorem 2.2 of [89].

Teleportation is required to ensure that all courses have nonzero stationary probability. When the stationary distribution is determined entirely by $\mathbf{P}$ ($\alpha = 0$), many entries in $\mathbf{q}_\infty$ are 0 as $t \to \infty$. For example, if a student takes Calculus I (Math 31A), this is his/her first math course. We exclude Precalculus in our network construction because fewer than 1% of math majors take this course. As a result, there are no in-edges for Calculus I in our network when $\alpha = 0$ and the stationary probability associated to Calculus I is 0. Similarly, when a student takes Calculus II (Math 31B), it is either the first math course taken or taken after Math 31A. As a result, the stationary probability of Calculus II is 0 as its only in edge is 0. Therefore, we cannot differentiate the order of Calculus I and Calculus II when $\alpha = 0$. Similar problems exist for the six lower-division calculus courses: Math 31AB, 32AB, and 33AB. In our applications, we select $\alpha = .15$ as in the original work [166]. We make

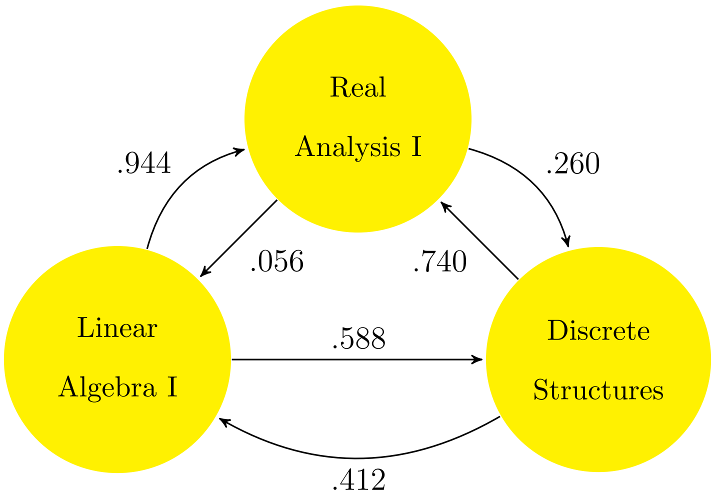

Figure 3.1: A subgraph corresponding to the proportion matrix $\mathbf{P}$ defined Eq. (3.9) for Applied Mathematics majors. Each node represents a course; for this subgraph, we selected Linear Algebra I (Math 115A), Real Analysis I (Math 131A), and Discrete Structures (Math 61). The edge weight P_{ij} from course i to j indicates the proportion of students that took i in an earlier quarter than j out of all those students that took the pair of courses in different quarters.

this selection not to align with prior applications of PageRank, but to ensure that the the six introductory courses are ordered as Math 31A, Math 31B, Math 32A, Math 32B, 33A, and Math 33B (see Section 3.3 for a discussion). In our experiments, these introductory math courses were correctly ordered for α between .13 and .17. We examine a type of personalized PageRank [89] to further differentiate early and late coursework. Specifically, we first compute $\mathbf{q}_\infty$ using Eq. (3.13) and then set $\mathbf{v} = \mathbf{1}_n - \mathbf{q}_\infty$ when we apply Eq. (3.14) again.

3.5.3 Rank Centrality

In [152], the method of Rank Centrality was proposed to recover the parameters associated to the BTL model from a set of pairwise comparisons (Section 3.4). Let $\mathbf{x}$ be the vector of parameters associated to the BTL model. The goal of the network construction is to produce a Markov chain with transition probability T_{ij} proportional to $\frac{x_i}{x_i+x_j}$. Rank Centrality defines a Markov chain on the n_c courses with the following transition matrix

$$\mathbf{S}^{\mathrm{rc}} = \frac{1}{d_{\max}}\mathbf{P} + \left(\mathbf{I}_{n_c} - \frac{1}{d_{\max}}\mathbf{D}\right), \tag{3.16}$$

where $\mathbf{D}$ is the diagonal matrix of out-degrees given as $d_{ii} = \sum_j P_{ij}$, $d_{\max}$ is the maximum out-degree of all course nodes in the network, and $\mathbf{I}_{n_c}$ is the $n_c \times n_c$ identity matrix. To obtain the rankings from the Markov chain of Eq. (3.16), we determine the stationary distribution $\mathbf{q}_\infty$ by computing the top eigenvector of $(\mathbf{S}^{\mathrm{rc}})^T$. This is the numerical method prescribed in [152], which is guaranteed to be the stationary distribution because $\mathbf{S}^{\mathrm{rc}}$ has both row and column sums 1 [152]. Again, the smaller $(\mathbf{q}_\infty)_i$, the more likely a student takes course i early in his/her sequence. Rank Centrality recovers $\mathbf{x}$ as long as the pairwise comparison data is distributed uniformly among pairs (see Theorem 2 of [152]). In our numerics in Section 3.6, Rank Centrality does poorly in certain cases. Specifically, Rank Centrality poorly orders advanced classes that are offered infrequently. We conjecture that such classes are highly correlated with a particular sequence within a major and are not compared to the full range of classes that are taken. One possible way to explore this poor performance would be to extract sequences of students that took these poorly ordered courses and compare them to the larger population. Because the other five rank aggregation methods produced sequences that were in relative agreement (see Table 3.2 and Table 3.2), we did not examine this aspect of Rank Centrality further.

3.5.4 SerialRank

SerialRank [81] adapts the seriation problem proposed in [11] to determine a global ranking of items, which we now detail. The seriation problem is the problem of determining an ordering of n items given a real-valued similarity function f so that items closer together in the ordering are more similar than items farther apart [11]. Precisely, if $\pi(i) < \pi(j) < \pi(k)$ is an ordering of the three elements i, j, and k, then $f(i,j) \geq f(i,k)$ and $f(j,k) \geq f(i,k)$. For SerialRank, one defines a similarity function that counts how frequently two courses are ordered similarly relative to other courses. To construct the similarity matrix, we first define the *comparison matrix* $\mathbf{A}_k$ for course k as

$$(A_k)_{ij} = 1 - \frac{|P_{ik} - P_{jk}|}{2} \quad \text{whenever } P_{ik} \neq 0 \text{ and } P_{jk} \neq 0$$

where P_{ij} is the proportion matrix (Eq. (3.9)). If either course i or course j has not been taken in sequence with k, we define $(A_k)_{ij} = \frac{1}{2}$. The comparison matrix A_k counts how frequently course i and course j are ordered similarly relative to k. The similarity matrix $\mathbf{S}^{\text{sr}}$ is then determined by summing over all possible comparison matrices

$$\mathbf{S}^{\text{sr}} = \sum_{k=1}^{n_c} \mathbf{A}_k.$$

We can then subtract the minimum value of $\mathbf{S}^{\text{sr}}$ from all the entries of $\mathbf{S}^{\text{sr}}$ so that those courses with minimum similarity now have similarity of 0. To determine a ranking from $\mathbf{S}^{\text{sr}}$, we form the *(combinatorial) graph laplacian* $\mathbf{L}$ and rank the courses using the components of the Fiedler vector [81]. The graph laplacian $\mathbf{L}$ is defined as

$$\mathbf{L} = \mathbf{D} - \mathbf{S}^{\text{sr}} .$$

The *Fiedler vector* is the eigenvector associated to the smallest nonzero eigenvalue of $\mathbf{L}$. Our rankings can are extracted from $\mathbf{q}$. We interpret $\mathbf{q}$ as approximation to a NP-hard ranking problem described in [11]:

$$\mathbf{q} = \underset{\mathbf{p} \in S_{n_c}}{\arg\min} \sum_{i,j} s_{ij}^{\text{sr}} (p_i - p_j)^2 , \tag{3.17}$$

where S_{n_c} is the subset of vectors with integer entries representing permutations on the set $\{1, 2, \ldots, n_c\}$ such that $i \mapsto p_i$. First, we observe that $\sum_{i,j} s_{ij}^{\text{sr}} (p_i - p_j)^2 = (\mathbf{p})^T \mathbf{L} \mathbf{p}$. Then, we allow $\mathbf{p} \in \mathbb{R}^{n_c}$ and relax Eq. (3.17) into a minimization that is solved by the the eigenvector associated to the smallest nonzero eigenvalue of $\mathbf{L}$:

$$\mathbf{q} = \underset{\mathbf{p} \in \mathbb{R}^{n_c} \,:\, ||\mathbf{p}||=1}{\arg\min} (\mathbf{p})^T \mathbf{L} \mathbf{p} .$$

After ordering the n_c courses using the components of $\mathbf{q}$, we obtain a course sequence. In [81] (Proposition 2.4), the authors provide guarantees on recovery of the ranking if the pairwise comparisons are drawn from a BTL model and sufficiently many comparisons from each possible pair are obtained. In [81], the authors rank teams in the English Premier Soccer League and competitors on TopCoder.com and both compare favorably to the true rankings of each data set.

3.5.5 SyncRank

In [53], Cucuringu formulated rank aggregation as an instance of *angular synchronization*, which we now discuss. *Group synchronization* reconstructs a finite subset $S \subset G$ of a group G given a set M of measurements of the form

$$M = \left\{ m_{ij} \;\mid\; m_{ij} = g_1 g_2^{-1}, \;\; g_1, g_2 \in S \right\}.$$

In [188], Singer studied the angular synchronization problem, a special case of the above where $G = SO(2) = \{\mathbf{S} \mid \mathbf{S} \in \mathbb{R}^{2\times 2}, \; \det(\mathbf{S}) = 1\}$. Elements of $SO(2)$ can be identified with $z \in \mathbb{C}$ with $|z| = 1$, where $|\cdot|$ is the norm of a complex number. If we write $z = e^{\mathrm{i}\theta}$, the group operation is given as complex multiplication: $e^{\mathrm{i}\theta_1} e^{\mathrm{i}\theta_2} = e^{\mathrm{i}(\theta_1+\theta_2)}$ whenever $e^{\mathrm{i}\theta_1}, e^{\mathrm{i}\theta_2} \in SO(2)$. We can also identify each element $e^{\mathrm{i}\theta} \in \mathbb{C}$ with $\theta \in [0, 2\pi)$ so that the complex multiplication becomes addition modulo 2π. The angular synchronization problem can be stated as a set of measurements M with elements

$$\Theta_{ij} = \theta_i - \theta_j \pmod{2\pi}. \tag{3.18}$$

Singer assumed that each Θ_{ij} of M is corrupted with additive zero-mean Gaussian noise and that $|M| \ll \binom{|S|}{2}$. Singer introduced a spectral method for approximating the set $S = \{\theta_1, \ldots, \theta_n\}$ from Θ_{ij} [188]. We observe that, for any $\omega \in [0, 2\pi)$, the set $S + \omega = \{\theta + \omega \pmod{2\pi} \mid \theta \in S\}$ produces the same set of Θ_{ij}. Accordingly, once we recover $\theta_1, \ldots, \theta_n$, we must use some additional information to determine a suitable phase ω to add to each angle.

We now relate the angular synchronization problem to rank aggregation. As in [53], we refer to this method as SyncRank. Suppose we have cardinal comparisons Θ_{ij} that determine a skew-symmetric matrix as in Eq. (3.18). The spectral method of [188] guarantees we can recover real numbers $\theta_i \in [0, 2\pi)$ such that $\theta_i - \theta_j \approx \Theta_{ij}$ as long as there are sufficiently many measurements Θ_{ij} and the pairs are uniformly distributed among possible pairs. After suitable rotation, we can then rank courses according to the recovered θ_i. To obtain a suitable skew symmetric Θ_{ij} for this method, we define $\Theta_{ij} = \pi F_{ij}$ (Eq. (3.10) in Section 3.5.1). Note that there are several other methods to construct a skew-symmetric matrices from ordinal (or cardinal) comparisons as in [90]. With this skew-symmetric $\pi\mathbf{F}$, SyncRank correctly orders the six introductory math courses (Math 31AB, Math 32AB, Math 33AB) for all seven math majors. W use this ordering of courses to tune α in our application of PageRank in Section 3.5.2 and noted in that section that a majority of students do not violate this sequence. As a result, we did not explore other skew-symmetric matrices.

We now discuss the matrix formulation of angular synchronization and its spectral relaxation [188]. We first build a $n_c \times n_c$ Hermitian matrix $\mathbf{H}$ with

$$H_{ij} = \begin{cases} e^{\mathrm{i}\Theta_{ij}}, & \text{if } C_{ij} + C_{ji} > 0 \\ 0 & \text{otherwise} \end{cases} .$$

where $\mathrm{i} = \sqrt{-1}$. First, we note that

$$\left|e^{-\mathrm{i}\theta_j} H_{ij} e^{\mathrm{i}\theta_i}\right|^2 = \left|e^{-\mathrm{i}\theta_j} e^{\mathrm{i}\Theta_{ij}} e^{\mathrm{i}\theta_i}\right|^2 \leq 1 \; . \tag{3.19}$$

Suppose that $\Theta_{ij} = \theta_i - \theta_j \pmod{2\pi}$ for angles $\theta_1, \ldots, \theta_{n_c}$. Then, for each $i = 1, \ldots, n_c$, Eq. (3.19) obtains its maximum value of 1. We thus write the angular synchronization problem as

$$\mathbf{z} = \underset{\mathbf{w} \in \mathbb{C}^{n_c} \,:\, |w_i| = 1}{\arg\max} \; ||\overline{\mathbf{w}}^T \mathbf{H} \mathbf{w}||_2 \; . \tag{3.20}$$

Note the constraint on $\mathbf{w}$ in Eq. (3.20) is non-convex. We solve the angular synchronization problem via its spectral relaxation

$$\mathbf{v} = \underset{\mathbf{w} \in \mathbb{C}^{n_c} \,:\, ||w||_2 = n_c}{\arg\max} \; ||\overline{\mathbf{w}}^T \mathbf{H} \mathbf{w}||_2 \; . \tag{3.21}$$

Note that the constraint that $|w_i| = 1$ is stronger than $||\mathbf{w}||_2 = n_c$. We solve Eq. (3.21) finding the largest eigenvector of $\mathbf{H}$. We approximate $\mathbf{z}$ from Eq. (3.20) as

$$z_i = e^{\mathrm{i}\theta_i} = \frac{v_i}{|v_i|}$$

for $i = 1, 2, \ldots, n_c$. We extract the corresponding angles $\theta_1, \ldots, \theta_{n_c}$. These angles are correct up to a circular permutation because, for any $\omega \in [0, 2\pi)$, the vector $e^{\mathrm{i}\omega}\mathbf{v}$ is also an eigenvector of $\mathbf{H}$. To determine the correct ranking, we use the consistency coefficient that we introduce in Section 3.5.8 (Eq. (3.26)).

3.5.6 Least Squares

We now discuss the method of [97] for course-sequences discovery. This method uses the framework introduced in Eq. (3.8) in Section 3.4. Assume we are given a network with a skew symmetric weight matrix $\mathbf{W}$. Let $k = 1, \ldots, |E_M|$ be enumeration of edges $e_k \in E_M$ of the measurement graph G_M. Define the gradient operator associated to this enumeration as

$$B_{ik} = \begin{cases} 1 & \text{if } e_k = (i,j) \text{ and } i > j \\ -1 & \text{if } e_k = (i,j) \text{ and } i < j \ . \end{cases} \tag{3.22}$$

Observe that $\mathbf{B} \in \mathbb{R}^{|E_M| \times n_c}$. Let $\mathbf{w}$ be a vector of size $|E_M| \times 1$ that includes only the nonzero entries of $\mathbf{W}$. We assume that $W_{ij} = W_{ji} = 0$ precisely when i and j have not been compared and so there is no edge in the measurement graph G_M. The enumeration of edges to construct $\mathbf{B}$ should agree with $\mathbf{w}$. Then Eq. (3.8) can be rewritten as

$$\underset{\mathbf{x} \in \mathbb{R}^{n_c} \,:\, \mathbf{1}_n^T \mathbf{x} = 0}{\text{minimize}} \ ||\mathbf{B}\mathbf{x} - \mathbf{w}||_2^2. \tag{3.23}$$

We assume that $n_c < |E_M|$; this is always the case in our data set as the number of courses is much less than the pairs of courses that co-occurr in a student's schedule. This assumption means that Eq. (3.23) is an over-determined system. We apply least-squares [60] to determine $\mathbf{x}$. In our applications, we use the skew-symmetric $\mathbf{F}$ (Eq. (3.10)) as a weight matrix $\mathbf{W}$.

3.5.7 Ranking via Singular Value Decomposition

We now discuss a rank aggregation method that assumes a skew-symmetric weight matrix $\mathbf{W}$ has a low-rank approximation. These methods were introduced in [53,90]. We follow [53] and apply the *Singular Value Decomposition* (SVD) to obtain a low-rank approximation. Recall a special case of the Singular Value Decomposition of a real $n_c \times n_c$ matrix $\mathbf{W}$ is

$$\mathbf{W} = \mathbf{U}\mathbf{\Sigma}\mathbf{V}^T \,,$$

where $\mathbf{U} = [\mathbf{u}_1 \mathbf{u}_2 \ldots \mathbf{u}_{n_c}]$ and $\mathbf{V} = [\mathbf{v}_1 \ldots \mathbf{v}_{n_c}]$ are unitary matrices such that each $\mathbf{u}_i$, $\mathbf{v}_i$ are unit-length column vectors and $\mathbf{\Sigma}$ is a diagonal matrix of *singular values* given by $\sigma_1, \ldots, \sigma_n$

[60]. Each $\mathbf{u}_i$ is a *left singular vector* and each $\mathbf{v}_i$ is the *right singular vector*. If all but the top two singular values are negligible in size relative to σ_1 and σ_2, then we can approximate $\mathbf{W}$ as a rank-2 matrix. Specifically,

$$\mathbf{W} \approx \sigma_1 \mathbf{u}_1 \mathbf{v}_1^T + \sigma_2 \mathbf{u}_2 \mathbf{v}_2^T \, . \tag{3.24}$$

We observe that the rank of $\mathbf{W}$'s approximation is determined entirely by $\mathbf{v}_1$ and $\mathbf{v}_2$ and we refer to these as the *top (right) singular vectors*. In [90], Gleich applied techniques from compressive sensing to determine a low-rank approximation of $\mathbf{W}$.

For our application, we assume that $\mathbf{v}$ is an $n_c \times 1$ vector such that v_i provides a numerical score associated to the rank of a course. Let $\mathbf{R}$ be the matrix of rank offsets associated to this vector $\mathbf{v}$ given as $R_{ij} = v_i - v_j$ (see Eq. (3.5)). We observe that $\mathbf{R}$ has rank 2 because

$$\mathbf{R} = \mathbf{v}\mathbf{1}_{n_c}^T - \mathbf{1}_{n_c}\mathbf{v}^T \, , \tag{3.25}$$

where $\mathbf{1}_{n_c}$ denotes the all-ones column vector of size $n_c \times 1$. We assume that a skew-symmetric weight matrix $\mathbf{W}$ can be approximated by $\mathbf{R}$. To obtain a decomposition as in Eq. (3.25) of $\mathbf{W}$, we assume $\mathbf{v}$ is approximately a scalar multiple of one of the top two singular vectors $\mathbf{v}_1$ or $\mathbf{v}_2$ given in Eq. (3.24). As in Section 3.5.6, we set $\mathbf{W} = \mathbf{F}$ (Eq. (3.10)). Because we obtain singular vectors $\mathbf{v}_1$ and $\mathbf{v}_2$ up to sign, we must also compare (the reversed) rankings associated to $-\mathbf{v}_1$ and $-\mathbf{v}_2$. We choose the ranking that has the highest consistency coefficient that we introduce in Section 3.5.8 (Eq. (3.26)).

3.5.8 Evaluating a Course Sequence

To compare extracted course sequences from each of the methods above, we need a measure that demonstrates how well a particular sequence agrees with our student data. We assume that a hidden course sequence determines the order in which courses are taken. However, there is no underlying ground truth course sequence that we can use to measure the accuracy of an extracted sequence. Moreover, rank aggregation should not be viewed as a model for forecasting course orders, but rather a tool to better analyze high-dimensional space of course schedules. Also, we do not expect exact agreement of course orders from the different rank aggregation methods we apply. For example, in [53, 81], English Premier soccer teams were ranked using several different methods according to the head-to-head matchups played during the regular season. Of the eight methods applied, there was no consensus on the top ranked team.

There are several different methods for evaluating rankings when ground truth is known and when it is not [44, 53, 71, 152]. We define a measure similar to a measure that can be found in [53, 152]. Let $\mathbf{q}$ be the score vector of our courses such that $q_i < q_j$ implies that course i comes before course j in the sequence. If two courses i and j can be taken in any order and are offered with similar frequency, our null hypothesis is that $P_{ij} = P_{ji}$. Because $P_{ij} + P_{ji} = 1$, we also have that $P_{ij} = P_{ji} = .5$. However, if two courses are offered with similar frequency and course i depends on course j or course j depends on course i, then the alternate hypothesis is $P_{ij} \neq .5$. We define the consistency coefficient $\mathrm{K}(\mathbf{q})$ to measure the refutation of our null hypothesis over every possible pair in our ordered sequence. Specifically, the formula is

$$\mathrm{K}(\mathbf{q}) = \frac{4}{n^2 - n} \sum_{q_i < q_j} (P_{ij} - .5) = \frac{2}{n^2 - n} \sum_{q_i < q_j} (P_{ij} - P_{ji}) \,. \tag{3.26}$$

The coefficient in front of the sum ensures that $\mathrm{K}(\mathbf{q}) \in [-1, 1]$. When the courses are taken in random order by students, we expect $\mathrm{K}(\mathbf{q}) \approx 0$ for any ranking $\mathbf{q}$. On one hand, if all students take their courses in a single linear order determined by $\mathbf{q}$, then $\mathrm{K}(\mathbf{q}) = 1$. On the other hand, if the courses were all taken the reverse order determined by $\mathbf{q}$, then $\mathrm{K}(\mathbf{q}) = -1$. We can use the consistency coefficient to compare a pair of courses. If we consider two vectors $\mathbf{q}_1$ and $\mathbf{q}_2$ from different rank aggregation methods, with $\mathrm{K}(\mathbf{q}_1) \geq \mathrm{K}(\mathbf{q}_2)$, we conclude that for any course i coming before course j in the extracted sequence of $\mathbf{q}_1$ the mean difference $P_{ij} - P_{ji}$ over all such pairs is greater than or equal to the same mean for $\mathbf{q}_2$. Additionally, using $\mathrm{K}(\mathbf{q})$, we can measure how consistently a particular population takes courses in the same order as $\mathbf{q}$. No population we consider is aligned perfectly with the extracted course sequence so $\mathrm{K}(\mathbf{q}) < 1$. The closer $\mathrm{K}(\mathbf{q})$ is to 1, the closer the mean $P_{ij} - P_{ji}$ is to 1 for each course i coming before course j in the extracted sequence.

There are several ways to refine the consistency coefficient $\mathrm{K}(\mathbf{q})$, which we will explore in future work. First, it would be helpful to incorporate the number of terms between course i and course j in a meaningful way. However, as noted in Section 3.4, students go through course offerings at different speeds and spend different amounts of time completing their required coursework (e.g. incoming transfers versus freshman). Moreover, the distance between each term is not uniform (e.g. summer break discussed in Section 3.3 breaks up spring and fall terms). Second, comparing the numerical scores associated to q_i and q_j may be interesting as we expect from most methods $q_i \ll q_j$ means not only that course i comes after j, but more frequently. A natural avenue for exploration would be the modification

$$\widetilde{\mathrm{K}}(\mathbf{q}) = \frac{4}{n^2 - n} \sum_{q_i < q_j} (q_j - q_i)(P_{ij} - .5),$$

where we have normalized $||\mathbf{q}||_2 = 1$. Third, the measure we define in Eq. (3.26) views each course comparison as equally important, but the number of students taking a pair of courses is ignored. For instance, a ranking that correctly orders a pair of required courses both with high enrollment should be more valuable than a ranking that orders a pair of specialized courses with relatively low enrollment. These improvements will be explored in future work.

3.6 Course-Sequence Discovery

We now apply the six methods discussed in Section 3.5 to the student data described in Section 3.3. This section is organized as follows. We compare each of the course sequences obtained by the six matrix methods. We also discuss how the extracted course sequence compares to the prerequisites in the UCLA general catalog [161] and the recommendations provided by the UCLA department of mathematics [157]. In Section 3.6.2, we then compare the course sequences of high and low performing students and identify possible hidden dependencies between courses.

3.6.1 Evaluating the Matrix Methods

In this section, we discuss some of the results when we apply rank aggregation to various segments of the student population (see Section 3.3). When applying a method, we construct

Table 3.2: Course Sequences for Applied Mathematics Majors obtained by three of the six methods discussed in this chapter.

PageRank	**Rank Centrality**	**SerialRank**
Linear Algebra I	Linear Algebra I	Linear Algebra I
Discrete Structures	Discrete Structures	Discrete Structures
Real Analysis I	Applied Algebra	Real Analysis I
Probability I	Partial Diff. Equations	Probability I
Numerical Analysis I	Mathematical Modeling	Numerical Analysis I
Nonlinear Systems	Real Analysis I	Nonlinear Systems
Complex Analysis	Abstract Algebra I	Abstract Algebra I
Abstract Algebra I	Game Theory	Complex Analysis
Real Analysis II	Complex Analysis	Real Analysis II
Graph Theory	Numerical Analysis II	Graph Theory
Mathematical Modeling	Numerical Analysis I	Mathematical Modeling
Actuarial Mathematics	Graph Theory	Actuarial Mathematics
Ordinary Diff. Equations	Probability I	Ordinary Diff. Equations
Applied Algebra	Nonlinear Systems	Applied Algebra
Optimization	History of Mathematics	History of Mathematics
History of Mathematics	Probability II	Probability II
Probability II	Actuarial Mathematics	Optimization
Numerical Analysis II	Real Analysis II	Game Theory
Game Theory	Ordinary Diff. Equations	Numerical Analysis II
Partial Diff. Equations	Optimization	Partial Diff. Equations

Table 3.3: Course Sequences for Applied Mathematics Majors obtained by the three of the six methods discussed in this chapter.

SVD	**Least Squares**	**SyncRank**
Linear Algebra I	Linear Algebra I	Linear Algebra I
Discrete Structures	Discrete Structures	Discrete Structures
Real Analysis I	Real Analysis I	Real Analysis I
Probability I	Probability I	Probability I
Nonlinear Systems	Numerical Analysis I	Numerical Analysis I
Numerical Analysis I	Nonlinear Systems	Nonlinear Systems
Complex Analysis	Complex Analysis	Complex Analysis
Abstract Algebra I	Abstract Algebra I	Abstract Algebra I
Real Analysis II	Real Analysis II	Actuarial Mathematics
Graph Theory	Graph Theory	Graph Theory
Actuarial Mathematics	Mathematical Modeling	Real Analysis II
Mathematical Modeling	Actuarial Mathematics	Applied Algebra
Applied Algebra	Applied Algebra	Mathematical Modeling
Ordinary Diff. Equations	Ordinary Diff. Equations	Ordinary Diff. Equations
History of Mathematics	History of Mathematics	History of Mathematics
Probability II	Optimization	Probability II
Optimization	Probability II	Optimization
Numerical Analysis II	Numerical Analysis II	Numerical Analysis II
Game Theory	Game Theory	Game Theory
Partial Diff. Equations	Partial Diff. Equations	Partial Diff. Equations

the relevant matrix (e.g. the flow matrix **F**) using only students from this population. In all of our applications, we remove courses in which fewer than 10% of a population enrolled in order to more easily identify trends. We did not observe relative changes in an extracted sequence when we lowered the enrollment threshold from 5–15% in our numerical experiments. Specifically, when we compared a sequence in which we excluded courses with fewer than 5% enrollment to a sequence with fewer than 10%, the relative positions of individual courses in both sequences was unchanged except for Rank Centrality, which we detail below.

We first discuss how the extracted course sequence matched the prerequisites in the course catalog [161] and capture trends in student course selection we discussed in Section 3.3. First, all the methods ordered the six introductory math courses (Section 3.3) as Calculus I (Math 31A), Calculus II (Math 31B), Multivariable Calculus I (Math 32A), Multivariable Calculus II (Math 32B), Linear Algebra for Applications (Math 33A), and Differential Equation (Math 33B), for each math major. This provides some indication that all the methods correctly identify that a majority of students take introductory courses in this order (see Section 3.3). In Table 3.2 and Table 3.3, we compare the output sequences beyond these introductory courses for all six methods on Applied Mathematics majors with A-range GPAs. We inspect Applied Math majors because they are the largest of the seven possible math majors. We focus A students because we expect this smaller population ($n_s = 140$) to select similar coursework. When we further subdivided students between A-, A, and A+ GPAs, we did not notice variation in the extracted course sequence. In Table 3.2 and Table 3.3, all methods place Linear Algebra I and Real Analysis I early in the sequence as these are courses required for all math majors. In fact, the department explicitly encourages students to take Linear Algebra I as their first proof course [157]. All the methods consistently placed Real Analysis I before Real Analysis II and III and similarly for other courses that span a single topic over many quarters (e.g. Numerical Methods I, II). Although no two methods were in total agreement, we observed that Rank Centrality produced results that were largely different than the others for this particular population. Specifically, Rank Centrality placed Applied Algebra and Partial Differential Equations much earlier than the other methods.

Approximately 10% of students in the Applied Mathematics major took these classes, which was the minimum for a class to be considered in our course sequence. When Rank Centrality was applied to all Applied Math majors (not shown), Real Analysis II, which is only taken by 10% of the population, was placed before Real Analysis I in the sequence. When we consider courses with at least 5% (as opposed to 10%), courses with low enrollment frequently are moved up and even the introductory courses (see Section 3.3 are not ordered correctly). We conjecture that this method does poorly when a class is infrequently taken.

After we extract a sequence, we can inspect the heat map of the weight matrix according to the extracted sequence to obtain a granulated view of the data. For example, in Figure 3.2, we construct $\mathbf{P}$ of Pure Mathematics students with A-range GPAs. See Appendix A.1 for a reference of course name of each course number in the axes. Again, we can see from the same Figure 3.2 that the introductory course sequence (31A, 31B, 32A, 32B, 33A, 33B) is taken earliest in the sequence and a majority of students take this sequence in this order. We observe $P_{ij} + P_{ji} = 1$ when both i and j have been taken by at least one in different quarters. There are some pairs of classes for which $P_{ij} + P_{ji} = 0$, which occurs when either no student takes both course i and j or there are no students that take these courses in different quarters. For instance, we can see from Figure 3.2 that this is the case for Math 61 (Discrete Structures) and Math 133 (Fourier Series).

We also evaluate each course sequence using the consistency coefficient introduced in Section 3.5.8. In Table 3.4, we provide values of $\mathrm{K}(\mathbf{q})$ for all six methods and their corresponding rankings $\mathbf{q}$ for three different majors across four different performance categories. The majors shown are Applied Mathematics, Applied Science and Pure Mathematics; we computed similar consistency coefficients for the other four majors not shown. The first two majors are the largest mathematics majors of those seven in the mathematics department. These majors often allow students to allow requirements outside of the mathematics department (e.g. Statistics) [157]. Because we only have a student's record when they are enrolled in a Mathematics course, we expect some "noise" in the pairwise comparison data as students fulfill similar requirements with courses from different departments. Within each major, we also illustrate three GPA categories (see Section 3.3). Using the numerics listed in the table, we compare different populations as follows. We see that in general, K($\mathbf{q}$) is maximal for A range students and minimized when we consider the entire major population. The large value of K($\mathbf{q}$) for A students indicate their navigation through coursework is more homogeneous in terms of the ordering in which classes are taken (see Section 3.5.8). We also note that Rank Centrality has low consistency coefficient relative to the other methods for Applied Mathematics majors, reinforcing similar observations we made earlier in this section that several courses with low enrollment were placed early in an extracted sequence even though students did not generally follow this ordering. The low consistency coefficient means relative to the other methods that the extracted course sequence from Rank Centrality has Outside of Rank Centrality (specifically for Applied Mathematics majors), the coefficients for K($\mathbf{q}$) are all within .015 of each other. Again, we are not using the course sequence to forecast the order of students but rather identify possible trends in a very high dimensional space of students schedules. Specifically, we can extract a single linear sequence that reflects how students fulfill math major requirements to better identify courses that may be important for students to take early in their mathematics education or hidden dependencies between courses. We explore such dependencies in Section 3.6.2.

We can also apply rank aggregations to compare how different majors navigate their coursework. In Table 3.6, we apply SerialRank to students with A-range GPAs from five different math majors. We exclude Financial and Actuarial Mathematics and Mathematics for Teaching because these majors are much smaller than the other mathematics majors as discussed in Section 3.3 (there are only 6 students with A-range GPAs in the Mathematics for Teaching Major). We observe that the Applied Math disciplines (Applied Science, Mathematics & Economics, Mathematics for Computation, and Applied Mathematics) all take Probability I early, while Pure Mathematics students generally do not. In the next section, we identify possible hidden dependencies between courses.

Table 3.4: K($\mathbf{q}$) coefficients for Applied Mathematics, Applied Science, and Pure Mathematics. Each major has n_s total students. We subdivide each majors into GPA categories: All ([0, 4.3]), A-range ([3.7, 4.3]), B-range ([2.7, 3.7)), and C-range ([1.7, 2.7)).

Method	**Applied Mathematics** ($n_s = 672$)			
	All GPAs	**A-range**	**B-range**	**C-range**
PageRank ($\alpha = .15$)	0.652	0.691	0.669	0.674
Rank Centrality	0.531	0.671	0.546	0.670
SerialRank	0.657	0.696	0.674	0.678
SyncRank	0.657	0.696	0.669	0.679
Least Squares	0.654	0.697	0.676	0.679
SVD	0.657	0.701	0.674	0.678
	Applied Science ($n_s = 499$)			
PageRank ($\alpha = .15$)	0.707	0.772	0.722	0.757
Rank Centrality	0.727	0.743	0.740	0.757
SerialRank	0.725	0.768	0.737	0.767
SyncRank	0.725	0.763	0.737	0.768
Least Squares	0.725	0.760	0.727	0.771
SVD	0.715	0.746	0.735	0.766
	Pure Mathematics ($n_s = 346$)			
PageRank ($\alpha = .15$)	0.618	0.706	0.634	0.645
Rank Centrality	0.606	0.708	0.622	0.685
SerialRank	0.617	0.713	0.631	0.692
SyncRank	0.617	0.721	0.632	0.694
Least Squares	0.619	0.718	0.634	0.707
SVD	0.618	0.714	0.632	0.692

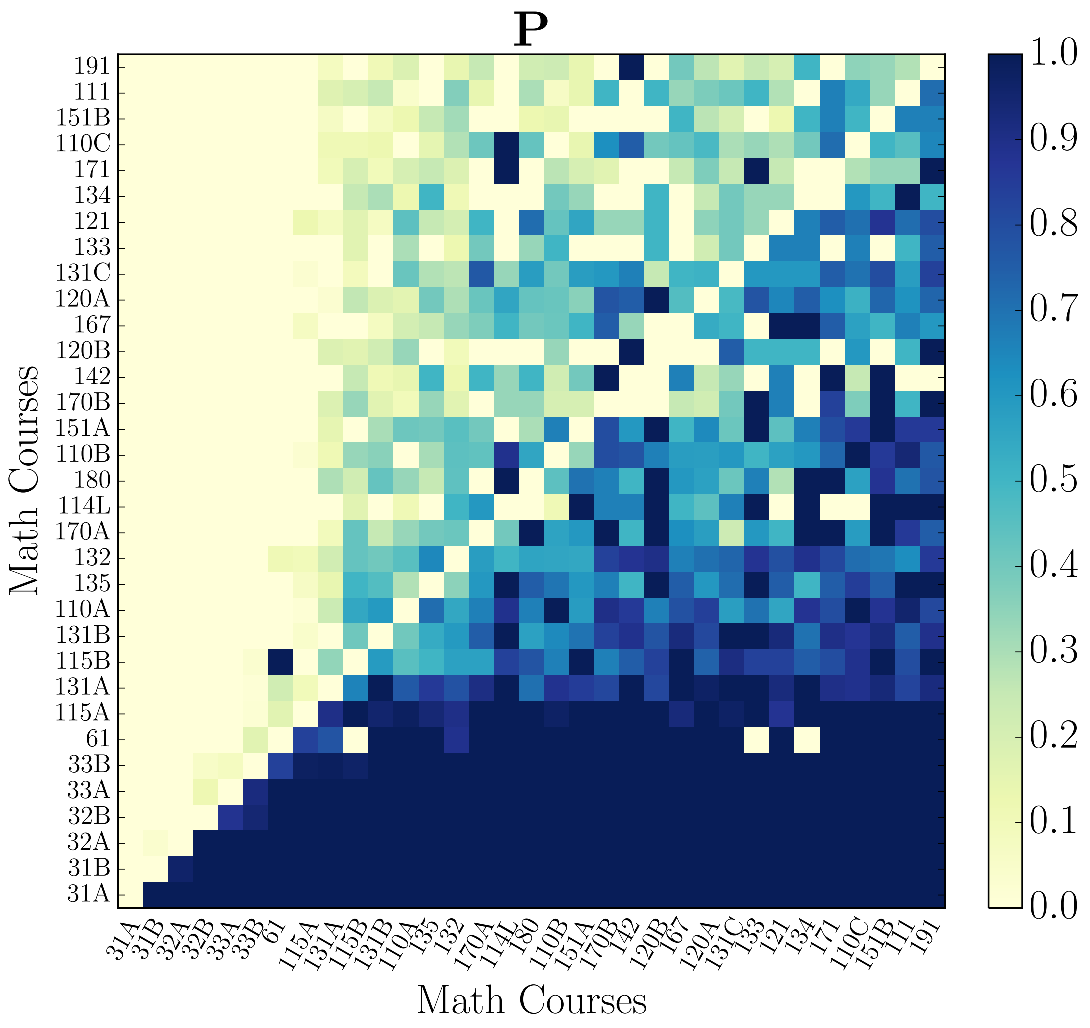

Figure 3.2: The proportion matrix **P** for Pure Mathematics students with A-range GPA. We order courses with PageRank.

3.6.2 Identifying Hidden Course Dependencies

One of the motivations for examining the manner students navigate through coursework is to be able to identify possible hidden course dependencies. Specifically, we want to identify courses, when taken earlier in a sequence, that may improve a student's performance overall and in a specific later course. Indeed, there are a number of factors that influence a student's performance (financial responsibilities, prior training, work ethic), and in this work, we do not demonstrate causal relationship between the order students take courses and their performance. In future work, we plan to design hypothesis tests on the possible hidden dependencies we identify. Our focus in this work is to introduce a tool to reduce the dimensionality of possible course schedules and more easily identify possible hidden course dependencies.

We first compare course sequences from two GPA categories: A and C students. In doing so, we attempt to identify possible hidden dependencies assuming in aggregate A students more successfully navigate their coursework than C students. This assumption should be viewed with caution. We expect that a stronger student is able to earn an A GPA taking courses in a variety of orders assuming he or she has a reasonable amount of prerequisites for each subsequent course in the sequence. In contrast, we expect weaker students to select fewer, less-challenging classes to fulfill the basic requirements and regardless of the order they take courses they will do poorly. Another flaw in this setup is that we completely omit B students. We chose to omit this population because the extracted course sequence of A and B students are similar with various methods (not shown). Specifically, the extracted sequences from A and B students had roughly 5 to 6 courses in identical order following there introductory lower-division coursework, which too were in the same order. We are uncertain if B students represent a population similar to A or C students, a mixture of A students and C students, or a wholly different population. Moreover, we expect that permutation of course orders should not drastically change a students GPA, and so B students offer insights into how possible permutations of course orders to impact a student's performance. Even with these flaws, the comparison of the extracted sequences from these vastly different performance categories have noticeable differences in the ordering of courses, and we can identify possible hidden course dependencies.

In Table 3.6, we use SyncRank (Section 3.5.5) to extract the course sequences within these two GPA categories from three different majors. We compare the first 11 courses for A-range students and C-range students (excluding the required the six introductory courses discussed in Section 3.3). A-range students have Discrete Structures (Math 61) earlier in their sequence than do C-range students. Discrete structures is not a required course and it's only prerequisite is Calculus I (Math 31A). The course introduces proof techniques and basic combinatorics. However, there are several challenges associated to validating that Discrete Structures may improve overall GPA or performance in a specific course when taken earlier. First, the number of Pure Mathematics students constitutes a fairly small population ($n_s = 346$) and the number of A-range Pure Mathematics students is even smaller ($n_s = 86$). Second, only 20% of mathematics students in our sample take Discrete Structure. This implies that our conclusions are based on a relatively small population and careful statistical hypothesis tests are needed. Nonetheless, the ability to identify possible hidden dependencies between courses from a large set of possibilities is valuable for guiding statistical analysis.

In a similar fashion, we observe that Probability I is taken early by A students who major in Mathematics of Computation (Table 3.5). Probability I is not required, although this course can serve as an upper-division elective course requirement (an upper-division mathematics course is numbered 100-199) [157]. Mathematics of Computation majors are required to take six upper division elective courses in addition to a list of required courses. Numerical Analysis I is on the list of required courses that all Math of Computation majors must take. However, the extracted course sequence indicates Numerical Analysis I is taken significantly later than Probability I. Numerical Analysis I requires Linear Algebra I, usually the first proof-based course, whereas Probability I does not. However, if Probability I is taken much earlier, certain unique skills and knowledge acquired in this course may help a student in future Mathematics courses. We inspect all the 203 students that were Mathematics of Computation majors and we find that their sequence extracted from SerialRank is Linear Algebra I (Math 115A), Discrete Structures (Math 61), Real Analysis

I (Math 131A), Numerical Analysis I (Math 151A), and then Probability I (Math 170A). Because there are only 20 students in Mathematics of Computation with A-range GPAs, this observation regarding course ordering must be viewed with a healthy level of skepticism. It is beyond the scope of this work to provide detailed statistical evidence that Probability I influences mathematics performance in this major. However, rank aggregation is a tool to uncover possible trends in student schedules.

We mention a few more observations that we draw from the extracted sequences in Table 3.6. First, A-range Pure Mathematics students tend to take Real Analysis I and Real Analysis II within two courses of each other whereas C students tend to take Real Analysis II much later (not in the 11 courses shown). Real Analysis I and II are both required—approximately 90% of the Pure Mathematics students in this data set took both. The department recommends enrolling in Real Analysis after Linear Algebra I [157]. This recommendation suggests that sufficient experience with proof-based mathematics is important for a students taking Real Analysis I [157]. Strong mathematics students may continue through the sequence faster, whereas poor-performing students may postpone the completion the completion of this course. Similarly, for Applied Science students, we can see from Table 3.6 that a majority of A students take Actuarial Math I much earlier than a majority of C students. Rank aggregation identifies these possible trends easily and can guide future analysis (statistical or otherwise) to better quantify these differences in student behaviors.

3.7 Conclusions and Future Work

In this chapter, we applied rank aggregation methods to examine how UCLA mathematics students navigate their coursework. We used rank aggregation to identify possible hidden course dependencies and investigate patterns in the order students select courses. The space of possible course schedules is large and studying all related order statistics is infeasible. However, if we assume that the order that courses are selected is the result of an underlying course sequence, we can extract a sequence with rank aggregation and investigate patterns associated with this sequence. For example, in our application of rank aggregation, we were

Table 3.5: First 11 courses for A students in five different majors using SerialRank.

Applied Mathematics	**Pure Mathematics**	**Applied Sciences**	**Mathematics & Economics**	**Mathematics for Computation**
$n_s = 140$	$n_s = 86$	$n_s = 75$	$n_s = 101$	$n_s = 20$
Linear Algebra I	Discr. Struct.	Linear Algebra I	Linear Algebra I	Linear Algebra I
Discr. Struct.	Linear Algebra I	Probability I	Discr. Struct.	Probability I
Real Analysis I	Real Analysis I	Discr. Struct.	Probability I	Real Analysis I
Probability I	Linear Algebra II	Act. Math	Real Analysis I	Discr. Struct.
Nonlinear Systems	Real Analysis II	Probability II	Applied Algebra	Probability II
Num. Analysis I	Algebra I	Real Analysis I	Optimization	Act. Math
Graph Theory	Ord. Diff. Eqns.	Num. Analysis I	Probability II	Math Modeling
Complex Analysis	Complex Analysis	Act. Models II	Num. Analysis I	Math Econ.
Real Analysis II	Probability I	Graph Theory	Real Analysis II	Act. Models II
Math Modeling	Algebra II	Optimization	Game Theory	Num. Analysis I
Algebra I	Graph Theory	Act. Models II	Math Econ.	Loss Models I

Table 3.6: Comparing the A and C students in three majors using SyncRank.

Applied Mathematics		**Applied Sciences**		**Pure Mathematics**	
A ($n_s = 140$)	**C** ($n_s = 198$)	**A** ($n_s = 75$)	**C** ($n_s = 162$)	**A** ($n_s = 86$)	**C** ($n_s = 95$)
Linear Algebra I	Linear Algebra I	Linear Algebra I	Linear Algebra I	Discr. Struct.	Linear Algebra I
Discr. Struct.	Discr. Struct.	Probability I	Discr. Struct.	Linear Algebra I	History of Math
Real Analysis I	Probability I	Discr. Struct.	Probability I	Real Analysis I	Real Analysis I
Probability I	Real Analysis I	Real Analysis I	Real Analysis I	Linear Algebra II	Discr. Struct.
Complex Analysis	Algebra I	Act. Math	Nonlinear Systems	Algebra I	Algebra I
Nonlinear Systems	Num. Analysis I	Num. Analysis I	Math Modeling	Real Analysis II	Ord. Diff. Eqns.
Num. Analysis I	Graph Theory	Probability II	Graph Theory	Ord. Diff. Eqns.	Complex Analysis
Math Modeling	Real Analysis II	Graph Theory	Game Theory	Complex Analysis	Game Theory
Real Analysis II	Act. Math	Act. Models II	Num. Analysis I	Probability I	Probability I
Algebra I	Nonlinear Systems	Act. Models II	Optimization	Algebra II	Graph Theory
Graph Theory	Math Modeling	Ord. Diff. Eqns.	Ord. Diff. Eqns.	Graph Theory	Num. Analysis I
Ord. Diff. Eqns.	History of Math	Num. Analysis II	Act. Math	Real Analysis III	Optimization
Game Theory	Complex Analysis	Optimization	Probability II	Num. Analysis I	Number Theory
Research Seminar	Probability II	Math Econ.	Act. Models II	Logic	Algebra II

investigated how five of the different mathematics majors at UCLA navigate their coursework. The extracted sequence of all the methods that we investigated when applied to an entire major population ordered the introductory Mathematics courses that a majority of students follow (3.3). Now, the teleportation probability α was *selected* so that PageRank ordered these introductory Mathematics courses correctly. However, the other five methods that we investigated did not require a parameter. The other methods depend on the particular weight matrix that encodes student data between courses. The matrices we investigated all crucially relied on the proportion matrix. Moreover, when we inspected the entire major population, each method also placed Linear Algebra I (Math 115A) directly after this introductory sequence, consistent with the recommended selection of courses at the departmental website [157].

We were also able to identify possible hidden course dependencies by comparing high-performing (A-range GPA) students to low-performing (C-range GPA) students. This approach compares two populations with vastly different grades. We selected this methodology because our setup was able to distinguish differences in the extracted sequence between these GPA categories. We omitted B students because their extracted course sequence was similar to the extracted sequences of A students and identifying possible hidden course dependencies would be more tenuous. Nonetheless, our work provides an important first step to more easily identify possible course orders that may impact an overall students performance.

Using our comparison of A and C students, we observed that high-performing Pure Mathematics students tend to take Discrete Mathematics earlier than low-performing mathematics. Another observation was that A students in the Mathematics of Computation majors [157] tend to take Probability I relatively early in the course sequence even though it is not required. Unfortunately, although our data set spans 15 years of grade data, there is not enough data to avoid examining small, specialized populations. For example, there are only 86 A students that major in Pure Mathematics and 20 A students in the Mathematics of Computation major. As a result, statistical analysis to validate our findings is hardly possible without further assumptions. We hope that this preliminary work will prompt future investigations as the UCLA Department of Mathematics collects more data and larger data sets in different academic departments are made available.

To validate the application of rank aggregation in this context of extracting course sequences, we compared six different matrix methods: PageRank, Rank Centrality, SerialRank, SyncRank, Least Squares, and SVD ranking. To compare these methods, we examine a consistency coefficient $\mathrm{K}(\mathbf{q})$ in Section 3.5.8. The consistency coefficient measures the mean proportion of students who move between ordered pairs of courses that are drawn from the extracted sequence. We observed that the output of all the ranking methods have comparable consistency coefficients (Section 3.6.1). Rank Centrality, however, produced output very different than the other methods on certain populations. In particular, it incorrectly ranked courses with low enrollment. Although we removed courses in which fewer than 10% of a population enrolled, Rank Centrality incorrectly placed courses with low enrollment early in a course sequence—including placing Real Analysis II before Real Analysis I for Applied Mathematics majors. Despite the failure of Rank Centrality in certain instances, the comparability of the consistency coefficient among methods suggests that these methods perform similarly for course sequence discovery.

In future work, we plan to examine the differences among ranking methods more carefully particularly on synthetic generative models that include parameters and systems for the uneven comparison of courses and noise within comparison data. Specifically, we plan to generate proportion matrices $\mathbf{P}$ (Eq. (3.9)) from comparison data generated from appropriate synthetic models. The addition of noise into generative comparison models was numerically explored in [53] and more theoretically in [171]. Moreover, the original works of Rank Centrality [152] and Serial Rank [81] provide theoretical investigations about missing comparisons for particular generative models. The analysis require an assumption that there are enough comparisons to ensure the proportion matrix of Eq. (3.9) converges to the probability dictated by the particular generative process producing comparison data (e.g. the BTL model from Eq. (3.2)). There is no explicit discussion as to how many comparisons are required to ensure exact recovery of rankings from a particular generative pairwise comparison model, nor is there indication of the effect when these comparisons are unevenly distributed. Such exploration will help us better understand the effect on extracted course sequences of low enrollment courses—particularly those that are more advanced, infrequently offered, or not required. For example, if only two students take course i in a population, then $P_{ij} \in \{0, .5, 1\}$ for all courses j and our rank aggregation method can incorrectly place course i in a particular sequence due to the selection of these two students. To more directly account for such courses, we also plan to integrate the number of times a course was offered and the number of students enrolled in a particular course (or pair of courses) into the edge weights of our various network model. Additionally, we plan to build models that integrate the time between them (cardinal comparisons) in order to more effectively describe course dependencies. We also plan to build upon our consistency coefficient to reflect more complex network models (see our discussion in Section 3.5.8).

Ultimately, we want to use this methodology to understand optimal course sequences that provide the greatest (in a measurable sense) opportunity for students to succeed in their coursework. This will likely require the integration of grade data directly into network models to better capture a student's navigation patterns and the direct impact on his/her performance. More specifically, we plan to explore the impact of only comparing courses for a particular student when the grade in both courses are within 1 standard deviation of a student's overall GPA and then appropriately encode this data into the matrix $\mathbf{P}$. We also wish to explore network models that only compare courses when there is an improvement in course grade and exclude any comparison of courses when a course grade declined. Our ability to identify possible trends using ordinal comparison data can serve as a foundation for future, more detailed investigations into course navigation and optimal course selection.

CHAPTER 4

Core–Periphery Structure in Frugivore–Seed Networks

Local, intermediate (mesoscale), and global structures each help describe the function and organization of a network. Local structures are structures at the level of nodes and edges. For example, local structures may be an edge weight or a node degree. Global structures are those that aggregate various local structures throughout a network. For example, a global structure is the average node degree or the total number of edges in a network. Mesoscale structures lie between local and global scales and help to capture intermediate modes of organization and function. Core–periphery structure is a mesoscale structure that has attracted attention [176,216] due to varied application in fields such as in economics [115], sociology [117], and political science [190]. For simplicity, we first describe a core–periphery structure on an undirected, unweighted network. A core–periphery structure for such a network is a structure that describes a *core* that is well connected to the network and a *periphery* that is poorly connected to itself. In this case, there has been several methods for quantifying well-connected and poorly-connected nodes to describe core–periphery structure [98, 120, 176, 216]. This suggests that formalizing this intuitive definition (even in the simple case of an undirected, unweighted networks) must be done with some care. When more general network structures are considered, core–periphery structure must be extended to account for heterogeneous edge traits. For example, when edges are directed, each pairwise connection is asymmetric, and therefore, the notion of a well-connected core must be adapted appropriately [52]. Additionally, when edges are weighted, there are additional considerations that must be made because a well-connected node may be stipulated as one with large total edge weight, total number of neighbors, a combination of the previous two, or an entirely different measure altogether [52]. Due to the varied structure of networks, core–periphery structure frequently must be adapted for each particular application [52, 176].

Once a specific core–periphery structure is identified, then one can either look to partition the set of network nodes into core and periphery; score nodes based on their core (or peripheral) position within a network; or perform some combination of these two approaches. In the seminal work of Borgatti and Everett in [30], they explored core–periphery structure both as a partition of nodes into core and periphery in addition to measuring core in terms of a node centrality. Methods for examining core–periphery structure have been applied to political networks [176], transportation networks [98, 176], internet networks [98, 216], and others. In this chapter, we apply a method of core–periphery structure proposed in Rombach et al. [176] to frugivore–seed dispersal networks.

This chapter consists of three parts. The first part (Section 4.1) reviews graph calculus, which we use for our discussion of core–periphery structure for undirected networks (weighted and unweighted). The second part (Section 4.2) is an overview of models of core–periphery structure in networks. The third and final part (Section 4.3) is an application of the core–periphery framework described in [176] to describe core–periphery structure in an frugivore–seed dispersal network.

4.1 Notations and Related Graph Calculus

We review the graph calculus useful for graph cuts and network analysis [99, 138, 199]. This framework allows us to discuss core–periphery structure in a unified framework. Let $G = (V, E)$ be a network, where V is the node set and E the edge set. For simplicity, we identify V with $\{1, 2, \dots, n\}$ and edges E as pairs $\{ij \mid i, j \in V\}$ of vertices. Although we assume all networks are undirected, we associate two orientations with each edge. Specifically we write ij for the orientation of edge ij beginning at i and ending at j and ji for the reverse. We also use an $n \times n$ weight matrix $\mathbf{W}$ that indicates the edge weight between node i and node j. In many cases, we identify the weight matrix with the adjacency matrix for which $w_{ij} = 1$ if i is adjacent to j and 0 otherwise. Because we assume that our networks we consider are undirected, we assume that $w_{ij} = w_{ji}$.

We define the set of *real-valued functions on the node* set as

$$\mathcal{F}_V := \{\mathbf{f} : V \to \mathbb{R}\} . \tag{4.1}$$

We write $\mathbf{f} = (f_1, \ldots, f_n)$ for $\mathbf{f} \in \mathcal{F}_V$, identifying the function with a vector in $\mathbb{R}^n$. In particular, we write f_i to mean the output of $\mathbf{f}$ at node i, or in functional notation $\mathbf{f}(i)$. Because $\mathcal{F}_V$ is the set of real-valued functions, we also define the product $\mathbf{fg}$, the sum $\mathbf{f} + \mathbf{g}$, and the absolute value $|\mathbf{f}|$ for any $\mathbf{f}, \mathbf{g} \in \mathcal{F}_V$.

Using this functional notation, we specify node centrality measures as real-valued functions on V. For instance, the *degree of node i* in an undirected network is defined to be $d_i := \sum_{j \in V} w_{ij}$. When $\mathbf{W}$ is the adjacency matrix, d_i is the number of neighbors of node i. We then define $\mathbf{d} \in \mathcal{F}_V$ as $\mathbf{d}(i) = d_i$.

We also study partitions using this functional notation. Specifically, consider a *characteristic function* χ_A of a fixed subset of nodes A contained in V. The characteristic function χ_A has range $\{0, 1\}$ such that $\chi_A(i) = 1$ if $i \in A$ and 0 otherwise.

We define the set of *skew-symmetric functions on the edge set E* as

$$\mathcal{F}_E := \{\mathbf{a} : E \to \mathbb{R},\ \mathbf{a}(ij) = -\mathbf{a}(ji)\} . \tag{4.2}$$

Often such functions are construed as *flows* from one node to another so skew symmetry is a natural property [199]. Because we view each edge ij as also carrying two orientations, each $\mathbf{a} \in \mathcal{F}_E$ can be interpreted as measuring the flow with respect to one of two orientations. We define $\mathbf{ab}$, $\mathbf{a} + \mathbf{b}$, and $|\mathbf{a}|$ for $\mathbf{a}, \mathbf{b} \in \mathcal{F}_E$, though to do so, we first must fix an orientation for every edge first. After an orientation on each edge is fixed, we define the operation on functions for each edge as $(\mathbf{ab})_{ij} = \mathbf{a}_{ij} \cdot \mathbf{a}_{ij}$ for the appropriate orientation of ij. One possible way to fix an orientation on a network is to orient edges so that an edge ij is oriented from i to j such that $i < j$. For clarity, we orient networks in this fashion for the remainder of our discussion. We equip $\mathcal{F}_V$ and $\mathcal{F}_E$ with inner products and these become finite-dimensional

Hilbert Spaces [199]. Specifically,

$$\langle \mathbf{f}, \mathbf{g} \rangle := \sum_{i \in V} f_i g_i \ , \qquad \mathbf{f}, \mathbf{g} \in \mathcal{F}_V \ , \tag{4.3}$$

$$\langle \mathbf{a}, \mathbf{b} \rangle := \sum_{\substack{ij \in E: \\ i<j}} a_{ij} b_{ij} \ , \quad \mathbf{a}, \mathbf{b} \in \mathcal{F}_E \ . \tag{4.4}$$

Observe that the inner product over edges is depends on how we fix our orientation. In Eq. (4.4), we assume that each edge ij is oriented from i to j such that $i < j$. We also define the *gradient operator* $\nabla : \mathcal{F}_V \to \mathcal{F}_E$ as follows:

$$(\nabla \mathbf{f})_{ij} = \sqrt{w_{ij}}(f_j - f_i) \ . \tag{4.5}$$

In other words, gradient operator of a function $\mathbf{f}$ in Eq. (4.5) takes as input an oriented edge and outputs the difference in $\mathbf{f}$ along this edge with respect to the reverse orientation. The *normalized gradient operator* $\nabla_{nor} : \mathcal{F}_V \to \mathcal{F}_E$ is defined as

$$(\nabla_{\text{nor}} \ \mathbf{f})_{ij} = \sqrt{w_{ij}} \left(\frac{f_j}{\sqrt{d_i}} - \frac{f_i}{\sqrt{d_j}} \right) \ , \tag{4.6}$$

where again d_i is the degree of node i.

The *divergence operator* div : $\mathcal{F}_E \to \mathcal{F}_V$ is the adjoint of the gradient. The divergence (written as div) is characterized by the relation

$$\langle \nabla \mathbf{f}, \mathbf{a} \rangle_{\mathcal{F}_E} = \langle \mathbf{f}, \text{div } \mathbf{a} \rangle_{\mathcal{F}_V} \ , \quad \mathbf{f} \in \mathcal{F}_V, \mathbf{a} \in \mathcal{F}_E. \tag{4.7}$$

From the metrics on $\mathcal{F}_V$ and $\mathcal{F}_E$ given in Eq. (4.3) and Eq. (4.4) respectively, we obtain the explicit formula for the divergence and normalized divergence as

$$(\text{div } \mathbf{a})_i = \sum_{j \in V} \sqrt{w_{ij}}(a_{ij} - a_{ji}). \tag{4.8}$$

$$(\text{div}_{\text{nor}} \ \mathbf{a})_i = \sum_{j \in V} \sqrt{w_{ij}} \left(\frac{a_{ij}}{\sqrt{d_i}} - \frac{a_{ji}}{\sqrt{d_j}} \right) \ . \tag{4.9}$$

The divergence of an $\mathbf{a} \in \mathcal{F}_E$ at node i (Eq. (4.8)) can be interpreted as the net change of $\mathbf{a}$ moving outward from all edges incident to node i. Now, we can define the the *(combinatorial)*

Laplacian and *normalized Laplacian* as

$$\Delta := \text{div } \circ \nabla \ , \tag{4.10}$$

$$\Delta_{\text{nor}} := \text{div}_{\text{nor}} \ \circ \nabla_{\text{nor}} \ , \tag{4.11}$$

respectively. The quantity $(\Delta \mathbf{f})_i$ measures the total flow associated to $\nabla \mathbf{f}$ that leaves node i. A computation shows that the definitions of Laplacians given above agree with the combinatorial and normalized Laplacian given in [201] as

$$\Delta = \mathbf{D} - \mathbf{W} \ , \tag{4.12}$$

$$\Delta_{\text{nor}} = \mathbf{I} - \mathbf{D}^{-1/2}\mathbf{W}\mathbf{D}^{-1/2} \ , \tag{4.13}$$

where $\mathbf{W}$ is the weight matrix and $\mathbf{D}$ is the diagonal matrix in which the i^{th} diagonal element is the degree of i^{th} node. Clustering nodes using the eigenvectors associate to the Laplacians defined in Eq. (4.12) and Eq. (4.13) has been applied to problems in image-segmentation and data science [22].

We now define the integration of functions in $\mathcal{F}_V$ and $\mathcal{F}_E$ as

$$\int_V \mathbf{f} := \sum_{i \in V} f_i = \langle \mathbf{f}, \mathbf{1}_V \rangle \ , \quad \mathbf{f} \in \mathcal{F}_V \ ,$$

$$\int_E \mathbf{a} := \sum_{\substack{ij \in E: \\ i<j}} a_{ij} = \langle \mathbf{a}, \mathbf{1}_E \rangle \ , \quad \mathbf{a} \in \mathcal{F}_E \ ,$$

where $\mathbf{1}_V : V \to \mathbb{R}$ is the constant function with $\mathbf{1}(i) = 1$ and $\mathbf{1}_E$ is defined similarly for a fixed orientation on E. Note that the integral over E depends on how edges are oriented; for simplicity, we select edges to be oriented as $i < j$. We can now write our inner products as the integrals

$$\langle \mathbf{f}, \mathbf{g} \rangle = \int \mathbf{f}\mathbf{g} \ , \quad \mathbf{f}, \mathbf{g} \in \mathcal{F}_V \ ,$$

$$\langle \mathbf{a}, \mathbf{b} \rangle = \int_E \mathbf{a}\mathbf{b} \ , \quad \mathbf{a}, \mathbf{b} \in \mathcal{F}_E \ .$$

Using this notation, we have the following divergence theorems [199]:

$$\int_V \Delta \mathbf{f} = 0 \ , \quad \mathbf{f} \in \mathcal{F}_V \ ,$$

$$\int_E \text{div } \mathbf{a} = 0 \ , \quad \mathbf{a} \in \mathcal{F}_E \ .$$

We define harmonic functions as those functions that satisfy $\Delta f = 0$. As in a continuous setting, harmonic functions are constant on each *connected component* as shown in [201]. Recall a connected component on a graph is a set of nodes such that each pair can be joined with a path. The eigenvectors of higher eigenvalues are also important for determining subgraphs with high edge density relative to the rest of the graph [45, 191].

Finally, we define L^p norms for functions on nodes and edges for $p \in \mathbb{N}$ such that $p \geq 1$. Let $\mathbf{f} \in \mathcal{F}_V$ and

$$||\mathbf{f}||_p := \sqrt[p]{\int_V |\mathbf{f}|^p} = \sqrt[p]{\sum_{i \in V} |f_i|^p} ,$$

where $|\mathbf{f}| = (|f_1|, \ldots, |f_n|)$. For $\mathbf{a} \in \mathcal{F}_E$, we define two different L^p norms. One is a local norm relative to a node i and the other is a quantity associated to the whole network [138, 178]. They are respectively

$$||\mathbf{a}||_p(i) := \sqrt[p]{\sum_{j \in V} |a_{ij}|^p} ,$$

$$||\mathbf{a}||_p := \sqrt[p]{\int_E |\mathbf{a}|^p} = \sqrt[p]{\sum_{ij \in E} |a_{ij}|^p} .$$

Using the L^p norms, we define the total-variation (TV) norms of a function $\mathbf{f} \in \mathcal{F}_V$ as in [34, 178]. The *anisotropic total-variation norm* is given as

$$||\nabla \mathbf{f}||_1 := \int_E |\nabla \mathbf{f}| = \sum_{ij \in E} \sqrt{w_{ij}} |f_i - f_j| .$$

The *isotropic total-variation* is given as

$$||\nabla \mathbf{f}||_1^{\text{iso}} := \int_{V_i} ||\nabla \mathbf{f}||_1(i) = \sum_{i \in V} \sqrt{\sum_{j \in V} w_{ij}(f_i - f_j)^2} .$$

These TV norms are important tools for image denoising, inpainting, and segmentation [93, 178], to name a few. This framework and its techniques have also used successfully for graph clustering and machine learning [22, 34, 138]. For example, let A be a subset of nodes V. Define $\textsc{Cut}(A, A^c)$ from A to A^c as

$$\textsc{Cut}(A, A^c) = \sum_{i \in A, j \in A^c} w_{ij} .$$

We can write the cut in terms of the anisotropic total-variation norm associated to the characteristic function on A. Specifically,

$$\textsc{Cut}(A, A^c) = \sum_{\substack{i\in A,\\ j\in A^c}} \sqrt{w_{ij}} = \sum_{\substack{i\in A,\\ j\in A^c}} w_{ij} = \sum_{ij\in E} w_{ij}|(\chi_A)_i - (\chi_A)_j| = ||\nabla \chi_A||_1 \ .$$

In fact, this this relationship between graph cuts and TV norms fashions a variational framework for many important graph cut problems that are NP-hard. For example, in [34], the authors demonstrated the *Cheeger cut* $C(G)$ of a graph admits a continuous relaxation that can be solved efficiently. The Cheeger cut is

$$C(G) := \min_{A\subset V} \frac{\text{Cut}(A, A^c)}{\min(|A|, |A^c|)} \ ,$$

and can write the Cheeger cut as

$$C(G) = \min_{\substack{\mathbf{f}\in\mathcal{F}_V:\\ \mathbf{f}=\chi_A}} \frac{||\nabla \mathbf{f}||_1}{||\mathbf{f} - \text{med}(\mathbf{f})||_2} \ . \tag{4.14}$$

where med($\mathbf{f}$) is the median of all the values in the range of $\mathbf{f}$. If one removes the restriction that $\mathbf{f} = \chi_A$, Eq. (4.14) is solved efficiently in [34]. The graph calculus discussed in this section connects the methods of image processing [178] to those of classical graph cuts [201]. We also define some foundational graph-cut quantities for subsets S, S_1, S_2 of nodes as in [45]. Let the *volume* vol(S), the *boundary* $|\partial S|$, *total edge weight* $E(S_1, S_2)$ from S_1 to S_2, and *total edge weight* $|E_S|$ in S be defined (respectively) as

$$\text{vol}(S) := \sum_{i\in S} d_i \ , \tag{4.15}$$

$$|\partial S| := \sum_{\substack{i\in S,\\ j\in V\setminus S}} w_{ij} \ , \tag{4.16}$$

$$E(S_1, S_2) := \sum_{\substack{i\in S_1,\\ j\in S_2}} w_{ij} \ , \tag{4.17}$$

$$|E_S| := \sum_{\substack{i\in S_1,\\ i<j}} w_{ij} \ . \tag{4.18}$$

This implies that $|\partial S| = \text{Cut}(S, S^c)$ and that

$$\text{vol}(S) = 2|E_S| + |\partial S| \ . \tag{4.19}$$

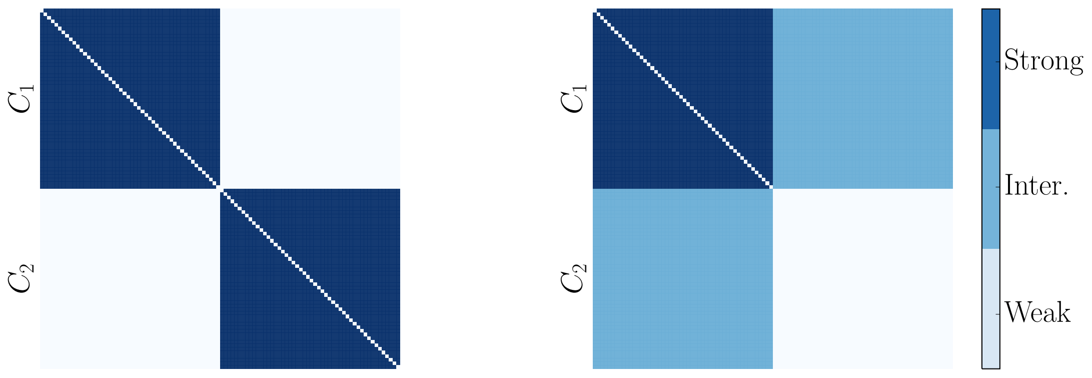

(a) Community Structure **(b)** Core–Periphery Structure

Figure 4.1: Two examples weight matrices for networks with characteristic mesoscale structures: community structure (a) and core–periphery structure (b). We illustrate strong, intermediate, and weak edge weight. In Figure 4.1a, C_1 and C_2 are two disjoint communities with strong edge weight within a community and weak edge weight between communities. In Figure 4.1b, C_1 is the core and C_2 the periphery such that the core is strongly connected to itself, the core is connected to the periphery with intermediate weight, and the periphery is connected weakly to itself.

We also define the *edge expansion* e_S of a set of nodes S contained in a network (as in [9]) to be

$$e_E(S) := \frac{|\partial S|}{\min(|S|, |V \backslash S|)}. \tag{4.20}$$

These quantities arise often in spectral graph theory [45, 191].

4.2 Core–Periphery Structure

Core–periphery structure is a mesoscale structure that describes a network's so-called *core* and *periphery* [52, 176]. For simplicity, we first discuss the undirected, unweighted case, although our focus will return to the weighted case shortly as this latter structure is what concerns us for ecological applications. A core structure is interpreted as a set of nodes that is well connected a network, whereas a periphery structure is poorly connected to itself. This definition is not mathematically precise (even in this limited context), and core–periphery structures continue to be actively developed and explored [52, 98, 176, 216]. Specifically, the notions of "well connected" and "poorly connected" must be properly specified to describe this structure. For example, we can quantify a nodes connections via adjacency. In other situations, a courser resolution of connections (or proximity) may be quantified using shortest path lengths or the distribution of a walkers starting at a particular node [54, 120, 130]. Once a suitable definition for core–periphery structure is selected, one can score nodes according to a related measure [120, 176], partition a network into core and periphery [216], or provide combination of both scoring and partitioning [54, 176].

Core–periphery structure for undirected, unweighted networks can be transferred to weighted networks, but notions of "well connected" and "poorly connected" must be appropriately specified. In this chapter, we quantify how "well connected" two nodes are relative to the weight of an edge connecting them. More generally, we quantify how well connected a particular node v is to a fixed set S of nodes using the total weight of edges from v to S. Even though this definition appears reasonable, we remark that there are still caveats that may produce unintended consequences in certain applications. For example, let v be a node and S a fixed set of nodes in a network. Let's assume that $S \gg 1$. According to our definition, a node v can be measureably well connected to S even if it has but one neighbor in S if its edge weight connecting it to a node in S is high enough relative to other edge weights in the network. We note that the edge density (counting the number of edges per node) is a wholly separate measure than the edge weight and the total edge weight associated to a node. We attempt to highlight this distinction for core–periphery structures in weighted networks. We will not consider directed networks in this chapter.

Core–periphery structure contrasts another mesoscale structure known as *community structure*. Just as with core–periphery structure, we begin our discussion our discussion in an undirected, unweighted network. Intuitively, a community structure may be thought of as a division (or sometimes a set of partitions at different resolutions) of nodes into *communities*, in which nodes within a community are well connected to each other but not to the rest of the network. However, this intuitive explanation is imprecise and runs into several complications when applied to empirical networks. For example, communities can overlap and each node may have mixed membership; a node's community membership can be determined as a probability distribution (not a partition); there can be several different community structures valid within a network (and possibly organized hierarchically); or nodes may be sorted into communities based on similarities of local or global structures rather than adjacency. Reviews of community detection methods and analyses can be found in [82, 170]. When extending our preliminary notion to weighted networks, we quantify how well two nodes are connected via the weight of an edge connecting them. We again remark that this particular generalization is not suitable for all applications due to the distinction between edge density and weight.

To compare community and core–periphery structures, we illustrate two weight matrices that represent particular forms of community and core–periphery structures. For this brief discussion that occupies the remainder of the section, we assume that the blocks (either core and periphery or two communities) can be partitioned into separate sets of nodes. In Figure 4.1a, we illustrate a weight matrix and a division into two communities, C_1 and C_2. In this representation, each node within a community is strongly connected with one another but connections between each community is weak. This representation focuses on edge weight and ignores edge density. We can also interpret Fig 4.1a as probabilities that an edges connects two nodes with the assumption that all nodes are equally weighted. In this interpretation, we ignore edge weights and focus on the edge density. In either interpretation of Figure 4.1a, a form of community structure in a weighted network is highlighted. In Figure 4.1b, we illustrate a weight matrix of a core–periphery structure in a network. We have a core C_1 that is strongly connected to every core other node in the network and connected with intermediate strength to each peripheral node C_2. We also see that peripheral nodes are weakly connected to each other. We can also interpret this as probabilities that two nodes connected assuming edge weights are again uniform throughout a network. Again, each different interpretation highlights a different aspect of core–periphery structure in weighted networks, namely edge density and edge weights. Even in the scenario that a core and peripheral nodes can be divided, a network can have multiple cores or can be separated into

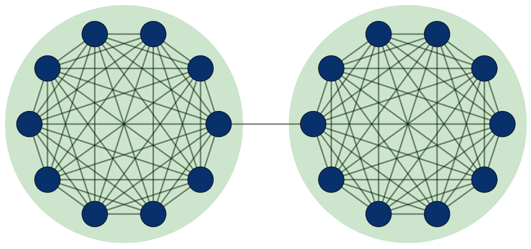

Figure 4.2: The barbell graph in which there are two complete graphs on 10 vertices connected by a single edge. The shaded regions indicate the disconnected subgraphs when a single edge connecting these two subgraphs is removed.

communities each with their own core–periphery structure as discussed in [176]. In practice, one must carefully select and possibly adapt a particular core–periphery structure for an application.

4.2.1 Combinatorial Quantities Related to Core–Periphery Structure

In this section, we discuss some combinatorial quantities and graph structures related to core–periphery structure. Because we consider graphs, such discussions center on unweighted networks. Although these methods have frequently been applied to empirical networks, many of the methods and models were described within graph theory or theoretical computer science. We indicate whenever possible which structures can be extended to the weighted case. We also provide examples of how a combinatorial quantity or structure may differ from a particular core–periphery heuristic.

Let $G = (V, E)$ be an unweighted network (or a graph). We write $H \subset G$ to denote a *subnetwork* (or *subgraph*) if $H = (V_H, E_H)$ when $V_H \subset V$ and $i, j \in V_H$ and $ij \in E$ for every $ij \in E_H$. Therefore, one may wish to phrase core–periphery structure as finding a particular subgraph with a certain graph-theoretic property. This particular choice would correspond to determining core–periphery structure as a partition, though this may not be suitable for all applications.

One may define a core structure as a *maximal clique* [28]. To define a maximal clique, we first define a *complete graph*, which is a graph in such that every node is adjacent to all others. A *maximal clique* is is the maximal subgraph that is complete subgraph. In general, a *maximal subgraph* with respect to a property is a subgraph with the greatest number of nodes that still possesses this property. A maximal subgraph is not unique. For example, there are two maximal cliques in Figure 4.2. When a small fraction of edges are removed from a clique, the clique structure is destroyed and this combinatorial definition may be too restrictive for analyzing possible core–periphery structure [176]. Also, this combinatorial structure ignores the notion of periphery. To our knowledge, there is not a generalization of this structure to weighted networks.

Another possible way to analyze core structure in unweighted, undirected networks is a *k-core* for fixed $k \in \mathbb{N}$ with $k > 0$ [63, 98]. A k-core is the maximal subgraph such that every node is connected to at least k other nodes in the subgraph. For social network analysis, the k-core can model social cohesion [18]. A interesting feature of the k-core is that it decomposes a network into nested core structures as if G_k is a k-core of a network G, then $G_k \supset G_{k+1}$. In Figure 4.3, we illustrate a sequence of k-cores for $k = 1, 2, 3$. We note that the largest degree node is not included in the top most k-core as it is connected to many degree one nodes in Figure 4.3. Finding a k-core has time complexity $O(|E|) = O(|V|^2)$ [18], so it can be found in large empirical networks. Recently, the notion of a k-core has been studied in weighted networks [87] by defining the notion of a *weighted degree* d_i^w of node i. In [87], they defined the weighted degree d_i^w of node i with d incident edges and w as the total edge weight of incident edges as

$$d_w^i = (d_i^\alpha w_i^\beta)^{\frac{1}{\alpha+\beta}} \,,$$

for $\alpha, \beta \geq 0$. W remark that there are other combinatorial notions for unweighted networks that identify core structures using shortest path distance. For example, a k-clan is a maximal subgraph with *diameter* exactly k [141]. The diameter of a subgraph is the maximal edge distance between any two nodes. See [141] for a survey of combinatorial core quantities related to k-core and k-clan in unweighted networks.

Core structures can also be examined in terms of the *connectivity* of a network. The *edge*

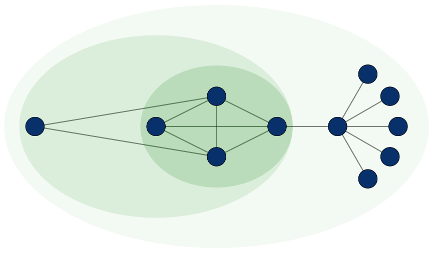

Figure 4.3: The k-cores for $k = 1, 2, 3$ enclosed in increasingly dark concentric ellipses, respectively. Note that the largest degree node is not considered part of the core for $k > 1$ as it is connected to several degree one nodes. Using the k-core requires a core structure to be well connected with itself, though not necessarily with the periphery.

connectivity is defined to be the minimal number of edges that disconnects a graph when they are removed [76]. Similarly, the *node connectivity* is the minimal number of nodes when removed that disconnects a graph when they are removed [76]. For edge connectivity, we can associate a subgraph to the network structure after edges are removed. One may elect to view the remaining edge set as representing a peripheral structure. However, the resulting connected components may be well connected unto themselves and not reflect that a periphery structure is poorly connected onto itself. For example, in Figure 4.2, we see that once a single edge is removed, we have two complete subgraphs. We can similarly examine peripheral structures when we remove nodes and incident edges. Node connectivity can be examined for weighted networks as in [173]. Specifically, they examine those nodes and edges when removed have minimal total edge weight.

Some core-structures are also related to the combinatorial optimization problem of *dense subgraphs* in unweighted networks. There are several nonequivalent ways to define a maximal dense subgraphs, each depending on how we define subgraph density. Ultimately, finding a dense subgraph is finding a subgraph with maximum density.

We first discuss *edge–edge density* related to a subgraph. Let $H = (V_H, E_H)$ be a subgraph of $G = (V, E)$. We define the edge–edge density of H as

$$d_E(H) := \frac{|E_H|}{\begin{pmatrix} |V_H| \\ 2 \end{pmatrix}} \in [0, 1] \, . \tag{4.21}$$

We see that d_E is maximum on any complete subgraph H and minimum on a subgraph H with $E_H = \emptyset$. Many subgraphs of very different sizes within the same graph may have maximum edge–edge density. For instance, every subgraph in the complete graph with at least 2 vertices has maximal edge–edge density 1. In particular, the subgraph of two nodes connected by a single edge has maximum edge–edge density. As a result, one must specify a range of acceptable sizes for possible. An algorithmic framework for studying the edge–edge density is still nascent [23], and to our knowledge, has not been directly applied to core–periphery detection. Moreover, we are not aware of extensions of the edge–edge density to weighted networks. The challenge of this extension comes in part because the denominator of Eq. (4.21) may have several different extensions for a weighted network.

The *edge–node density* [92] of a subgraph H is defined as

$$d_V(H) := \frac{|E_H|}{|V_H|} \, . \tag{4.22}$$

Finding a maximal edge–node density subgraph can be translated into a MIN-CUT problem [23, 92]. The MIN-CUT problem is the task on a weighted undirected graph that partitions the network into two subsets S and S^c such that $|\partial S|$ is minimized. Note that $2d_V(H)$ is the average degree of the subgraph H. One can rephrase the maximal edge–node dense subgraph problem as finding a subgraph with maximal degree (here, degree is the degree in H rather than in G). Let $S \subset V$ be a subset of nodes. We define $d_V(S)$ and $d_E(S)$ to be $d_V(H_S)$ and $d_E(H_S)$, where H_S is the *induced subgraph* on the nodes of S. When we think of core–periphery structure as a partition, it is useful to have notation for this induced subgraph density. The notion of a dense subgraph can be generalized to weighted networks using total edge weight and enjoys the same computational efficiency [92].

Although a maximal edge–node density can be extracted in $O(|V|)$-time when $G = (V, E)$ is unweighted or weighted [23], edge–node density may not be desirable to examine core–periphery structure. We illustrate this with a family of synthetic unweighted networks $G_n = (V, E)$ indexed by a size parameter $n > 1$ with a core C and periphery P such that $|C| = |P| = n$. Let $G_n = (V, E)$ such that C and P partition V and both C and P each have n nodes. Let C be a complete subgraph. Let each node of P be connected to each node of C. Further assume no pair of nodes in P are connected to each other. We show that any maximal edge–node density subgraph of G_n that contains C must also include all nodes of G_n. In general, if we consider a subgraph $H \subset G_n$ and add a node v in $V \backslash V_H$ such that v is adjacent to more nodes in H than $d_V(H)$, then the edge–node density increases. This follows from the fact that

$$\begin{aligned} d_V(H \cup \{v\}) &> \frac{|E_H| + d_V(H)}{|V_H| + 1} \\ &= \frac{|E_H| + \frac{|E_H|}{|V_H|}}{|V_H| + 1} \\ &= \frac{|E_H|}{|V_H|} \times \frac{1 + \dfrac{1}{|V_H|}}{1 + \dfrac{1}{|V_H|}} \\ &= d_V(H)\,, \end{aligned}$$

where $H \cup \{v\}$ is the subgraph adding v to H and all incident edges of v that connect to nodes in H. For any proper subgraph H of G_n that contains C, $d_V(H)$ is bounded from above by $\frac{1}{2}(2n-1)$ because the maximum degree in G_n is $2n-1$. However, whenever a new node of P is added, we introduce n new edges since we assume $C \subset H$. Therefore, the number of incident edges to a new node from C is larger than $d_V(H)$ because $n > \frac{1}{2}(2n-1)$. From our heuristic, we expect that for G_n, the node sets C and P provide a partition that describes a core–periphery structure. Specifically, core nodes are connected to the entire network and peripheral nodes are not well connected to each other (there are no edges connecting any pair of peripheral nodes). Unfortunately, the subgraph with largest edge–node density does not partition G_n as we expect.

In general, one must be careful when adapting combinatorial quantities or methods to examine core–periphery structure. First, many quantities and methods are defined for unweighted networks and may not suitable for weighted networks. Additionally, some networks may admit a particular core–periphery description that is incompatible with a combinatorial quantity or method. For example, when we describe core–periphery structure as a partition of a G_n into C and P above, this was not compatible with the notion of a dense subgraph with respect to edge–node density.

4.2.2 Models for Core–Periphery Structure

As we discussed at the beginning of Section 4.2, core–periphery structure can be described with the heuristic that core nodes are well connected to the entire network, while peripheral nodes are poorly connected to each other. We introduced this heuristic specifically for the unweighted case and discussed it appropriate adaption to the weighted case. In this section, we overview models for core–periphery and their related models that arise outside of graph-theoretic setting. Although many of the methods that we introduce in Section 4.2.1 have been explored in empirical settings, many of the models for core–periphery structure that we discuss now frequently require numerical simulations and consider more general network structures. We will focus on weighted and unweighted networks, and will make sure the particular structure is apparent. As usual, we assume our networks are undirected, unless otherwise specified.

We first discuss *stochastic block models* that describe core–periphery structure in unweighted networks. It is convenient to consider generative network models that specify blocks of nodes and the inter– and intra–connection probabilities of connections as in [168]. We investigate stochastic block models that represent a particular form core–periphery structure. In this case, we assume that core and periphery are blocks of nodes and hence are described with a partition of our network. Although these models are not historically the first to describe core–periphery structure in networks, they have been used to explore core–periphery structure in synthetic networks [54, 176, 216]. For stochastic block models with core–periphery structure, we consider two blocks, C and P. Set $|C| = n_c$ and $|P| = n_p$. One defines the the stochastic symmetric matrix $\mathbf{S}$ as in [168, 216] to specify the edge probability across and within core/periphery blocs as

$$\mathbf{S} = \begin{array}{c c} & \begin{array}{cc} C & P \end{array} \\ \begin{array}{c} C \\ P \end{array} & \begin{pmatrix} p_{cc} & p_{cp} \\ p_{cp} & p_{pp} \end{pmatrix} \end{array} . \tag{4.23}$$

For instance, we place an edge between two nodes in C with probability p_{cc}. One additionally stipulates that

$$p_{cc} \geq p_{cp} \geq p_{pp} \ , \tag{4.24}$$

with at least one strict inequality so that we do not have the Erdős-Rényi model [75]. Assuming we measure how well connected a node according to which nodes and how many a particular node is adjacent to, this block model (Eq. (4.23)–(4.24)) satisfies the heuristic that a core node is well-connected to a network and periphery connected is poorly connected to itself. Moreover, the constraints in Eq. (4.24) imply that a core has highest expected degree and periphery has the lowest expected degree. Frequently, a coarse measure for core–periphery structure is to group nodes according to their degree. For stochastic block models described according to Eq. (4.23)–(4.24), degree can in fact be used to partition nodes and extract the desired structure. In general, we cannot expect that core–periphery structure to be entirely determined from the distribution of degrees and even in the case of the stochastic block model we consider, more advanced methods can be used to partition nodes with greater accuracy. In Figure 4.4, we illustrate the adjacency matrix of a stochastic block model with $n_p = n_c = 50$ and its distribution of degrees as in [216]. We set $p_{cc} = .8$ and $p_{cp} = p_{pp} = .5$. In Figure 4.4b, we see the degree distribution of core nodes minimally overlaps from the degree distribution of peripheral nodes. In [216], the parameters of the stochastic block models were inferred using an iterative statistical inference algorithm. Specifically, they applied belief propagation [146, 150] to infer which nodes are members of the core and periphery blocks. A powerful feature of the approach is that all the parameters (n_c, n_p, p_{cc}, p_{cp}, and p_{pp}) of the stochastic block model are approximately recovered. Unfortunately, general convergence of belief propagation requires either sparse [5] or "locally tree-like" networks [216]. Clauset et al. proposed stochastic block models for weighted networks

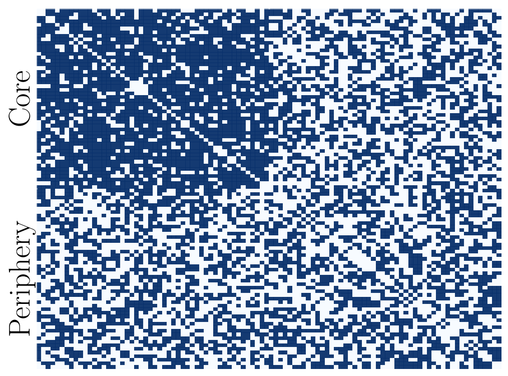

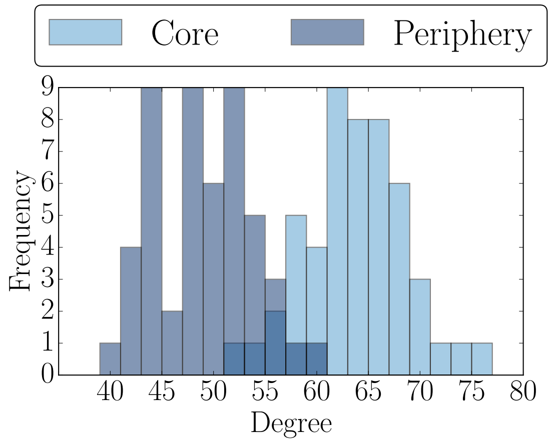

(a) **(b)**

Figure 4.4: (a) A realization of a network from the stochastic block model from Eq. (4.23)–(4.24) with parameters $n_c = n_p = 50$, $p_{cc} = .8$, and $p_{cp} = p_{pp} = .5$ specified. (b) A histogram of degrees in the same network.

in [5] and discuss possible core–periphery structures on such networks. To our knowledge, the methods in [216] do not provide a measure to compare the strength of core–periphery structures in networks. Specifically, given a particular network, it is useful to have a measure to numerically compare a networks mesoscale structure to synthetic networks (e.g. networks with identical degree distributions) or other empirical networks with similar functions. For example, we do not expect a block structure in a complete graph; in particular, we do not expect a core–periphery structure for such a graph when core–periphery structure is stipulated as a connection patterns of blocks as in Eq. (4.23)–(4.24). We remark that the work of Jeub et al. [103] provided a general discussion regarding a class of unweighted networks (expander graphs) that have poor block structure with respect to edge expansion (Eq. 4.20).

Continuing with unweighted networks, core–periphery structure can also be described in terms of low-rank matrix models [30, 54]. These models assume that the observed network's adjacency matrix is a perturbation of a low-rank matrix. In [54], Cucuringu et al. assumed that a weight matrix $\mathbf{W}$ is a perturbation of a rank-2 matrix when core–periphery structure is present. For example, Figure 4.5a shows a rank-2 matrix with self-loops at each core node. To find a rank two-approximation of an adjacency matrix $\mathbf{W}$, one computes the diagonalization $\mathbf{W} = \mathbf{Q}\mathbf{\Lambda}\mathbf{Q}^T$, where $\mathbf{Q}$ is an orthonormal matrix whose columns are eigenvectors of $\mathbf{W}$ and $\mathbf{\Lambda}$ is a diagonal matrix of eigenvalues. The rank-2 approximation is

$$\mathbf{W} \approx \mathbf{Q}\widetilde{\mathbf{\Lambda}}\mathbf{Q}^T \,, \tag{4.25}$$

where $\widetilde{\mathbf{\Lambda}}$ is the diagonal matrix with all but the top two eigenvalues of $\mathbf{W}$ set to 0. When $\mathbf{W}$ is an adjacency matrix, they also thresholded each entry of $\mathbf{Q}\widetilde{\mathbf{\Lambda}}\mathbf{Q}^T$ to 0 or 1 such that each entry greater than or equal to .5 is set to 1 and those less than .5 set to 0. In Figure 4.5, we apply this method on a stochastic block model with parameters $n_c = n_p = 50$ and $p_{cc} = p_{cp} = .8$ and $p_{pp} = .5$. One can inspect the degree distribution of the low-rank approximation of $\mathbf{W}$ and then extract a possible core–periphery division. This degree of each node associated to the low-rank approximation can also be seen as numerical scoring of core position [54]. This low-rank model can in practice be applied to weighted networks without modification. However, given possible distribution of edge weights, this approach requires careful consideration when using this model to examine core–periphery structure in weighted networks.

In [30], Everett and Borgatti provided another low-rank model to examine possible core–periphery structure for unweighted networks. They assumed that the adjacency matrix $\mathbf{W}$ of a network with core–periphery structure is rank-1. The rank is then determined according to a single vector $\mathbf{c}_{\text{cp}}$, which approximates off-diagonal elements. (They only considered networks without self-loops). Specifically, they defined $\mathbf{c}_{\text{cp}} \in \mathcal{F}_V$ as

$$\mathbf{c}_{\text{cp}} := \arg\min_{\mathbf{c}\in\mathbb{R}^n} \sum_{i\neq j} (w_{ij} - c_i c_j)^2 = \arg\min_{\mathbf{c}\in\mathbb{R}^n} ||\mathbf{P}_O(\mathbf{W} - \mathbf{c}^T\mathbf{c})||_2^2 \,, \tag{4.26}$$

where $\mathbf{P}_O : \mathbb{R}^{n^2} \to \mathbb{R}^{n^2-n}$ is the projection onto the off-diagonal of a matrix. Eq. (4.26) can be solved iteratively as in [49]. As with rank-2 approximation, this rank-1 model can be applied to weighted networks without any modification. However, the interpretation given in [30] is only for unweighted networks and must be cautiously applied to weighted networks.

Core structures can also be characterized in terms of shortest paths. In [54, 120], core nodes are characterized as those frequently occurring in short paths, while peripheral nodes

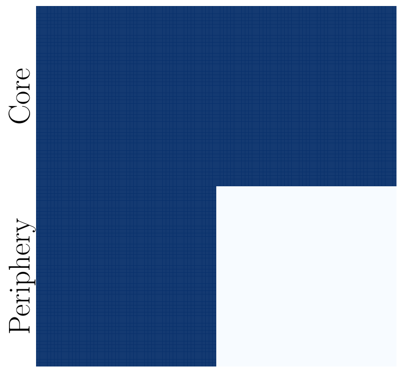

(a) Rank-2 Adjacency Matrix

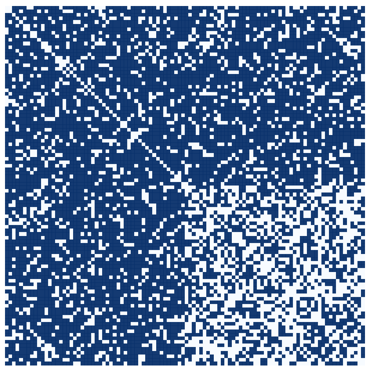

(b) Adjacency matrix

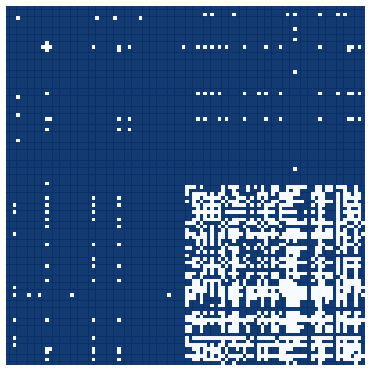

(c) Rank-2 Approximation

Figure 4.5: (a) A rank-2 adjacency matrix of a core–periphery structure. (b) An adjacency matrix that we generate from a stochastic block model with parameters $p_{cc} = p_{cp} = .8$ and $p_{pp} = .5$. (c) A rank-2 approximation of the adjacency matrix with entrywise thresholding such that each entry $\widetilde{w}_{ij}$ in rank-2 matrix is set to 0 if $\widetilde{w}_{ij} < .5$ else we set $\widetilde{w}_{ij}$ to 1.

are rarely occurring. In [120], they similarly describe core edges as those that are frequently occurring in short paths, while periphery edges are rarely occurring. In many networks, short paths between nodes represent the pathway that information is transmitted [154]. A well-known way of quantifying this heuristic for nodes is *betweenness centrality* [154, 176]. Let σ_{st} be the number of shortest paths between $s, t \in V$. Let $\sigma_{st}(i)$ be the number of shortest paths between $s, t \in V$ that pass through i. In either case, if no such path exists, we define this quantity to be 0. The betweenness centrality b_i of a node i is defined as

$$b_i = \sum_{\substack{s,t \in V \setminus i\, : \\ s<t}} \frac{\sigma_{st}(i)}{\sigma_{st}} \, . \tag{4.27}$$

For simplicity, we assume that the network is connected so there is no division by 0. For fixed $s, t \in V$, if the ratio of shortest paths $\left(\frac{\sigma_{st}(i)}{\sigma_{st}}\right)$ between s and t that pass through i is large relative to other nodes, then node i has a core position relative to nodes s and t. Summing this ratio for all possible pairs is what determines betweenness centrality and can be used to assess core position in a network. In [176], a family of stochastic block models (specifically, Eq. (4.23)–(4.24) with $p_{cc} = k^2/4$ and $p_{cp} = p_{pp} = k/4$ for $k \in [1, 2]$ and $n_c = n_p = 50$) had nodes from the specified core block with much smaller betweenness centrality than nodes from the periphery block. In [54, 120], Cucuringu et al. improve betweenness centrality for core–periphery detection making the observation that in the rare case two peripheral nodes are adjacent, any shortest path that avoids this edge should pass through the core. Let $E\backslash i := \{st \in E | s, t \neq i\}$. Let $G\backslash st$ to be the graph omitting $st \in E$. The *path score* p_i of a node i is defined as

$$p_i := \sum_{st \in E \setminus i} \frac{\sigma_{st}(i)|_{G\setminus st}}{\sigma_{st}|_{G\setminus st}} \, . \tag{4.28}$$

When there are not paths in $G\backslash st$, the ratio in Eq. (4.28) is set to 1. The removal of st of the graph differentiates Eq. (4.28) from betweenness Eq. (4.27) [175]. Cucuringu et al. expected that many short paths should pass through the core: the removal of any edge between core nodes should not impact the betweenness centrality. However, if two peripheral nodes are connected by an edge, the removal of this edge should force shortest paths to travel through the core. An analogous measure for edges is defined in [120]. The time complexity of computing the vector $\mathbf{p}$ of path scores is $O(|E|^2)$ [54], which is prohibitive for large dense graphs.

One can also measure for core–periphery structure is using the stationary distribution of a random walker in a network. We employ the terminology of a discrete-time random walk described in Section 3.5.1. Such measures are easily adapted to weighted networks if one assumes that a random walker travels to an adjacent node with probability proportional to the weight of the incident edge connecting the edges. We assume that the walker has probability 0 of remaining at the same node. Consider a random walker that begins a discrete time random walk at node i with probability $(q_0)_i$. The $n \times 1$ column vector of all such probabilities is $\mathbf{q}_0$. Let $\mathbf{q}_t$ be the vector of probabilities associated that a random walker is at node i at time $t \in \mathbb{N}$. We specify the time-homogeneous transition between discrete times as

$$\mathbf{q}_t^T = \mathbf{q}_t^T \mathbf{T} \ , \tag{4.29}$$

where $\mathbf{T}$ is the transition matrix. In this discussion, we set $\mathbf{T} = \mathbf{D}^{-1}\mathbf{W}$, where $\mathbf{D}$ is the diagonal matrix of degrees and $\mathbf{W}$ is the weight matrix. Each entry of $\mathbf{T}$ has the form

$$T_{ij} = \frac{w_{ij}}{d_i} \ . \tag{4.30}$$

The stationary distribution $\mathbf{q}_\infty$ is the solution to the linear system $\mathbf{q}_\infty^T = \mathbf{q}_\infty^T \mathbf{T}^T$. As in [130], we note that

$$(q_\infty)_i = \frac{d_i}{\sum_{i',j' \in V} w_{i'j'}} = \frac{d_i}{\sum_{j' \in V} d_j} \tag{4.31}$$

for undirected weighted networks. In [59], core structure of a set S was measured in terms of the probability that a random walker stays in S after a single time step and its initial state is $\mathbf{q}_\infty$. This is

$$\alpha_S = \frac{\sum_{i,j \in S} (q_\infty)_i T_{ij}}{\sum_{i \in S} (q_\infty)_i} \ . \tag{4.32}$$

Substituting Eq. (4.30) and Eq. (4.31) into Eq. (4.32), we obtain

$$\alpha_S = \frac{\sum_{i,j \in S} w_{ij}}{\sum_{i \in S} d_i} \ . \tag{4.33}$$

We expect a set S of peripheral nodes to have $\alpha_S \approx 0$. In [59, 130], a randomized greedy algorithm was employed to incrementally add nodes from a network to build a periphery set S with low α_S. Nodes of a network can also be ranked in the order they are added to a periphery set S using this greedy algorithm. Let S_k be the set S after k nodes have been added. Let i_k be the k^{th} node added to S. The node i_k may be different with different runs of the randomized algorithm in [59]. The authors in [59] measured the core quality of a node as $\alpha_{i_k} = \alpha_{S_k} - \alpha_{S_{k-1}}$. Using this ranking of nodes, they profiled a core–periphery structure by incrementally adding nodes to S and inspecting the curve α_{i_k} versus $k = 1, \ldots, n$. Their null model for assessing the presence of core-periphery in *unweighted* networks is the complete graph, where α_{i_k} increases linearly as $\alpha_{i_k} = k/n$. Networks with more core–periphery structure have α_{i_k}-curves below this curve and candidate periphery sets P are those with $\alpha_P \approx 0$. The authors suggested with various numerical experiments that these curves can be used to compare the presence of core–periphery structure in networks. We remark that, in the recent work of Jeub et al. [103], the authors suggested that expander graphs do not have identifiable block structure. It seems a natural question to ask if α_{S_k} has a similar contour as a complete graph. We do not agree with the authors of [59] that complete graphs are an appropriate null model. A large sparse unweighted network has such different global structure than a complete graph of the same size that it doesn't seem appropriate to compare these two networks. However, expander graphs may serve as a more appropriate null model assuming they have similar α_{i_k}-curves.

In the early pioneering work on core–periphery structure [98], Holme provided another distance-based measure to assess core–periphery structure in unweighted networks. Recall that the *closeness centrality* $C_C(i)$ of a node is

$$C_C(i) = \sum_{j \in V} \frac{1}{d(i,j)} \ ,$$

where $d(i,j)$ denotes the shortest path distance from node i to j [154]. The closeness centrality of a node i measures when the shortest path length between i and other nodes is small. In [98], Holme defined the closeness centrality of a subset U of nodes V as

$$C_C(U) = \langle C_C(i) \rangle_{i \in U} \tag{4.34}$$

Holme defined the core vertices $V_{\text{core}}(G)$ of a network G as the k-core (see Section 4.2.1) that maximizes the closeness centrality in Eq. (4.34). He also defined the core coefficient c_c for evaluating if a network possessed core–periphery structure as

$$c_c(G) = \frac{C_C(V_{\text{core}}(G))}{C_C(V)} - \left\langle \frac{C_C(V_{\text{core}}(G'))}{C_C(V')} \right\rangle_{G' \in \mathcal{G}(G)} , \tag{4.35}$$

where $\mathcal{G}(G)$ is the set of networks with the same degree distribution as G generated using a configuration model (self-loops permitted) [83]. In this case, the null model is taken to be a configuration model and the core–periphery structure in a given network is compared to networks generated from this null model. We observe that the null model selected (a configuration model) is highly constrained when dealing with unweighted networks with a core that is well connected to the entire network such as G_n from Section 4.2.1. Specifically, if we consider a network with the same degree distribution as G_n, there are no other possible networks if we forbid self-loops. Additionally, because degree can serve as a preliminary way to classify core and peripheral nodes for certain core and periphery structures, we expect that certain degree distributions may be much more likely to exhibit particular core–periphery structures. As a result, the configuration model may not serve as null model that effectively differentiates networks with high core–periphery structure and those that do not.

Ecologists have also developed their own notions of core–periphery structure to study animal–plant interactions. The so-called *mutualistic frugivore–seed networks* are networks that encode the interactions between fruit-eating species (frugivores) and the seeds they spread [136, 137, 183]. These networks are *bipartite networks*. A bipartite network is a network with two *independent sets* S_1 and S_2 of nodes. Subsets S_1 and S_2 of nodes are said to be independent if no edges have both endpoints in the same set. An important core quantity associated to such mutualistic networks is *nestedness*. There is a lot of debate among ecologists and network scientists as to the appropriate definition of nestedness in mutualistic networks [52]. We discuss a few notions of nestedness in this chapter. According to [52], a heuristic that frequently guides the notion of a perfectly nested mutualistic network is a network with the following property: if the degrees d_i and d_j of nodes i and j respectively obey $d_i < d_j$, then all of the adjacent nodes of i are also adjacent to j. To measure nestedness in unweighted bipartite networks, the authors in [167] proposed a *nestedness coefficient* N_c. They labeled nodes by degree so that $i < j$ implies that $d_i < d_j$. They first defined the *matching coefficient*

$$N_{ij} = \frac{|N_i \cap N_j|}{|N_i|} = \frac{|N_i \cap N_j|}{d_j} \; ,$$

where N_i is the set of adjacent nodes of i. The nestedness coefficient is then

$$N_c = \frac{\sum\limits_{\substack{i,j \in S_1, \\ i<j}} N_{ij} + \sum\limits_{\substack{i,j \in S_2, \\ i<j}} N_{ij}}{\binom{|S_1|}{2} + \binom{|S_2|}{2}} \; . \tag{4.36}$$

The authors in [6] extended nestedness to weighted networks. First, they defined the *weighted matching coefficient*

$$N_{ij}^{w} = \sum_{\substack{l \in V: \\ l \in N_i \cap N_j}} \min(w_{il}, w_{jl}) \; . \tag{4.37}$$

This weighted matching coefficient is then substituted into Eq. (4.36). In [120], N_{ij}^{w} is defined as $\sum_{\substack{l \in V: \\ l \in N_i \cap N_j}} 1_{w_{il} < w_{jl}}$, where $1_{w_{il} < w_{jl}} = 1$ if $w_{il} < w_{jl}$ and 0 otherwise. In [120], Lee explores particular core–periphery structures and nestedness on synthetic and ecological networks and found high correlation between the measures he investigated. He suggests that core–periphery and nestedness are related, and are "two sides of the same coin." There are several other related definitions of nestedness on bipartite networks [52, 208]. Nestedness can also be extended to general non-bipartite networks in [118]. We remark that for many notions of nestedness including the unweighted coefficient N_c in Eq. (4.36) assumes that degree determines how nested a node is in a network. While nestedness does not explicitly score nodes according to its core position or partition nodes into different blocks, the basic assumption that a nested core are those with highest degree contrasts many models of core–periphery structure such as k-core used by Holme [98].

In the seminal work of [30], Everett and Borgatti first to formalized the study of core-periphery structure in networks. We discuss a model they proposed using the graph calculus that we discussed in Section 4.1. Let us first consider $G = (V, E)$ to be a weighted network.

In this model, Everett and Borgatti viewed core–periphery structure as a partition of nodes into a core C with $|C| = n_c$ and periphery P with $|P| = n_p$. Let $\mathcal{B}_V(n_c)$ be the set of binary-valued functions on V that map n_c vertices to 1. Specifically,

$$\mathcal{B}_V(n_c) = \{\mathbf{f} \in \mathcal{F}_V \mid \mathrm{ran}(\mathbf{f}) = \{0,1\},\ \mathbf{1}_n^T\mathbf{f} = n_c\}\ , \tag{4.38}$$

where $\mathbf{1}_n$ is the $n \times 1$ vector of 1s. The set $\mathcal{B}_V(n_c)$ specifies candidate core sets of size n_c. Let $F_a : \mathbb{R}^2 \to \mathbb{R}$ for $a \in [0,1]$ be the function

$$F_a(x,y) = \begin{cases} 1 & \text{if } x = y = 1 \\ 0 & \text{if } x = y = 0 \\ a & \text{otherwise .} \end{cases}$$

We define a core–periphery structure as a maximization of a functional $\mathbf{E}_a : \mathcal{B}_V(n_c) \to \mathbb{R}$. Let $\mathbf{E}_a : \mathcal{F}_V \to \mathbb{R}$ be the functional

$$\mathbf{E}_a(\mathbf{f}) = \sum_{i,j \in V} w_{ij} F_a(f_i, f_j)\ . \tag{4.39}$$

One then determines

$$\chi_C = \underset{\mathbf{f} \in \mathcal{B}_V(n_c)}{\arg\max}\ \mathbf{E}_a(\mathbf{f})\ . \tag{4.40}$$

In this model, it is crucial to specify n_c (the size of the core) otherwise the functional is trivially maximized when $\mathbf{f} = \mathbf{1}_n$. The maximization in Eq. (4.39) can be expressed as

$$C = \underset{S \subseteq V;\ |S| = n_c}{\arg\max}\ \mathrm{vol}(S) + (2a - 1)|\partial S|\ , \tag{4.41}$$

where $\mathrm{vol}(S)$ and ∂S were defined in Eq. (4.15) and Eq. (4.16), respectively. This follows from the following computation for $\mathbf{f} = \chi_S$:

$$\begin{aligned}
\sum_{i,j\in V} w_{ij}F_a(f_i,f_j) &= \sum_{i,j\in S} w_{ij}F_a(f_i,f_j) + 2\sum_{\substack{i\in S,\\ j\in V\setminus S}} w_{ij}F_a(f_i,f_j) + \sum_{i,j\in V\setminus S} w_{ij}F_a(f_i,f_j)\\
&= \sum_{i,j\in S} w_{ij} + 2a\sum_{\substack{i\in S,\\ j\in V\setminus S}} w_{ij}\\
&= \sum_{i,j\in S} w_{ij} + \sum_{\substack{i\in S,\\ j\in V\setminus S}} 1 - \sum_{\substack{i\in S,\\ j\in V\setminus S}} 1 + 2a\sum_{\substack{i\in S,\\ j\in V\setminus S}} w_{ij}\\
&= 2|E_S| + |\partial S| - |\partial S| + 2a|\partial S|\\
&= \mathrm{vol}(S) + (2a-1)|\partial S|\ .
\end{aligned}$$

We now investigate the parameter a using Eq. (4.41). When $a = 1/2$, the solution to the cut problem is precisely the set of n_c nodes with highest degree in G as vol(S) is the sum of degrees of nodes in S. When $a = 0$, the cut problem of Eq. (4.41) is equivalent to finding the maximum edge–node density subgraph of fixed size [77] because we are maximizing $|E_S|$ (Eq. (4.19)). Recall the extraction of subgraph with maximum edge–node density is equivalent to a minimum cut, where there is no restriction on the possible size of a subgraph [92]. However, if we restrict our search to only those subgraphs of fixed size, the problem becomes NP-hard [77]. When $a = 1$, Eq. (4.41) becomes $2|E_S| + 2|\partial S|$. In other words, the number of edges contained entirely in S and the number of edges from S to S^c are weighted equally. We are not aware of related combinatorial quantities.

We can relate Eq. (4.41) to the edge–node densest subgraph problem (see Section 4.2.1) for all $a \in [0,1]$. Let $n_c \leq |V|/2$. We can divide both sides of Eq. (4.41) by $|S|$ without affecting the maximum S since n_c is fixed. The cut energy is given by

$$\frac{\mathrm{vol}(S)}{|S|} + \frac{(2a-1)|\partial S|}{|S|} = 2d_V(G_S) + 2a\cdot e_E(G_S), \tag{4.42}$$

where e_E is the edge expansion (Eq. (4.20)). We assumed that $|S| \leq |V|/2$ to ensure the equality of Eq. (4.42) holds.

We now relate Eq. (4.39) to *eigenvector centrality* $\mathbf{e}$ as in [30]. Borgatti and Everette viewed eigenvector centrality as a numerical score to measure each node's core position in the network. We note this is a different approach from their model that assumed there was an underlying partition of core and periphery nodes. Eigenvector centrality $\mathbf{e} \in \mathcal{F}_V$ is defined to be a unit-length $n \times 1$ eigenvector associated to the largest eigenvalue of the weight matrix $\mathbf{W}$ [175]. Because $w_{ij} \geq 0$, the Perron–Frobenius theorem guarantees that there is a unit-length $\mathbf{e}$ with $e_i \geq 0$ for all $i = 1, \ldots, n$ [191] . If we set $a = 0$ in Eq. (4.39), then

$$\begin{aligned}\mathbf{E}_0(\mathbf{f}) &= \sum_{i,j \in V} w_{ij} F_0(f_i, f_j) \\ &= \sum_{i,j \in V} w_{ij} f_i f_j \\ &= \mathbf{f}^T \mathbf{W} \mathbf{f} \ ,\end{aligned}$$

for binary $\mathbf{f} \in \mathcal{F}_V$. Let the quadratic form $\mathbf{Q_W}$ for $\mathbf{f} \in \mathcal{F}_V$ be

$$\mathbf{Q_W}(\mathbf{f}) := \mathbf{f}^T \mathbf{W} \mathbf{f} \ . \tag{4.43}$$

The largest eigenvector of $\mathbf{W}$ maximizes $\mathbf{Q_W}$ over the set of unit vectors [191]. Thus, if change the constraint on $\mathbf{f}$ in Eq. (4.39) to those with $||\mathbf{f}|| = 1$ and set $a = 0$, we recover eigenvector centrality. We can view this eigenvector as a ranking of a each node's "coreness", which we refer to as a nodes *core score*. A node's core score is a numerical score assigned to each node according to a particular core–periphery model. We specify a core score using an $\mathbf{f} \in \mathcal{F}_V$.

In [176], the core–periphery models from Eq. (4.39) and Eq. (4.40) were generalized so that the constraint on $\mathbf{f}$ is relaxed to a broader classes of functions to obtain core scores. We focus on a particular case discussed in which the functions were piecewise-linear. First, they defined the sets

$$S_1(\alpha, \beta, n) := \left\{ \frac{k(1-\alpha)}{2\lfloor \beta n \rfloor} \ \middle| \ k = 1, \ldots, \lfloor \beta n \rfloor \right\} \ , \tag{4.44}$$

$$S_2(\alpha, \beta, n) := \left\{ \frac{(k - \lfloor \beta n \rfloor))(1-\alpha)}{2(n - \lfloor \beta n \rfloor} \ \middle| \ k = \lfloor \beta n \rfloor + 1, ..., n \right\} \ , \tag{4.45}$$

$$S(\alpha, \beta, n) := S_1(\alpha, \beta, n) \cup S_2(\alpha, \beta, n) \ , \tag{4.46}$$

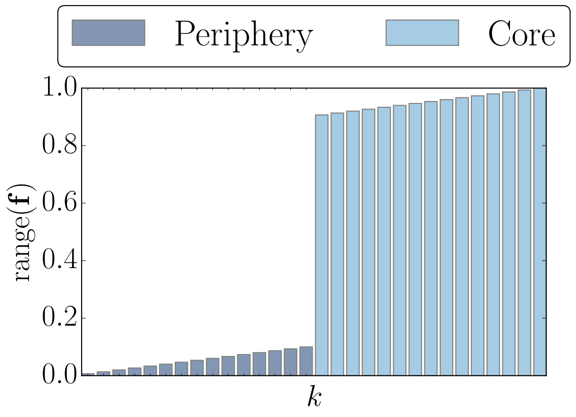

Figure 4.6: $S(\alpha, \beta, n)$ where $\alpha = .7$, $\beta = .5$, and $n = 30$. We consider $\mathbf{f}_{\alpha,\beta}$ with range $S(\alpha, \beta, n)$.

where $n \in \mathbb{N}$, $\alpha \in [0, 1]$, and $\beta \in (0, 1)$. For this discussion, let $n = |V|$. In Figure 4.6, we show $S(\alpha, \beta, n)$ with $\alpha = .7$, $\beta = .5$, and $n = 30$. Rombach et al. then replace $\mathcal{B}_V(n_c)$ of candidate binary functions (Eq. 4.38) with the set

$$\mathcal{P}_V(\alpha, \beta) = \{\mathbf{f}_{\alpha,\beta} \in \mathcal{F}_V \mid \text{ran}(\mathbf{f}_{\alpha,\beta}) = S(\alpha, \beta, n)\} \; . \tag{4.47}$$

Note that $|S(\alpha, \beta)| = n$ so $\mathbf{f}_{\alpha,\beta}$ hits precisely each element of $S(\alpha, \beta, n)$ exactly once. The function $\mathbf{f}_{\alpha,\beta}$ maps peripheral nodes to $S_1(\alpha, \beta, n)$ and core nodes to $S_2(\alpha, \beta, n)$. The parameter β specifies the fraction of nodes to include into the periphery ($|P| = \lfloor \beta n \rfloor$), and the parameter α represents the discontinuity of $\mathbf{f}$ between peripheral node scores and core node scores.

In [176], the authors also considered more general F in the functional $\mathbf{E}_a$ (Eq. (4.39)). This function $F : \mathbb{R}^2 \to \mathbb{R}$ in [176] is called a *transition function*. In [176], the authors considered nonnegative functions that are monotonic in each component, that is for every fixed x_0, the function $F(x_0, y)$ is monotonic in y. For example, they considered the L^p norm on $\mathbb{R}^n$ to be a transition function $F_p(x, y) = ||x^p + y^p||^p$ and multiplication $F(x, y) = xy$.

With these constructions, Rombach et al. defined the functional

$$\mathbf{E}(\mathbf{f}) = \sum_{i,j \in V} w_{ij} F(f_i, f_j) \; . \tag{4.48}$$

We often consider $F(x,y) = xy$ because the functional E in Eq. (4.48) resembles the quadratic form in Eq. (4.43) discussed in [30]. A core score $\widehat{\mathbf{f}}_{\alpha,\beta}$ is obtained through the maximization procedure

$$\widehat{\mathbf{f}}_{\alpha,\beta} = \underset{\mathbf{f}_{\alpha,\beta}\in\mathcal{P}(\alpha,\beta)}{\arg\max}\ \mathbf{E}(\mathbf{f}_{\alpha,\beta}) \ . \tag{4.49}$$

Numerically, the function $\widehat{\mathbf{f}}_{\alpha,\beta}$ is obtained through a stochastic optimization technique known as simulated annealing. We briefly discuss simulated annealing for this application in Appendix B.1. To assess the validity of a particular core score $\widehat{\mathbf{f}}_{\alpha,\beta}$, the authors of [176] defined the *core quality* $R_{\alpha,\beta}$ as

$$R_{\alpha,\beta} = E(\widehat{\mathbf{f}}_{\alpha,\beta}) = \sum_{i,j\in V} w_{ij}\ \widehat{\mathbf{f}}_{\alpha,\beta}(i)\widehat{\mathbf{f}}_{\alpha,\beta}(j) \ . \tag{4.50}$$

To obtain a core score independent of the parameters α and β, Rombach et al. defined the *aggregate core score* as the weighted mean with respect to the core quality of a core score for fixed α and β. Specifically,

$$\mathbf{f}_{\text{cp}}(i) = \frac{1}{Z}\sum_{\alpha,\beta}\widehat{\mathbf{f}}_{\alpha,\beta}(i)R_{\alpha,\beta} \ , \tag{4.51}$$

where Z is a normalizing constant so that $\mathbf{f}_{\text{cp}}(i) \in [0,1]$ for all $i \in V$. The aggregate core score $\mathbf{f}_{\text{cp}}$ is quite computationally expensive to compute because to obtain this vector, the maximization problem Eq. (4.49) must be solved for each (α,β) on a mesh of $[0,1]\times(0,1)$ (these restrictions on α and β are required by Eq. (4.46)).

Although core scores provide extra information about a core–periphery structure, there is not a standard way of obtaining a partition. In [54], Cucuringu et al. defined the following core–periphery cut CP-Cut(C,P) for a given partition C and P in V:

$$\text{CP-}\textsc{Cut}(C,F) = \frac{1}{n}\left(\frac{|E_C|}{\binom{|C|}{2}} + \frac{E(C,P)}{|C||P|} - \frac{|E_P|}{\binom{|P|}{2}}\right) \ . \tag{4.52}$$

This is related to the densities discussed in Section 4.2.1, as one can write

$$\text{CP-}\textsc{Cut}(C,P) = \frac{1}{n}\left(d_E(C) + \frac{E(C,P)}{|C||P|} - d_E(P)\right) \ . \tag{4.53}$$

Cucuringu et al. [54] also discussed an optional term to control the core-size in Eq. (4.52). To determine a cut from a general core score $\mathbf{f}$, Cucuringu et al. outlined the following process in [54]. First, one orders $\mathbf{f}$ as $f_{i_1} \leq f_{i_2} \leq \ldots \leq f_{i_n}$ or as $f_{i_1} \geq f_{i_2} \geq \ldots \geq f_{i_n}$ so that i_1 is the most core-like node and i_n is the most periphery-like node with respect to $\mathbf{f}$. One then computes the cut in Eq. (4.52) for C_k of the form $\{i_1, \ldots, i_k\}$ and $P_{n-k} = V \backslash C$. The final C and P are those sets with maximum $\text{CP-Cut}(C_k, P_{n-k})$ such that $k, n-k > \tau$ for some fixed $\tau \in \mathbb{N}$. Although the cut from Eq. (4.52) captures the heuristic associated with core–periphery structure, there are some challenges. Define the function $L : \{1, \ldots, n\} \to \mathbb{R}$ as $L(k) = \text{CP-Cut}(C_k, P_{n-k})$. In general, because we expect the landscape of Eq. (4.52) to be nonconvex with many local maxima according to all possible partitions C and P, the 1-dimensional view of this cut (i.e. L) can still be nonconvex, too [54]. Moreover, the core score $\mathbf{f}$ that we select may be measuring a different core–periphery structure and it is not clear the relative size of L's maximum relative to the absolute maximum of the cut for all possible partitions.

Lastly, there are some exploratory methods for core–periphery detection related to Eq. (4.39) and Eq. (4.48) [30]. Given a centrality $\mathbf{c}$ or a vector of core scores $\mathbf{f}$, one defines a *core matrix* $\mathbf{K}$ as

$$K_{ij} = w_{ij} F(f_i, f_j) \, . \tag{4.54}$$

As in [30], we consider $F(x, y) = xy$. One can rescale $\mathbf{K}$ to ensure that $K_{ij} \in [0, 1]$ by dividing entrywise by the maximum value in $\mathbf{K}$. One can explore the core matrix directly or further threshold low-weight edges to 0. Specifically,

$$\widetilde{K}_{ij} = \begin{cases} K_{ij} & \text{if } K_{ij} > t, \\ 0 & \text{otherwise,} \end{cases} \tag{4.55}$$

with $t \in \mathbb{R}$ a thresholding constant. In this discussion, we have thresholded $\mathbf{K}$ using the median of $\mathbf{K}$'s nonzero entries. In Figure 4.7, we provide some examples of core matrices. We use degree centrality, eigenvector centrality, and Pagerank with $\alpha = .15$.

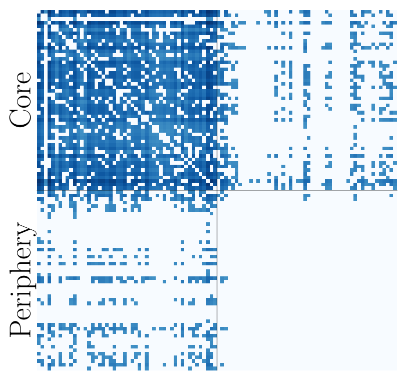

(a) Degree

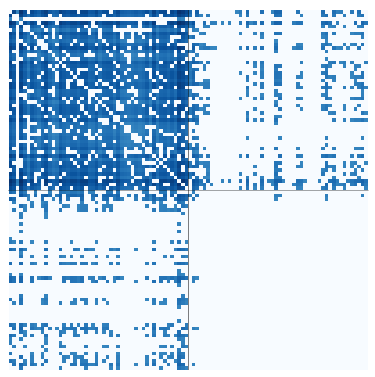

(b) PageRank ($\alpha = .15$)

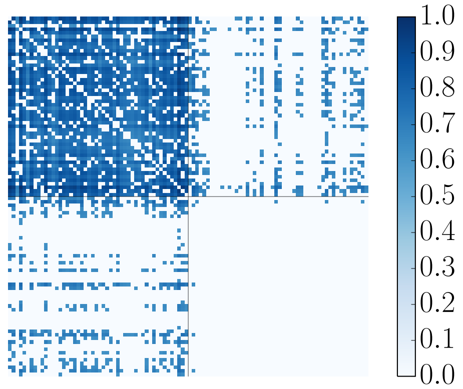

(c) Eigenvector

Figure 4.7: Core matrices for an instance of a stochastic block model using three different centralities. The network was generated using tje stochastic block model specified with Eq. (4.23)–(4.24) and parameters $n_c = n_p = 50$, $p_{cc} = .8$, $p_{cp} = p_{pp} = .5$. We set t in Eq. (4.55) to be the median of nonzero entries.

4.3 Core–Periphery Structure in Frugivore–Seed Networks

Ecological systems are not easily transferred into a network structure. The interaction patterns of two species are much more nuanced than simply counting the number of times two species interact. For example, within a particular ecological system, there are varying interaction types (e.g. avian–seed versus. predator–prey), time dependencies, and environmental factors (e.g. seasons or weather) [169]. Nonetheless, networks can provide a simplified structure to measure biological systems and quantify certain ecological phenomena [136,137,181]. For example, the community structure of seed dispersion provides insights into the precise organization of particular mutualistic networks [137,162]. In this section, we briefly discuss our joint investigation of core–periphery structure in frugivore–seed dispersion networks [179]. The focus in this section is the examination of core–periphery structure.

We model each mutualistic networks as a weighted bipartite network. We consider data collected from ecologists' observations of fruit-eating bird (frugivorous birds) and seed dispersion at 10 sites in northwestern Argentina [179, 180]. A node represents an animal or plant species. We weight each edge by the number of interactions between a bird species and a seed species during observation. This construction was also used in [6, 137]. A discussion on how this data was collected can be found in [179, 180]. Although this simple network construction is common for ecological applications, there are many potential problems with this approach [169]. In this data set, we only consider 3–4 days during the rainy season. The types of interaction patterns frequently change in different seasons [169]. In our network, the various seed types of fruits often lead to different types of dispersal by the birds. Nonetheless, we stick with this relatively simple construction because forms of core–periphery structures other than nestedness have been less studied in ecological systems. To illustrate the network structure, we show the weighted adjacency matrix and related network at Pozo Verde in Figure 4.8 and Figure 4.9, respectively.

We apply a core–periphery methods introduced in [54, 176] and that we discussed in Section 4.2.2. Specifically, we first obtain core–scores $\widehat{\mathbf{f}}_{\alpha,\beta}$ using Eq. (4.49) for $(\alpha, \beta) \in [0, 1] \times (0, 1)$ using a multiplicative transition function. We then compute aggregate core

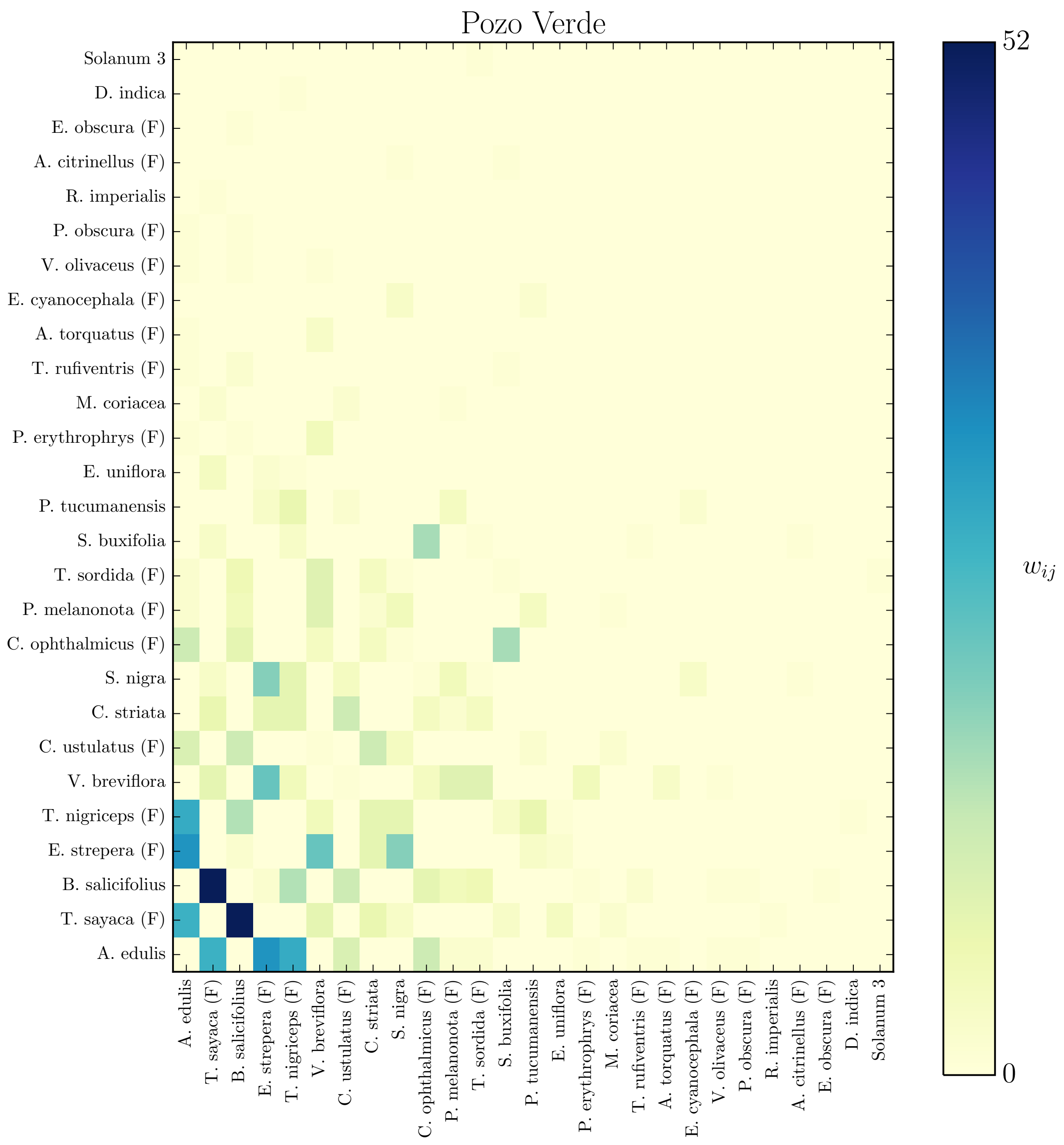

Figure 4.8: The weight matrix associated to Pozo Verde, one of the 10 sites. Each frugivore is labeled with an '(F)'. The weight between frugivores and plants is determined from the number of recorded interactions. A related network visualization is in Figure 4.9.

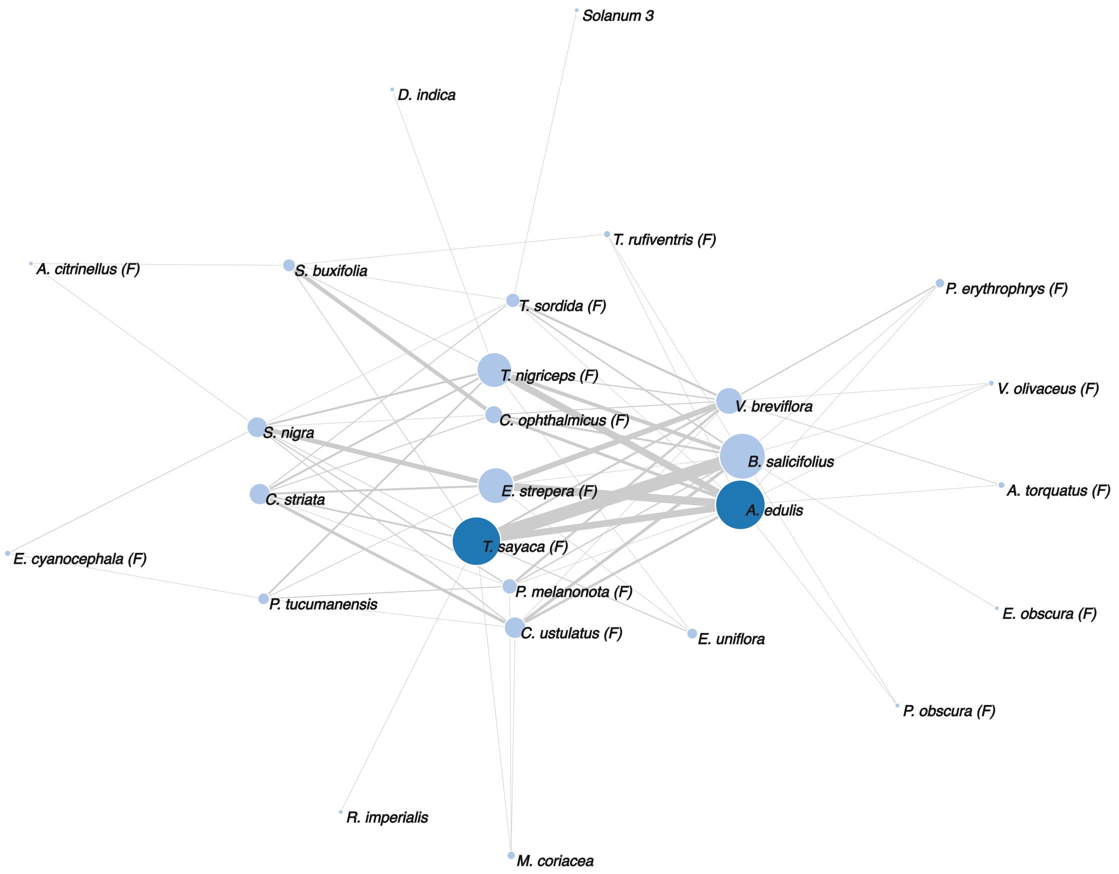

Figure 4.9: The network from Pozo Verde with weight matrix shown in Figure 4.8. The nodes's sizes are proportional to their aggregate core score (Eq. (4.51)). The edges are proportional to the weight. The two darker nodes are core-nodes. These nodes define a cut that maximizes CP-CUT from (Eq. (4.52)).

scores using Eq. (4.51). We finally propose a core–periphery partition according to the CP-Cut proposed in [54]. To obtain a partition, we order the aggregate core scores $(f_{\text{cp}})_{i_1} \geq (f_{\text{cp}})_{i_2} \geq \ldots \geq (f_{\text{cp}})_{i_n}$ and check each possible core and periphery partition of the form

$$C_k = \{(f_{\text{cp}})_{i_1}, \ldots, (f_{\text{cp}})_{i_k}\} \tag{4.56}$$

$$P_{n-k} = \{(f_{\text{cp}})_{k+1}, \ldots, (f_{\text{cp}})_{i_n}\}, \quad \text{for } k = 0, \ldots, n+1, \tag{4.57}$$

such that CP-Cut(C_k, P_{n-k}) from Eq. (4.52) is maximized. We note that when $k = 0$, C is empty and the cut takes a negative value. The definition of the cut CP-Cut(C_k, P_{n-k}) assumed an unweighted network, as two of the terms can be interpreted as an edge–edge density (Eq. (4.21)). To modify this cut for our weighted network by scaling each entry w_{ij} so that $w_{ij} \in [0, 1]$. Specifically, we divide each entry w_{ij} by the maximum over all possible entries in $\mathbf{W}$. We explore two other methods to rescale $\mathbf{W}$ as well. First, we set each nonzero to 1 and examine the underlying connections ignoring weights. Second, we divide each entry by the average of non-zero entries of $\mathbf{W}$. However, we find that these two alternative scalings of $\mathbf{W}$ produced identical cuts C and P at all 10 sites.

We select these particular core–periphery methodologies from [54,176] because this model numerically assigns a core score to each node (Eq. (4.51)) in addition to providing a partition. Moreover, the aggregate core scores from Eq. (4.51) have been applied to small (less than 100 nodes), weighted empirical networks and we believe it would be beneficial to investigate such structures in ecological networks [17, 176]. Additionally, we wanted to provide some more empirical comparisons of nestedness to core–periphery structure as in [120]. We remark that scoring nodes with Eq. (4.51) is computationally expensive. The greatest bottleneck is the computation of $R_{\alpha,\beta}$ (Eq. (4.50)) and $\widehat{f}_{\alpha,\beta}$ (Eq. (4.49)). Although each site has at most 50 nodes, the computation of the $R_{\alpha,\beta}$ and $\widehat{f}_{\alpha,\beta}$ on a 100×100 grid required approximately 2 hours per site on a quad 2.6 GHz Intel Core i7. In Figure 4.10, we display the grid of core-qualities $R_{\alpha,\beta}$ for the 100×100 grid. We note that the maximum values of $R_{\alpha,\beta}$ occur for $\beta \in (.92, .96)$. To obtain a partition from $R_{\alpha,\beta}$, we compute the aggregate core score $\mathbf{f}_{\text{cp}}$ (Eq. (4.51)) and then maximize the cut CP-Cut (Eq. (4.52)) using the ordering induced from the core scores. For all 10 sites, we find that $|C| = 2$. In Figure 4.11, we show the contour of the function $k \mapsto \text{CP-C}\textsc{ut}(C_k, P_{n-k})$. All the sites have a similar contour with maximum at $k = 2$.

We briefly verify that the core scores differ from degree. In Figure 4.12, we show a scatter plot for the degree and the core scores. We can see that for both sites, the two nodes with highest degree are the core-nodes (this was always the case). However, as we examine the group of seven nodes with highest degree, we see that there aggregate core score and degree are not perfectly correlated as in Figure 4.12b. We also compute the correlation coefficient for the entire network and find $\rho \geq .9$ at all sites.

Our colleagues used our core–periphery analysis along with additional ecological tools to identify those bird species that played a crucial role in seed dispersion [179]. We do our best to briefly discuss some of their findings. Because the cores we obtain from our methodology were rather small (precisely 2 core nodes), our collaborators used core scores to evaluate the core position of different species in a network. Our colleagues found that the bird species Austral Yungas had high core score at several sites (frequently ranked among the top five in aggregate core score). This bird species is a *masher* and often discards large seeds near the plant. As a result, many ecologists classify mashers as poor seed dispersers as opposed to gulpers that swallow fruit whole including the seeds [179]. However, the watery fruit that mashers in the ecological system ate have seeds are embedded inside the fruit and thus these seeds are more easily dispersed by mashers. Our collaborators also used our analysis to indicate that the core plant species across 10 sites were more heterogeneous than the bird species with respect to ecological metrics. Specifically, the fruits of each plant identified as core varied in shape, color, seed number, pulp mass, etc. across the 10 sites, whereas the birds had similar assemblage (bill morphology and size) across these sites. Our brief exploration of core–periphery structure in ecological networks can provide a template for more advanced core–periphery analysis in future ecological analysis. More often, nestedness is used as a measure for core structure in ecological networks. Here, we introduce a new tool for assessing core–periphery structure. Although we did not explore nestedness here, Lee in [119] explored the relationship between a particular definition of nestedness and a core–periphery model proposed in Rombac et al [176]. Lee found that the nestedness coefficient

N_c (Eq. (4.36)) was correlated with a aggregate core-quality (Eq. (4.50)) defined as:

$$R_{\mathrm{cp}} = \frac{\sum_{i,j\in V} w_{ij}\ \widehat{\mathbf{f}}_{\mathrm{cp}}(i)\widehat{\mathbf{f}}_{\mathrm{cp}}(j)}{\sum_{i,j\in V} w_{ij}\ \sum_{i,j\in V} \widehat{\mathbf{f}}_{\mathrm{cp}}(i)\widehat{\mathbf{f}}_{\mathrm{cp}}(j)}\ .$$

in synthetic and empirical networks. We hope to more carefully examine differences between possible core–periphery structure and nestedness for future ecological analysis.

4.4 Conclusions and Future Work

Core–periphery structure is a fundamental mesoscale structure. One can describe this structure as a core that is well connected to a network and a periphery that is poorly connected to itself. Even with this seemingly simple definition, there are many varied interpretations into how to quantify this structure in weighted and unweighted networks.

In Section 4.1, we reviewed graph calculus and then then used this framework to provide a mathematical overview of some of the models for core–periphery structure in 4.2. In particular, we related various combinatorial quantities in unweighted networks such as subgraph densities to the core–periphery structure, specifically to the seminal work of Everett and Borgatti [30]. We highlight those quantities that are easily generalized to the weighted case as this is our focus in our ecological application. Our original motivation for this research was to find methods to improve the computational overhead associated with methods introduced in [176] and to scale faster methods to larger networks. Although we did not accomplish this, we plan to use the research here to further explore methods for core–periphery structure and help illustrate the broad landscape of such models for related endeavors in the future.

In Section 4.3, we briefly discussed our joint work analyzing core–periphery structure in mutualistic frugivore–seed networks [179]. We identify core and periphery structures in these networks using methods from Rombach et al. [176] and discuss the interpretations of this analysis made our ecologist colleagues. For example, our colleagues found that birds classified as mashers were characterized as core at a variety of the 10 sites investigated. Our colleagues suggest that certain mashers are good dispersers at these sites because they feed on watery fruit with seeds embedded in the fruit's flesh. Typically, mashers are seen as poor

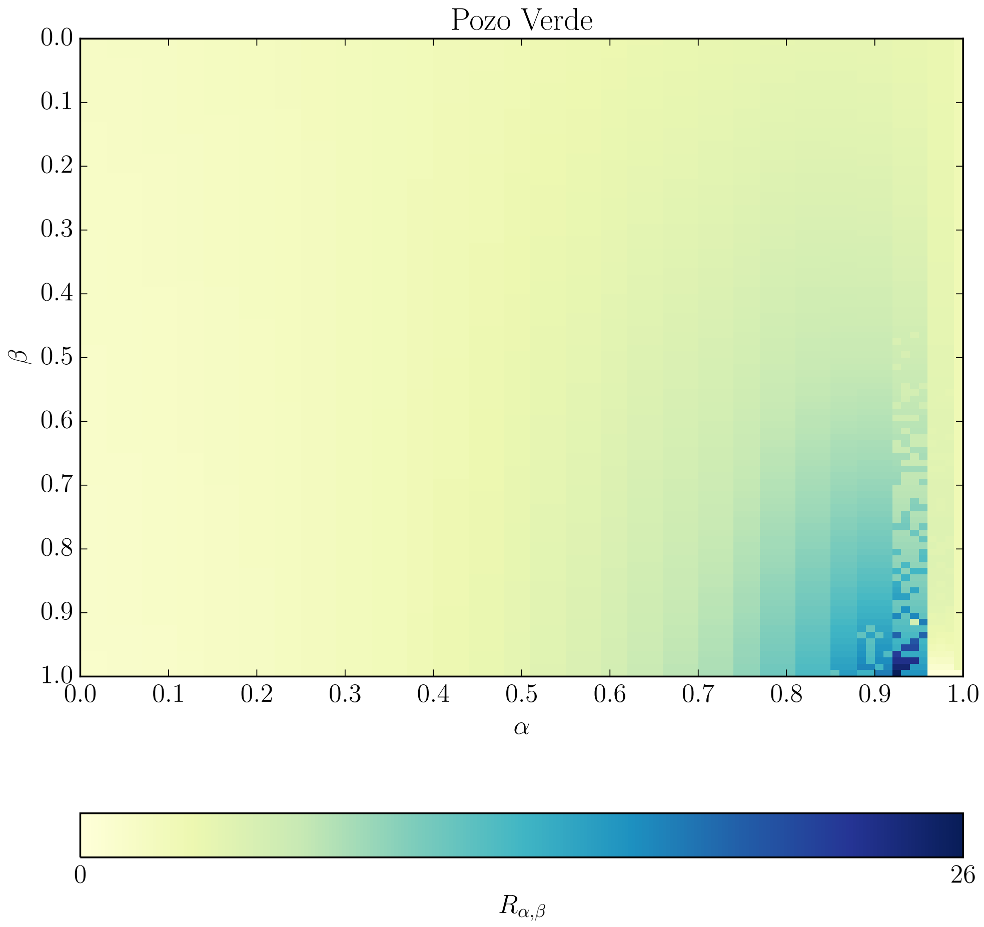

Figure 4.10: The matrix of $R_{\alpha,\beta}$ from Eq. (4.50).

dispersers because they use their beak as a sieve to sort out hard seeds when eating fruit. Admittedly, this exploration of core–periphery structure was brief, and in future work, we plan to more fully explore the bipartite nature of core–periphery structure as Larremore did for community structure [116] and Lee began to using a core–periphery structure proposed in [120]. We also hope to provide a more detailed analysis of the relationship between nestedness and core–periphery structure.

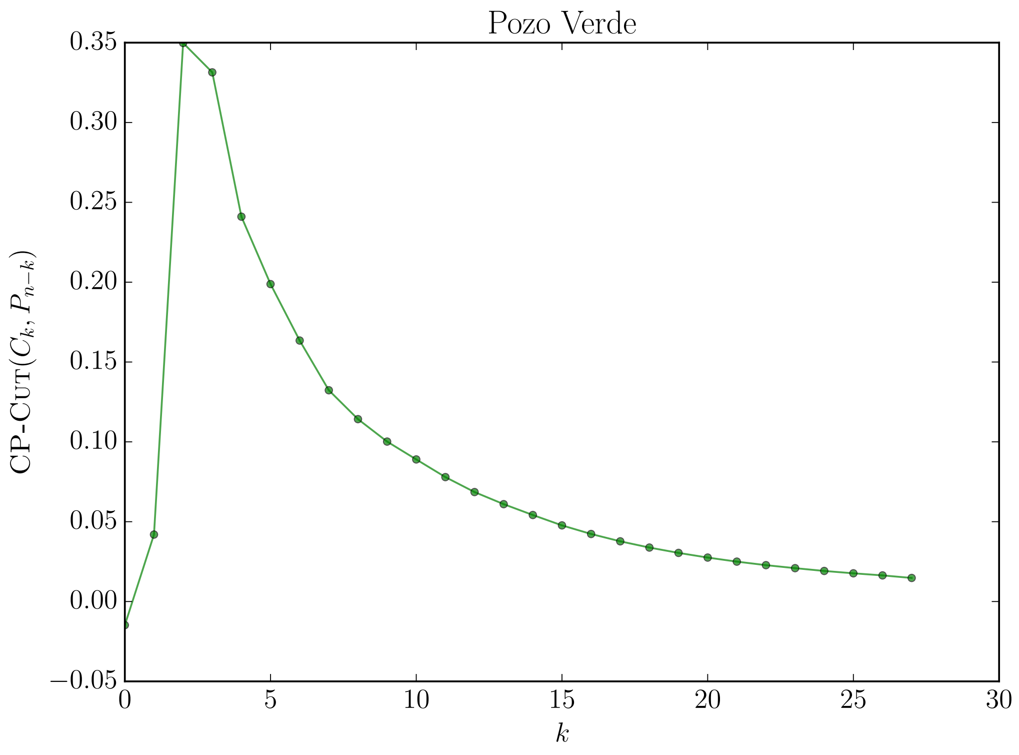

Figure 4.11: The profile of $\text{CP-CUT}(C_k, P_{n-k})$ as a function of k, where we scaled each entry of $\mathbf{W}$ dividing by the maximum entry.

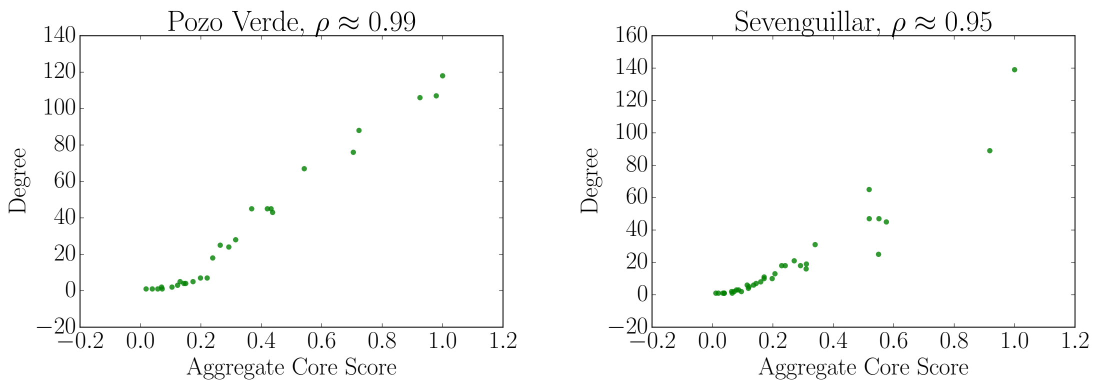

(a) **(b)**

Figure 4.12: A scatter plot for degree versus core scores for two sites. We compute the correlation coefficient ρ.

APPENDIX A

Rank Aggregation for Course–Sequence Discovery

A.1 Course Numbers

Table A.1 shows the official course numbers and the associated course names used throughout the paper. We shortened the official course names wherever possible, to make the tables more visually appealing. For example, "Introduction to Fourier Analysis" is simply labelled "Fourier Analysis". Also, A, B, C are substituted with I, II, and III respectively. A short description of each course in addition to the courses prerequisites is available in the UCLA general catalog [161].

Table A.1: Course names and numbers.

#	Course Name	#	Course Name	#	Course Name
31A	Calculus I	120A	Differential Geometry I	164	Optimization
31B	Calculus II	120B	Differential Geometry II	167	Game Theory
32A	Multi. Calculus I	121	Topology	170A	Probability I
32B	Multi. Calculus II	123	Axiomatic Geometry	170B	Probability II
33A	Applied Linear Algebra	131A	Real Analysis I	172A	Actuarial Mathematics
33B	Applied ODE's	131B	Real Analysis II	172B	Actuarial Models II
61	Discrete Structures	131C	Real Analysis III	172C	Actuarial Models II
106	History of Mathematics	132	Complex Analysis	173A	Casualty Loss Models I
110A	Abstract Algebra I	133	Fourier Analysis	173B	Casualty Loss Models II
110B	Abstract Algebra II	134	Nonlinear Systems	174	Mathematical Economics
110C	Abstract Algebra III	135	ODE's	180	Graph Theory
111	Number Theory	136	PDE's	182	Algorithms
115A	Linear Algebra I	142	Mathematical Modeling	184	Combinatorics
115B	Linear Algebra II	151A	Numerical Analysis I	191	Research Seminar
117	Applied Algebra	151B	Numerical Analysis II	199	Individual Research

APPENDIX B

Core-Periphery Structure in Fruigivore–Seed Networks

B.1 Simulated Annealing

Kirkpatrick et al. in [110] proposed simulated annealing as a stochastic minimization algorithm for combinatorial problems. We present pseudocode in Alg. 1 to represent the main idea of the minimization algorithm. Roughly speaking, Alg. 1 performs a local search, but rather than rejecting all states with higher cost J, we accept new states with a diminishing probability that depends on the difference in costs between the current state and possible new state.

Algorithm 1 Simmulated Annealing for Minimization

```
1: Inputs: Finite set of states $S$, cost function $J : S \to \mathbb{R}$, cooling schedule $C : \mathbb{R} \to (0, \infty)$ such that $\lim_n C(n) = 0$, randomized neighbor function $N : S \to S$; minimum temperature $T_{\min}$
2: Select $s \in S$; select $T$.
3: while $T > T_{\min}$ do
4:     $s' \leftarrow N(s)$
5:     if $J(s) < J(s')$ then
6:         $s \leftarrow s'$
7:     else
8:         $s \leftarrow s'$ with probability $\exp(-(J(s') - J(s))/T)$
9:     $T \leftarrow C(T)$ (cooling)
```

We use the `Matlab` code in [200]. The full pseudocode of this algorithm is given in Algorithm 2. We do not experiment with local search heuristics, neighboring functions and different cooling schedules, in part because we select parameters are designed to survey a large portion of the possible states [176]. We specify the inputs here. The set S of states from Line 1 of Alg. 2 is precisely the set $\mathcal{P}_V(\alpha, \beta)$ from Eq. (1). Recall that $\mathcal{P}(\alpha, \beta)$ is the set of all possible bijections of nodes V to $S(\alpha, \beta, n)$ (see Eq. (4.46)), where $n = |V|$. The cost function J is E from Eq. (4.48). Given an assignment $\mathbf{f}_{\alpha,\beta}$, we define the set of neighbors of $\mathbf{f}_{\alpha,\beta}$ as $\mathbf{g}_{\alpha,\beta}$ such that if $i_1, \ldots, i_n$ is an enumeration of the nodes V, then

1. $\mathbf{f}_{\alpha,\beta} = \mathbf{g}_{\alpha,\beta}$ on nodes $i_1, \ldots, i_{n-2}$,
2. $\mathbf{f}_{\alpha,\beta}(i_{n-1}) = \mathbf{g}_{\alpha,\beta}(i_n)$, and
3. $\mathbf{f}_{\alpha,\beta}(i_n) = \mathbf{g}_{\alpha,\beta}(i_{n-1})$.

In other words, the set of neighbors of $\mathbf{f}_{\alpha,\beta}$ are those functions in $\mathcal{P}_V(\alpha, \beta)$ whose assignment on two nodes are swapped. The randomized neighboring function N from Line 1 of Alg. 2 is a random selection of one of the possible neighbors. We used the cooling schedule $C(T) = .8T$ given as default in [200]. We also set $\text{att}_{\text{max}} = 5000$ and $\text{succ}_{\text{max}} = 1000$ using the code from [17].

Algorithm 2 Simmulated Annealing for Minimization from [200]

```
1: Inputs: Finite set of states $S$; cost function $J : S \to \mathbb{R}$; randomized neighbor function
   $N : S \to S$; minimum temperature $T_{\min}$; maximum consecutive rejections R; maximum
   number of attempts $\text{att}_{\max}$; maximum number of successes $\text{succ}_{\max}$; cooling schedule
   $C : \mathbb{R} \to (0, \infty)$ such that $\lim_{y\to\infty} C(y) = 0$.
2: Select state $s \in S$ uniformly at random (or using a heuristic).
3: Current consecutive rejections $r$ ($r \leftarrow 0$); current number of attempts att (att $\leftarrow 0$);
   current number of successful attempts succ (succ $\leftarrow 0$).
4: Temperature $T$ ($T \leftarrow 1$).
5: while $T > T_{\min}$ and $r < R$ do
6:     if att $> \text{att}_{\max}$ or succ $> \text{succ}_{\max}$ then
7:         $T \leftarrow C(T)$
8:         succ $\leftarrow 0$
9:         att $\leftarrow 0$
10:    $s' \leftarrow N(s)$.
11:    att $\leftarrow$ att $+ 1$
12:    if $J(s') < J(s)$ then
13:        $s \leftarrow s'$
14:        $r \leftarrow 0$
15:        succ $\leftarrow$ succ $+ 1$
16:    else
17:        $x \leftarrow \text{Rand}(0,\ 1)$
18:        if $x < \exp(J(s') - J(s)/T)$ then
19:            $s \leftarrow s'$
20:            $r \leftarrow 0$
21:            succ $\leftarrow$ succ $+ 1$
22:        else
23:            $r \leftarrow r + 1$
```

References

[1] Howard Abadinsky. *Organized Crime.* Cengage Learning, 2012.

[2] Lada A. Adamic and Bernardo A. Huberman. Power-law Distribution of the World Wide Web. *Science*, 287(5461):2115–2115, 2000.

[3] UCLA Undergraduate Admissions. Majors and Minors, December 2016. `https://www.admission.ucla.edu/prospect/coll_sch.htm` (Accessed: December 26th, 2016).

[4] Azam Ahmed and Randal Archibold. Mexican Drug Kingpin, El Chapo, Escapes Prison Through Tunnel, 2015. `http://nyti.ms/1K2b6em` (Accessed: January 6th, 2017).

[5] Christopher Aicher, Abigail Z. Jacobs, and Aaron Clauset. Learning Latent Block Structure in Weighted Networks. *Journal of Complex Networks*, 3(2):221–248, 2015.

[6] Mário Almeida-Neto and Werner Ulrich. A Straightforward Computational Approach for Measuring Nestedness using Quantitative Matrices. *Environmental Modelling & Software*, 26(2):173–178, 2011.

[7] Noga Alon and Joel H. Spencer. *The Probabilistic Method.* John Wiley & Sons, 2004.

[8] Ashton Anderson, Daniel Huttenlocher, Jon Kleinberg, Jure Leskovec, and Mitul Tiwari. Global Diffusion via Cascading Invitations: Structure, Growth, and Homophily. In *Proceedings of the 24th International Conference on World Wide Web*, pages 66–76. ACM, 2015.

[9] Sanjeev Arora, Satish Rao, and Umesh Vazirani. Expander Flows, Geometric Embeddings and Graph Partitioning. *Journal of the ACM*, 56(2):5, 2009.

[10] Luis Astorga and David A. Shirk. Drug Trafficking Organizations and Counter-Drug Strategies in the U.S.–Mexican Context. *Center for U.S.-Mexican Studies*, 2010.

[11] Jonathan E. Atkins, Erik G. Boman, and Bruce Hendrickson. A Spectral Algorithm for Seriation and the Consecutive Ones Problem. *SIAM Journal on Computing*, 28(1):297–310, 1998.

[12] Bruce Bagley. Drug Trafficking and Organized Crime in the Americas. *Woodrow Wilson Center: Update of the Americas*, 2012.

[13] John Bailey and Matthew M. Taylor. Evade, Corrupt, or Confront? Organized Crime and the State in Brazil and Mexico. *Journal of Politics in Latin America*, 1(2):3–29, 2009.

[14] Albert-László Barabási and Réka Albert. Emergence of Scaling in Random Networks. *Science*, 286(5439):509–512, 1999.

[15] Alain Barrat, Marc Barthelemy, Romualdo Pastor-Satorras, and Alessandro Vespignani. The Architecture of Complex Weighted Networks. *Proceedings of the National Academy of Sciences*, 101(11):3747–3752, 2004.

[16] Jordi Bascompte, Pedro Jordano, Carlos J Melián, and Jens M. Olesen. The Nested Assembly of Plant–Animal Mutualistic Networks. *Proceedings of the National Academy of Sciences*, 100(16):9383–9387, 2003.

[17] Danielle S. Bassett, Nicholas F. Wymbs, Puck Rombach, Mason A. Porter, and Scott T. Mucha, Peter J .and Grafton. Task-based Core-Periphery Organization of Human Brain Dynamics. *PLoS Computational Biology*, 9(9):e1003171, 2013.

[18] Vladimir Batagelj and Matjaz Zaversnik. An $O(m)$ Algorithm for Cores Decomposition of Networks. *arXiv preprint cs/0310049*, 2003.

[19] Nicola Bellomo, Francesca Colasuonno, Damian Knopoff, and Juan Soler. From a Systems Theory of Sociology to Modeling the Onset and Evolution of Criminality. *Networks and Heterogeneous Media*, 10(3):421–441, 2015.

[20] Bijan Berenji, Tom Chou, and Maria R. D'Orsogna. Recidivism and Rehabilitation of Criminal Offenders: a Carrot and Stick Evolutionary Game. *PLoS One*, 9:e85531, 2014.

[21] Noam Berger, Christian Borgs, Jennifer T. Chayes, and Amin Saberi. Asymptotic Behavior and Distributional Limits of Preferential Attachment Graphs. *The Annals of Probability*, 42(1):1–40, 2014.

[22] Andrea L. Bertozzi and Arjuna Flenner. Diffuse Interface Models on Graphs for Classification of High Dimensional Data. *Multiscale Modeling & Simulation*, 10(3):1090–1118, 2012.

[23] Aditya Bhaskara, Moses Charikar, Eden Chlamtac, Uriel Feige, and Aravindan Vijayaraghavan. Detecting High Log-Densities: an $O(1/4)$ Approximation for Densest k-Subgraph. In *Proceedings of the* 42^{nd} *ACM symposium on Theory of Computing*, pages 201–210. ACM, 2010.

[24] Ginestra Bianconi and Albert-László Barabási. Bose-Einstein Condensation in Complex Networks. *Physical Review Letters*, 86(24):5632, 2001.

[25] Marián Boguñá, Romualdo Pastor-Satorras, Albert Díaz-Guilera, and Alex Arenas. Models of Social Networks Based on Social Distance Attachment. *Physical Review E*, 70:056122, 2004.

[26] Béla Bollobás. The Evolution of Random Graphs. *Transactions of the American Mathematical Society*, 286(1):257–274, 1984.

[27] Béla Bollobás. *Modern Graph Theory*, volume 184. Springer, 2013.

[28] Immanuel M. Bomze, Marco Budinich, Panos M. Pardalos, and Marcello Pelillo. The maximum clique problem. In *Handbook of Combinatorial Optimization*, pages 1–74. Springer, 1999.

[29] Stephen P. Borgatti. Identifying Sets of Key Players in a Social Network. *Computational & Mathematical Organization Theory*, 12(1):21–34, 2006.

[30] Stephen P. Borgatti and Martin G. Everett. Models of Core-Periphery Structures. *Social Networks*, 21(4):375–395, 2000.

[31] Mark Bowden. *Killing Pablo: The Inside Story of the Manhunt to Bring Down the Most Powerful Criminal in History.* Atlantic Books, 2012.

[32] Ralph A. Bradley and Milton E. Terry. Rank Analysis of Incomplete Block Designs: I. The Method of Paired Comparisons. *Biometrika*, 39(3):324–345, 1952.

[33] Lori Breslow, David E. Pritchard, Jennifer DeBoer, Glenda S. Stump, Andrew D. Ho, and Daniel T. Seaton. Studying Learning in the Worldwide Classroom: Research into edX's First MOOC. *Research & Practice in Assessment*, 8:13–25, 2013.

[34] Xavier Bresson and Arthur D. Szlam. Total variation and cheeger cuts. In *Proceedings of the 27th International Conference on Machine Learning*, pages 1039–1046, 2010.

[35] Sergey Brin and Lawrence Page. The Anatomy of a Large-scale Hypertextual Web Search Engine. *Computational Networks and ISDN Systems*, 30(1-7):107–117, April 1998.

[36] F. Thomas Bruss. A Note on Extinction Criteria for Bisexual Galton–Watson Processes. *Journal of Applied Probability*, 21(4):915–919, 1984.

[37] Thomas Callaghan, Peter J. Mucha, and Mason A. Porter. Random Walker Ranking for NCAA Division IA Football. *American Mathematical Monthly*, 114(9):761–777, 2007.

[38] Alessio Cardillo, Jesús Gómez-Gardeñes, Massimiliano Zanin, Miguel Romance, David Papo, Francisco del Pozo, and Stefano Boccaletti. Emergence of Network Features from Multiplexity. *Scientific Reports*, 3:1344 EP–, 02 2013.

[39] Claudio Castellano, Santo Fortunato, and Vittorio Loreto. Statistical Physics of Social Dynamics. *Reviews of Modern Physics*, 81:591–646, 2009.

[40] Michele Catanzaro, Marián Boguñá, and Romualdo Pastor-Satorras. Generation of Uncorrelated Random Scale-Free Networks. *Physical Review E*, 71(2):027103, 2005.

[41] Manuela Cattelan. Models for Paired Comparison Data: A Review with Emphasis on Dependent Data. *Statistical Science*, pages 412–433, 2012.

[42] Bikas K. Chakrabarti, Anirban Chakraborti, and Arnab Chatterjee. *Econophysics and Sociophysics: Trends and Perspectives.* John Wiley & Sons, 2007.

[43] Sorathan Chaturapruek, Jonah Breslau, Daniel Yazdi, Theodore Kolokolnikov, and Scott G. McCalla. Crime Modeling with Lévy flights. *SIAM Journal on Applied Mathematics*, 73(4):1703–1720, 2013.

[44] Xi Chen, Paul N. Bennett, Kevyn Collins Thompson, and Eric Horvitz. Pairwise Ranking Aggregation in a Crowdsourced Setting. In *Proceedings of the Sixth ACM International Conference on Web Search and Data Mining*, pages 193–202, New York, NY, 2013. ACM.

[45] Fan Chung. *Spectral Graph Theory*, volume 92. American Mathematical Society, 1997.

[46] Fan Chung, Shirin Handjani, and Doug Jungreis. Generalizations of Polya's Urn Problem. *Annals of Combinatorics*, 7(2):141–153, 2003.

[47] Fan Chung and Linyuan Lu. Coupling Online and Offline analyses for Random Power Law Graphs. *Internet Mathematics*, 1(4):409–461, 2004.

[48] Douglas H. Clements and Julie Sarama. Learning Trajectories in Mathematics Education. *Mathematical Thinking and Learning*, 6(2):81–89, 2004.

[49] Andrew Comrey. The Minimum Residual Method of Factor Analysis. *Psychological Reports*, 11(1):15–18, 1962.

[50] Colin Cooper, Alan Frieze, and Juan Vera. Random Deletion in a Scale-Free Random Graph Process. *Internet Mathematics*, 1(4):463–483, 2004.

[51] Donald R. Cressey. *Theft of the Nation: The Structure and Operations of Organized Crime in America*. Harper & Row, 1969.

[52] Peter Csermely, Andrs London, Ling-Yun Wu, and Brian Uzzi. Structure and Dynamics of Core/Periphery Networks. *Journal of Complex Networks*, 1(2):93–123, 2013.

[53] Mihai Cucuringu. Sync-Rank: Robust Ranking, Constrained Ranking and Rank Aggregation via Eigenvector and SDP Synchronization. *IEEE Transactions on Network Science and Engineering*, 3(1):58–79, 2016.

[54] Mihai Cucuringu, Puck Rombach, Sang Hoon Lee, and Mason A. Porter. Detection of Core-Periphery Structure in Networks using Spectral Methods and Geodesic Paths. *European Journal of Applied Mathematics*, 27(6):846–887, 12 2016.

[55] H. A. David and D. M. Andrews. Nonparametric Methods of Ranking from Paired Comparisons. In *Probability Models and Statistical Analyses for Ranking Data*, pages 20–36. Springer, 1993.

[56] Cristobal de Brey, Thomas D. Snyder, and Sally A. Dillow. Mobile Digest of Education Statistics, 2014. *National Center for Education Statistics*, 2016.

[57] Pierre de Champlain. *Mobsters, Gangsters and Men of Honour: Cracking the Mafia Code*. Harper Collins (Canada), 2005.

[58] Derek J. de Solla Price. Networks of Scientific Papers. *Science*, 149(3683):510–515, 1965.

[59] Fabio Della Rossa, Fabio Dercole, and Carlo Piccardi. Profiling Core-Periphery Network Structure by Random Walkers. *Scientific Reports*, 3, 2013.

[60] James W. Demmel. *Applied Numerical Linear Algebra*. SIAM, 1997.

[61] James A. Densley. Street Gang Recruitment: Signaling, Screening, and Selection. *Social Problems*, 59(3):301–321, 2012.

[62] Jean-Pierre Dion. Estimation of the Mean and the Initial Probabilities of a Branching Process. *Journal of Applied Probability*, 11(4):687–694, 1974.

[63] Sergey N. Dorogovtsev, Alexander V. Goltsev, and Jose Ferreira F. Mendes. k-core Organization of Complex Networks. *Physical Review Letters*, 96(4):040601, 2006.

[64] Maria R. D'Orsogna, Michael McBride, Ryan Kendall, and Martin B. Short. Criminal Defectors Lead to the Emergence of Cooperation in an Experimental, Adversarial Game. *PloS One*, 8:e61458, 2013.

[65] Maria R D'Orsogna and Matjaz Perc. Statistical Physics of Crime. *Physics of Life Reviews*, 12:1–21, 2014.

[66] Steven S. Dudley. *Drug Trafficking Organizations in Central America: Transportistas, Mexican Cartels and Maras*, pages 63–93. Woodrow Wilson International Center for Scholars, 2010.

[67] Paul A. C. Duijn, Victor Kashirin, and Peter M. A. Sloot. The Relative Ineffectiveness of Criminal Network Disruption. *Scientific Reports*, 4(4238), 2014.

[68] Richard Durrett. *Random Graph Dynamics*. Cambridge University Press, 2007.

[69] Richard Durrett. *Essentials of Stochastic Processes*. Springer, 2012.

[70] Cynthia Dwork, Ravi Kumar, Moni Naor, and D. Sivakumar. Rank Aggregation Revisited, 2001. `http://www.eecs.harvard.edu/~michaelm/CS222/rank2.pdf` (Accessed: January 15th, 2017).

[71] Cynthia Dwork, Ravi Kumar, Moni Naor, and Dandapani Sivakumar. Rank Aggregation Methods for the Web. In *Proceedings of the 10th international conference on World Wide Web*, pages 613–622. ACM, 2001.

[72] David Easley and Jon Kleinberg. *Networks, Crowds, and Markets: Reasoning about a Highly Connected World*. Cambridge University Press, 2010.

[73] John Eid, Adrian Fehr, Jeremy Gray, Khai Luong, John Lyle, Otto, et al. Real-time DNA Sequencing from Single Polymerase Molecules. *Science*, 323(5910):133–138, 2009.

[74] Magdalini Eirinaki and Michalis Vazirgiannis. Web Mining for Web Personalization. *ACM Transactions on Internet Technology*, 3(1):1–27, 2003.

[75] Paul Erdős and Alfréd Rényi. On the Strength of Connectedness of a Random Graph. *Acta Mathematica Hungarica*, 12(1):261–267, 1961.

[76] Shimon Even and R. Endre Tarjan. Network Flow and Testing Graph Connectivity. *SIAM Journal on Computing*, 4(4):507–518, 1975.

[77] Uriel Feige, David Peleg, and Guy Kortsarz. The Dense k-Subgraph Problem. *Algorithmica*, 29(3):410–421, 2001.

[78] Marcus Felson. *The Ecosystem for Organized Crime*. European Institute for Crime Prevention and Control, 2006.

[79] Robert Filippone. The Medellin Cartel: Why We Can't Win The Drug War. *Studies in Conflict & Terrorism*, 17(4):323–344, 1994.

[80] Michael A. Fligner and Joseph S. Verducci. *Probability Models and Statistical Analyses for Ranking Data*, volume 80. Springer, 1993.

[81] Fajwel Fogel, Alexandre d'Aspremont, and Milan Vojnovic. SerialRank: Spectral Ranking using Seriation. In *Advances in Neural Information Processing Systems*, pages 900–908, 2014.

[82] Santo Fortunato. Community Detection in Graphs. *Physics Reports*, 486(3):75–174, 2010.

[83] Bailey K. Fosdick, Daniel B. Larremore, Joel Nishimura, and Johan Ugander. Configuring Random graph Models with Fixed Degree Sequences. *arXiv preprint arXiv:1608.00607*, 2016.

[84] Łukasz Gajewski, Jan Chołoniewski, and Janusz Hołyst. Key Courses of the Academic Curriculum Uncovered by Data Mining of Students' Grades. *arXiv preprint arXiv:1604.07074*, 2016.

[85] Francis Galton and Henry W. Watson. *On the Probability of Extinction of Families*, volume 4, pages 138–144. Wiley, 1875.

[86] John Gandar, Richard Zuber, Thomas O'Brien, and Ben Russo. Testing Rationality in the Point Spread Betting Market. *The Journal of Finance*, 43(4):995–1008, 1988.

[87] Antonios Garas, Frank Schweitzer, and Shlomo Havlin. A k-shell Decomposition Method for Weighted Networks. *New Journal of Physics*, 14(8):083030, 2012.

[88] James P. Gleeson, Davide Cellai, Jukka-Pekka Onnela, Mason A. Porter, and Felix Reed-Tsochas. A Simple Generative Model of Collective Online Behavior. *Proceedings of the National Academy of Sciences*, 111(29):10411–10415, 2014.

[89] David F. Gleich. PageRank Beyond the Web. *SIAM Review*, 57(3):321–363, 2015.

[90] David F. Gleich and Lek-Heng Lim. Rank Aggregation via Nuclear Norm Minimization. In *Proceedings of the 17th ACM SIGKDD International Conference on Knowledge Discovery and Data Mining*, pages 60–68, New York, NY, 2011. ACM.

[91] John Goddard and Ioannis Asimakopoulos. Forecasting Football Results and the Efficiency of Fixed-Odds Betting. *Journal of Forecasting*, 23(1):51–66, 2004.

[92] Andrew Goldberg. *Finding a Maximum Density Subgraph.* University of California Berkeley, CA, 1984.

[93] Tom Goldstein and Stanley Osher. The Split Bregman Method for ℓ_1-Regularized Problems. *SIAM Journal on Imaging Sciences*, 2(2):323–343, 2009.

[94] Alexander Gutfraind, Aric Hagberg, and Feng Pan. Optimal Interdiction of Unreactive Markovian Evaders. In *Integration of AI and OR Techniques in Constraint Programming for Combinatorial Optimization Problems: 6th International Conference*, pages 102–116. Springer Berlin, 2009.

[95] Jiawei Han, Hong Cheng, Dong Xin, and Xifeng Yan. Frequent Pattern Mining: Current Status and Future Directions. *Data Mining and Knowledge Discovery*, 15(1):55–86, 2007.

[96] William J. Hardin. *Mathematics, Prerequisites, and Student Success in Introductory Courses*, pages 352–360. Josey–Bass, 3 edition, 2008.

[97] Anil N. Hirani, Kaushik Kalyanaraman, and Seth Watts. Least Squares Ranking on Graphs, November 2011. `http://arxiv.org/abs/1011.1716` (Accessed: January 15th, 2017).

[98] Petter Holme. Core–Periphery Organization of Complex Networks. *Physical Review E*, 72(4):046111, 2005.

[99] Huiyi Hu, Thomas Laurent, Mason A. Porter, and Andrea L. Bertozzi. A Method Based on Total Variation for Network Modularity Optimization using the MBO-Scheme. *SIAM Journal on Applied Mathematics*, 73(6):2224–2246, 2013.

[100] David M. Hull. A Reconsideration of Galton's Problem (Using a Two-Sex Population). *Theoretical Population Biology*, 54(2):105–116, 1998.

[101] Hawoong Jeong, Zoltan Néda, and Albert-László Barabási. Measuring Preferential Attachment in Evolving Networks. *Europhysics Letters*, 61(4):567, 2003.

[102] Hawoong Jeong, Zoltan Néda, and Albert-László Barabási. Measuring Preferential Attachment in Evolving Networks. *Europhysics Letters*, 61(4):567, 2003.

[103] Lucas G. S. Jeub, Prakash Balachandran, Mason A. Porter, Peter J. Mucha, and Michael W. Mahoney. Think Locally, Act Locally: Detection of Small, Medium-Sized, and Large Communities in Large Networks. *Physical Review E*, 91:012821, 2015.

[104] Xiaoye Jiang, Lek-Heng Lim, Yuan Yao, and Yinyu Ye. Statistical Ranking and Combinatorial Hodge Theory. *Mathematical Programming*, 127(1):203–244, 2011.

[105] Katy Jordan. Initial Trends in Enrollment and Completion of Massive Open Online Courses. *The International Review of Research in Open and Distributed Learning*, 15(1):133–160, 2014.

[106] Norman Kaplan. The Multitype Galton–Watson Process with Immigration. *Annals of Probability*, 1(6):947–953, 1973.

[107] David G. Kendall. Branching Processes since 1873. *Journal of the London Mathematical Society*, 1(1):385–406, 1966.

[108] Michael Kenney. From Pablo to Osama: Counter–Terrorism Lessons from the War on Drugs. *Survival*, 45(3):187–206, 2003.

[109] Michael Kenney. The Architecture of Drug Trafficking: Network Forms of Organization in the Colombian Cocaine Trade. *Global Crime*, 8(3):233–259, 2007.

[110] Scott Kirkpatrick, C. Daniel Gelatt, and Mario P. Vecchi. Optimization by Simmulated Annealing. *Science*, 220(4598):671–680, 1983.

[111] Mikko Kivelä, Alex Arenas, Marc Barthelemy, James P. Gleeson, Yamir Moreno, and Mason A. Porter. Multilayer Networks. *Journal of Complex Networks*, 2(3):203–271, 2014.

[112] Krzysztof Koperski and Jiawei Han. Discovery of Spatial Association Rules in Geographic Information Databases. In *Proceedings of the 4th International Symposium on Advances in Spatial Databases*, pages 47–66, London, UK, 1995. Springer.

[113] Paul L. Krapivsky and Sidney Redner. Organization of Growing Random Networks. *Physical Review E*, 63(6):066123, 2001.

[114] Valdis Krebs. Mapping Networks of Terrorist Cells. *Connections*, 24(3):43–52, 2002.

[115] Paul R. Krugman. *Geography and Trade.* MIT press, 1991.

[116] Daniel B. Larremore, Aaron Clauset, and Abigail Z. Jacobs. Efficiently Inferring Community Structure in Bipartite Networks. *Physical Review E*, 90(1):012805, 2014.

[117] Edward O. Laumann and Franz Urban Pappi. New Directions in the Study of Community Elites. *American Sociological Review*, pages 212–230, 1973.

[118] Deok-Sun Lee, Seong Eun Maeng, and Jae Woo Lee. Scaling of Nestedness in Complex Networks. *Journal of the Korean Physical Society*, 60(4):648–656, 2012.

[119] Sang Hoon Lee. Network Nestedness as Generalized Core–Periphery Structures. *Physical Review E*, 93(2):022306, 2016.

[120] Sang Hoon Lee, Mihai Cucuringu, and Mason A. Porter. Density-Based and Transport-Based Core–Periphery Structures in Networks. *Physical Review E*, 89:032810, Mar 2014.

[121] Robert S. Leiken. *Mexico's Drug War.* Center for the National Interest, 2012. `http://www.cpimexico.org.mx/portal/wp-content/uploads/2014/01/Mexicos-drug-war.pdf`.

[122] Lun Li, David Alderson, John C. Doyle, and Walter Willinger. Towards a Theory of Scale–Free Graphs: Definition, Properties, and Implications. *Internet Mathematics*, 2(4):431–523, 2005.

[123] László Lovász. Random Walks on Graphs. *Combinatorics, Paul Erdős is Eighty*, 2:1–46, 1993.

[124] Robert D. Luce and Patrick Suppes. *Preference, Utility, and Subjective Probability.* Wiley, 1965.

[125] Tomasz Łuczak. Component Behavior Near the Critical Point of the Random Graph Process. *Random Structures & Algorithms*, 1(3):287–310, 1990.

[126] Hosam M. Mahmoud. Distances in Random Plane-Oriented Recursive Trees. *Journal of Computational and Applied Mathematics*, 41(1):237–245, 1992.

[127] Charles Z. Marshak, M. Puck Rombach, Andrea L. Bertozzi, and Maria R. D'Orsogna. Growth and Containment of a Hierarchical Criminal Network. *Physical Review E*, 93:022308, Feb 2016.

[128] Giovanni Mastrobuoni and Eleonora Patacchini. Understanding Organized Crime Networks: Evidence based on Federal Bureau of Narcotics Secret Files on American Mafia. *Carlo Alberto Notebooks*, 152:1–58, 2010.

[129] Giovanni Mastrobuoni and Eleonora Patacchini. Organized Crime Networks: An Application of Network Analysis Techniques to the American Mafia. *Review of Network Economics*, 11(3):1–43, 2012.

[130] Naoki Masuda, Mason A. Porter, and Renaud Lambiotte. Random Walks and Diffusion on Networks. *arXiv preprint arXiv:1612.03281*, 2016.

[131] Antonio L. Mazzitelli. Mexican Cartel Influence in Central America. *Western Hemisphere Security Analysis Center*, 2011.

[132] Julian J. McAuley and Jure Leskovec. Learning to Discover Social Circles in Ego Networks. In *Advances in Neural Information Processing*, volume 2012, pages 548–56, 2012.

[133] Michael McBride and Michael Caldara. The Efficacy of Tables versus Graphs in Disrupting Dark Networks: An Experimental Study. *Social Networks*, 35(3):406–422, 2013.

[134] Michael McBride and David Hewitt. The Enemy You Cannot See: An Investigation of the Disruption of Dark Networks. *Journal of Economic Behavior & Organization*, 93:32–50, 2013.

[135] Rachel McCulloch and Linda P. Rothschild. MOOCs: An Inside View. *Notices of the American Mathematical Society*, 61(8):866–872, 2014.

[136] Marco Aurelio Ribeiro Mello, Flávia Maria Darcie Marquitti, Paulo Roberto Guimarães, Jr., et al. The Missing Part of Seed Dispersal Networks: Structure and Robustness of Bat–Fruit Interactions. *PLoS One*, 6(2):1–10, 2011.

[137] Marco Aurelio Ribeiro Mello, Flávia Maria Darcie Marquitti, Paulo R. Guimaraes Jr., et al. The Modularity of Seed Dispersal: Differences in Structure and Robustness between Bat– and Bird–Fruit Networks. *Oecologia*, 167(1):131–140, 2011.

[138] Ekaterina Merkurjev, Tijana Kostic, and Andrea L. Bertozzi. An MBO Scheme on Graphs for Classification and Image Processing. *SIAM Journal on Imaging Sciences*, 6(4):1903–1930, 2013.

[139] Dillon V. P. Montag Mihai Cucuringu, Charlie Marshak and Puck Rombach. Rank Aggregation for Course Sequence Discovery, March 2016. `https://arxiv.org/abs/1603.02695` (In preparation).

[140] J. Mitchell Miller and Lance H. Selva. Drug Enforcement's Double-Edged Sword: An Assessment of Asset Forfeiture Programs. *Justice Quarterly*, 11(2):313–335, 1994.

[141] Robert J. Mokken. Cliques, Clubs and Clans. *Quality & Quantity*, 13(2):161–173, 1979.

[142] Cristopher Moore, Gourab Ghoshal, and Mark E. J. Newman. Exact Solutions for Models of Evolving Networks with Addition and Deletion of Nodes. *Physical Review E*, 74(3):036121, 2006.

[143] Carlo Morselli. *Contacts, Opportunities, and Criminal Enterprise.* University of Toronto Press, 2005.

[144] Carlo Morselli. *Inside Criminal Networks*, volume 8. Springer, 2008.

[145] Carlo Morselli. Assessing Vulnerable and Strategic Positions in a Criminal Network. *Journal of Contemporary Criminal Justice*, 26(4):382–392, 2010.

[146] Elchanan Mossel, Joe Neeman, and Allan Sly. Stochastic block models and reconstruction. *arXiv preprint arXiv:1202.1499*, 2012.

[147] Adilson E. Motter. Cascade Control and Defense in Complex Networks. *Physical Review Letters*, 93(9):098701, 2004.

[148] Adilson E. Motter and Ying-Cheng Lai. Cascade-Based Attacks on Complex Networks. *Physical Review E*, 66(6):065102, 2002.

[149] Peter J. Mucha, Thomas Richardson, Kevin Macon, Mason A. Porter, and Jukka-Pekka Onnela. Community Structure in Time-Dependent, Multiscale, and Multiplex Networks. *Science*, 328(5980):876–878, 2010.

[150] Kevin P. Murphy, Yair Weiss, and Michael I. Jordan. Loopy Belief Propagation for Approximate Inference: An Empirical Study. In *Proceedings of the Fifteenth Conference on Uncertainty in Artificial Intelligence*, pages 467–475, 1999.

[151] Roger B. Myerson. Analysis of Democratic Institutions: Structure, Conduct and Performance. *The Journal of Economic Perspectives*, 9(1):77–89, 1995.

[152] Sahand Negahban, Sewoong Oh, and Devavrat Shah. Iterative Ranking from Pair-wise Comparisons. In *Advances in Neural Information Processing Systems*, pages 2474–2482, 2012.

[153] Mark E. J. Newman. Clustering and Preferential Attachment in Growing Networks. *Physical review E*, 64(2):025102, 2001.

[154] Mark E. J. Newman. *Networks: An Introduction.* Oxford University Press, 2010.

[155] UCLA Department of Chemistry. The UCLA Chemistry Major, 2016. `http://www.chem.ucla.edu/dept/ugrad/majors/chemistry.htm` (Accessed: December 26th, 2016).

[156] Bureau of Labor Statistics. Economics News Release, 2016. `http://www.bls.gov/news.release/empsit.t04.htm` (Accessed: December 26th, 2016).

[157] UCLA Department of Mathematics. Majors, Minors & Specializations, December 2016. `https://www.math.ucla.edu/ugrad/majors` (Accessed: December 26th, 2016).

[158] Congressional Budget Office. National Defense Authorization Act for Fiscal Year 2017, 2016. `https://www.cbo.gov/publication/51570` (Accessed: January 6th, 2017).

[159] UCLA Registrar's Office. Class Levels, 2016. `hhttp://www.registrar.ucla.edu/Registration-Classes/Enrollment-Policies/Class-Levels` (Accessed: December 26th, 2016).

[160] UCLA Registrar's Office. Grades, 2016. `http://catalog.registrar.ucla.edu/ucla-cat2016-58.html` (Accessed: December 26th, 2016).

[161] UCLA Registrar's Office. UCLA General Catalog, 2016. `http://catalog.registrar.ucla.edu/` (Accessed: December 26th, 2016).

[162] Jens M. Olesen, Jordi Bascompte, Yoko L. Dupont, and Pedro Jordano. The Modularity of Pollination Networks. *Proceedings of the National Academy of Sciences*, 104(50):19891–19896, 2007.

[163] Braxton Osting, Christoph Brune, and Stanley Osher. Enhanced Statistical Rankings via Targeted Data Collection. In *International Conference on Machine Learning*, pages 489–497, 2013.

[164] Braxton Osting, Jérôme Darbon, and Stanley Osher. Statistical Ranking Using the ℓ_1-norm on Graphs. *AIMS Journal on Inverse Problems and Imaging*, 7(3):907–926, 2013.

[165] Elyssa Pachico. Mexico Defense of Kingpin Strategy Falls Short. *Insight Crime*, 2011.

[166] Lawrence Page, Sergey Brin, Rajeev Motwani, and Terry Winograd. The PageRank Citation Ranking: Bringing Order to the Web. Technical Report 1999-66, Stanford InfoLab, 1999. `http://ilpubs.stanford.edu:8090/422/1/1999-66.pdf` (Accessed: January 15th, 2017).

[167] Bruce D. Patterson and Wirt Atmar. Nested Subsets and the Structure of Insular Mammalian Faunas and Archipelagos. *Biological Journal of the Linnean Society*, 28(1-2):65–82, 1986.

[168] Tiago P. Peixoto. Hierarchical Block Structures and High-Resolution Model Selection in Large Networks. *Phys. Rev. X*, 4:011047, Mar 2014.

[169] Shai Pilosof, Mason A. Porter, Mercedes Pascual, and Sonia Kéfi. The Multilayer Nature of Ecological Networks. *arXiv preprint arXiv:1511.04453*, 2015.

[170] Mason A. Porter, Jukka-Pekka Onnela, and Peter J. Mucha. Communities in Networks. *Notices of the American Mathematical Society*, 56(9):1082–1097, 2009.

[171] Arun Rajkumar and Shivani Agarwal. A Statistical Convergence Perspective of Algorithms for Rank Aggregation from Pairwise Data. In *International Conference on Machine Learning*, pages 118–126, 2014.

[172] Karthik Raman and Thorsten Joachims. Methods for Ordinal Peer Grading. In *Proceedings of the 20th ACM SIGKDD International Conference on Knowledge Discovery and Data Mining*, pages 1037–1046. ACM, 2014.

[173] R. Ravi and D. P. Williamson. An Approximation Algorithm for Minimum–Cost Vertex–Connectivity Problems. *Algorithmica*, 18(1):21–43, 1997.

[174] Peter Reuter and Mark A. R. Kleiman. Risks and Prices: An Economic Analysis of Drug Enforcement. *Crime and Justice*, pages 289–340, 1986.

[175] Puck Rombach and Mason A. Porter. Discriminating Power of Centrality Measures. *arXiv preprint arXiv:1305.3146*, 2013.

[176] Puck Rombach, Mason A. Porter, James H. Fowler, and Peter J. Mucha. Core-periphery structure in networks. *SIAM Journal on Applied Mathematics*, 74(1):167–190, 2014.

[177] Jonathan B. Rothbard and William R. Taylor. A Sequence Pattern Common to T-cell Epitopes. *The EMBO Journal*, 7(1):93–100, 1988.

[178] Leonid Rudin, Stanley Osher, and Emad Fatemi. Nonlinear Total Variation based Noise Removal Algorithms. *Physica D: Nonlinear Phenomena*, 60(1):259–268, 1992.

[179] Román A. Ruggera, Pedro G. Blendinger, M. Daniela Gomez, and Charlie Marshak. Linking Structure and Functionality in Mutualistic Networks: Do Core Frugivores Disperse More Seeds than Peripheral Species? *Oikos*, August 2015.

[180] Román A. Ruggera, M. Daniela Gomez, and Pedro G. Blendinger. Frugivory and Seed Dispersal Role of the Yellow–Striped Brush–Finch (Atlapetes citrinellus), an Endemic Emberizid of Argentina. *EMU*, 114(4):343–351, 2014.

[181] Matthias Schleuning, Lili Ingmann, Rouven Strauss, Susanne A. Fritz, Bo Dalsgaard, D. Matthias Dehling, et al. Ecological, Historical and Evolutionary Determinants of Modularity in Weighted Seed–Dispersal Networks. *Ecology letters*, 17(4):454–463, 2014.

[182] Barbara Schneider, Christopher B. Swanson, and Catherine Riegle-Crumb. Opportunities for Learning: Course Sequences and Positional Advantages. *Social Psychology of Education*, 2(1):25–53, 1997.

[183] Eugene W. Schupp, Pedro Jordano, and José María Gómez. Seed Dispersal Effectiveness Revisited: a Conceptual Review. *New Phytologist*, 188(2):333–353, 2010.

[184] UCLA Summer Session. UCLA Summer Session, December 2016. `http://www.summer.ucla.edu/` (Accessed: December 26th, 2016).

[185] Martin B. Short, Andrea L. Bertozzi, and P. Jeffrey Brantingham. Nonlinear Patterns in Urban Crime: Hotspots, Bifurcations, and Suppression. *SIAM Journal on Applied Dynamical Systems*, 9(2):462–483, 2010.

[186] Martin B. Short, Maria R. D'Orsogna, Virginia B. Pasour, George E. Tita, P. Jeffrey Brantingham, Andrea L. Bertozzi, and Lincoln Chayes. A Statistical Model of Criminal Behavior. *Mathematical Models and Methods in Applied Science*, 18:1249–67, 2008.

[187] Herbert A. Simon. On a Class of Skew Distribution Functions. *Biometrika*, 42(3):425–440, 1955.

[188] Amit Singer. Angular Synchronization by Eigenvectors and Semidefinite Programming. *Applied Computational Harmonic Analysis*, 30(1):20–36, 2011.

[189] Robert T. Smythe and Hosam M. Mahmoud. A Survey of Recursive Trees. *Theory of Probability and Mathematical Statistics*, 51:1–28, 1995.

[190] David Snyder and Edward L. Kick. Structural Position in the World System and Economic Growth, 1955-1970: A Multiple-Network Analysis of Transnational Interactions. *American Journal of Sociology*, pages 1096–1126, 1979.

[191] Daniel A. Spielman. Spectral Graph Theory and Its Applications. In *IEEE 54th Annual Symposium on Foundations of Computer Science*, pages 29–38. IEEE, 2007.

[192] Alexey Stomakhin, Martin B. Short, and Andrea L. Bertozzi. Reconstruction of Missing Data in Social Networks based on Temporal Patterns of Interactions. *Inverse Problems*, 27(11):115013, 2011.

[193] Steven H. Strogatz. Exploring Complex Networks. *Nature*, 410(6825):268–276, 2001.

[194] Michael P. H. Stumpf and Mason A. Porter. Critical Truths about Power Laws. *Science*, 335(6069):665–666, 2012.

[195] Nguyen Thai-Nghe, Lucas Drumond, Artus Krohn-Grimberghe, and Lars Schmidt-Thieme. Recommender System for Predicting Student Performance. *Procedia Computer Science*, 1(2):2811–2819, 2010.

[196] David P. Thompson. Pablo Escobar, Drug Baron: His Surrender, Imprisonment, and Escape. *Studies in Conflict & Terrorism*, 19(1):55–91, 1996.

[197] L. L. Thurstone. The Method of Paired Comparisons for Social Values. *The Journal of Abnormal and Social Psychology*, 21(4):384–400, 1927.

[198] Amanda L. Traud, Peter J. Mucha, and Mason A. Porter. Social Structure of Facebook Networks. *Physica A: Statistical Mechanics and its Applications*, 391(16):4165–4180, 2012.

[199] Yves van Gennip, Nestor Guillen, Braxton Osting, and Andrea L. Bertozzi. Mean Curvature, Threshold Dynamics, and Phase field theory on Finite Graphs. *Milan Journal of Mathematics*, 82(1):3–65, 2014.

[200] Joachim Vandekerckhove. General Simulated Annealing Algorithm, 2006. `https://is.gd/fXikwf` (Accessed: January 3rd).

[201] Ulrike Von Luxburg. A Tutorial on Spectral Clustering. *Statistics and Computing*, 17(4):395–416, 2007.

[202] Haixun Wang, Wei Wang, Jiong Yang, and Philip S. Yu. Clustering by Pattern Similarity in Large Data Sets. In *Proceedings of the 2002 ACM SIGMOD International Conference on Management of Data*, SIGMOD, pages 394–405. ACM, 2002.

[203] Stanley Wasserman and Katherine Faust. *Social Network Analysis: Methods and Applications*, volume 8. Cambridge University Press, 1994.

[204] David Wen-Shung Tai, Hui-Ju Wu, and Pi-Hsiang Li. Effective e-Learning Recommendation System based on Self-Organizing Maps and Association Mining. *The Electronic Library*, 26(3):329–344, 2008.

[205] Walter Willinger, David Alderson, and John C. Doyle. Mathematics and the Internet: A Source of Enormous Confusion and Great Potential. *Notices of the AMS*, 56(5):586–599, 2009.

[206] James Q. Wilson. *The Investigators: Managing FBI and Narcotics Agents*. Basic Books, 1978.

[207] R. Kevin Wood. Deterministic Network Interdiction. *Mathematical and Computer Modelling*, 17(2):1–18, 1993.

[208] David H. Wright, Bruce D. Patterson, Greg M. Mikkelson, Alan Cutler, and Wirt Atmar. A Comparative Analysis of Nested subset Patterns of Species Composition. *Oecologia*, 113(1):1–20, 1997.

[209] Jennifer Xu and Hsinchun Chen. The Topology of Dark Networks. *Communications of the ACM*, 51(10):58–65, 2008.

[210] Jie Xu, Tianwei Xing, and Mihaela van der Schaar. Personalized Course Sequence Recommendations. *IEEE Transactions on Signal Processing*, 64(20):5340–5352, 2016.

[211] Jiong Yang, Wei Wang, and Philip S. Yu. Mining Asynchronous Periodic Patterns in Time Series Data. *IEEE Transactions on Knowledge and Data Engineering*, 15(3):613–628, 2003.

[212] Jiong Yang, Wei Wang, Philip S. Yu, and Jiawei Han. Mining Long Sequential Patterns in a Noisy Environment. In *Proceedings of the 2002 ACM SIGMOD International Conference on Management of Data*, pages 406–417. ACM, 2002.

[213] Yiming Yang, Hanxiao Liu, Jaime Carbonell, and Wanli Ma. Concept Graph Learning from Educational Data. In *Proceedings of the Eighth ACM International Conference on Web Search and Data Mining*, pages 159–168, New York, NY, 2015. ACM.

[214] H. P. Young. Condorcet's Theory of Voting. *The American Political Science Review*, 82(4):1231–1244, 1988.

[215] G. Udny Yule. A Mathematical Theory of Evolution. *Philosophical Transactions of the Royal Society of London*, 213(402-410):21–87, 1925.

[216] Xiao Zhang, Travis Martin, and Mark Newman. Identification of Core-Periphery Structure in Networks. *Physical Review E*, 91(3):032803, 2015.